

**Asphaltene Adsorption on Different Solid Surfaces from Organic Solvents**

**by**

**Adriana Briones**

**A thesis submitted in partial fulfillment of the requirements for the degree of**

**Master of Science**

**in**

**Chemical Engineering**

**Department of Chemical and Materials Engineering**

**University of Alberta**

**© Adriana Briones, 2016**

# Abstract

Adsorption of asphaltenes at liquid-liquid and solid-liquid interfaces is an undesirable phenomenon and considered to be the major contributor to several complications found in petroleum industry. Although the adsorption of asphaltenes on mineral surfaces has been extensively studied, little work has been performed on the adsorption of asphaltenes on metal surfaces. There remain some inconsistencies in findings reported in the literature and several unanswered questions regarding these topics.

In this study, the adsorption of asphaltenes on different solid surfaces from toluene and heptane/toluene (1:1 volume mixture) solutions was investigated. UV-Vis spectrophotometry was used to study the adsorption of asphaltenes on particles with different surface areas, chemical compositions and morphology ( $\text{SiO}_2$ ,  $\text{Al}_2\text{O}_3$ , kaolinite, and stainless steel). Adsorption of asphaltenes on solid particles was found to be highly sensitive to the aromaticity of organic solvents and the type of particles. In toluene, the equilibrium adsorption data were fitted better by the Langmuir isotherm model. In heptol, asphaltene adsorption on particles studied showed a continuous increase with asphaltene concentrations and exhibited Freundlich type adsorption isotherms.

To investigate the adsorption kinetics of asphaltenes and the structural properties of the adsorbed layer(s) onto different surfaces ( $\text{SiO}_2$ ,  $\text{Al}_2\text{O}_3$ ,  $\text{Fe}_3\text{O}_4$ , and stainless steel) coated on quartz crystals surfaces, a sensitive technique of Quartz Crystal Microbalance with Dissipation (QCM-D) was used. The adsorption process was identified as being rapid and able to form rigid film(s). It was found that the amount of asphaltenes desorbed represents less than 10 % of the mass of asphaltenes adsorbed. The adsorption capacity of asphaltenes on the surfaces investigated was also found to

be strongly dependent on the quality of the solvent and type of solid surfaces. Carboxylic, pyrrolic, and thiophenic functional groups were identified to play a critical role in the interactions between asphaltenes and the solid surfaces investigated.

# Acknowledgements

This work would not have been possible without the generous financial support provided by the Natural Sciences and Engineering Research Council of Canada (NSERC) under the Industrial Research Chair Program in Oil Sands Engineering.

First, I would like to express my sincere gratitude to my supervisor Dr. Zhenghe Xu for his support, patience, and guidance throughout this project. I am grateful for his encouragement to explore my scientific curiosity and for sharing his wide knowledge in the oil sands research field.

My very special thanks goes to Dr. Lan Liu, for her insightful comments, motivation, and for sharing her ideas and expertise with me. I am also grateful for her patience in revising, correcting and proofreading this thesis.

Thank you to Mr. Jim Skwarok, and Ms. Jie Ru for your technical assistance and help in different phases of this work. I would also like to thank Ms. Lisa Carreiro, Mr. Kevin Heidebrecht, and Ms. Lily Laser who provided administrative support to me for the duration of pursuing this degree.

I want to express my special gratitude to the Alberta Center for Surface Engineering and Science (ACSES) for providing surface analysis of my samples, and in particular would like to thank Dr. Anqiang He and Dr. Shihong Xu for their help with CasaXPS software. I would also like to thank the National Institute of Nanotechnology (NINT), the Clean Coal Lab along with Dr. Deepak Pudasainee for their collaboration in surface area measurements.

Additionally, I would like to thank all the members of our oil sands group for their kind help and friendship.

I would also like to thank my father for encouraging me to follow my dreams. I thank my beloved mother for her endless love, continuous motivation and encouraging words during my studies. To Luis Morales, I am so thankful for your patience, companionship, caring support and immense love, bringing a smile to my face.

## Table of Contents

<b>Chapter 1 Introduction</b> .....	<b>1</b>
1.1 Introduction .....	1
1.2 Objectives and Thesis Outline.....	5
<b>Chapter 2 Literature Review</b> .....	<b>6</b>
2.1 Bitumen .....	6
2.2 Asphaltene.....	7
2.2.1 Asphaltene Chemical Composition .....	7
2.2.2 Asphaltene Molecular Structure .....	7
2.2.3 Solubility Characteristics and Precipitation of Asphaltenes .....	8
2.2.4 Asphaltene-Crude Oil System .....	9
2.2.5 Interfacial Properties of Asphaltenes.....	10
2.2.5.1 Adsorption of Asphaltenes on Liquid-Liquid Interface.....	10
2.2.5.2 Adsorption of Asphaltenes on Mineral Surfaces .....	11
2.2.5.3 Adsorption of Asphaltenes on Metal Surfaces .....	12
<b>Chapter 3 Adsorption of Asphaltenes on Silica, Alumina, Kaolinite and Stainless Steel Particles using UV-Vis Spectrophotometry</b> .....	<b>14</b>
3.1 Introduction .....	14
3.2 Experimental .....	15
3.2.1 Materials.....	15
3.2.1.1 Chemicals.....	15
3.2.1.2 Asphaltenes Precipitation .....	15
3.2.1.3 Particles.....	16
3.2.2 Experimental Procedures.....	16
3.2.2.1 SEM Imaging.....	16
3.2.2.2 Surface Area .....	17
3.2.2.3 FTIR-DRIFT Spectroscopy .....	17
3.2.2.4 UV-Vis Spectrophotometric Measurements .....	17
3.2.2.5 Asphaltene Solubility in Toluene and Heptol (1:1 volume ratio).....	20
3.2.2.6 Adsorption Experiments .....	23
3.2.2.7 Thermo-Gravimetric Analysis .....	24
3.3 Results .....	24

3.3.1 Optimization of Adsorption Experimental Conditions.....	24
3.3.1.1 Kinetics of Asphaltene Adsorption on Different Particles .....	24
3.3.1.2 Effect of Particles to Liquid Ratio (S/L).....	26
3.3.2 Effect of Types of Particles .....	27
3.3.3 Effect of Solvents Properties .....	35
3.3.4 Thermally Treated Particles .....	37
3.3.5 Thermo-Gravimetric Analysis of Asphaltenes Adsorbed on Solid Particles .....	39
3.4 Conclusions .....	45
<b>Chapter 4 Adsorption of Asphaltenes on Silica, Alumina, Stainless Steel and Iron Oxide</b>	
<b>QCM-D Sensors .....</b>	<b>47</b>
4.1 Introduction .....	47
4.2 Experimental .....	49
4.2.1 Quartz Crystal Microbalance with Dissipation (QCM-D) .....	49
4.2.1.1 Principle .....	49
4.2.1.2 Instrumentation and QCM-D Crystals .....	51
4.2.2 Asphaltene Solutions .....	51
4.2.3 Asphaltene Adsorption Experiments .....	52
4.2.4 Wettability of Quartz Crystals-Contact Angle .....	53
4.2.5 X-ray Photoelectron Spectroscopy (XPS) .....	54
4.3 Results .....	54
4.3.1 Adsorption of Asphaltenes on Solid Surfaces using QCM-D Technique .....	54
4.3.1.1 Effect of Type of Surfaces .....	54
4.3.1.2 Effect of Solvents Properties .....	58
4.3.2 XPS Spectral Analysis.....	63
4.3.2.1 Survey Spectra .....	63
4.3.2.2 High Resolution Spectra .....	66
4.3.2.2.1 Carbon Spectra .....	66
4.3.2.2.2 Oxygen Spectra .....	67
4.3.2.2.3 Nitrogen Spectra.....	69
4.3.2.2.4 Sulfur Spectra.....	70
4.3.2.3 Summary and Further Discussion .....	71
4.4 Conclusions .....	72
<b>Chapter 5 General Conclusions and Future Work.....</b>	<b>74</b>

5.1 General Conclusions .....	74
5.2 Future Work .....	75
<b>References .....</b>	<b>77</b>

## List of Tables

Table 2.1. Elemental composition (wt. %) of typical Alberta oil sands asphaltenes.....	7
Table 3.1. Chemicals used in the experiments .....	15
Table 3.2. Composition of stainless steel nanoparticles used in this study reported by SkySpring Nanomaterials, Inc.....	16
Table 3.3. Intercept and slope values from linear fitting of calibration curves .....	20
Table 3.4. BET data and mass of particles used in the adsorption experiments .....	24
Table 3.5. Model parameters of asphaltene adsorption on different particles from toluene solutions .....	29
Table 3.6. Freundlich model parameters for adsorption of asphaltene on different particles from heptol solutions .....	37
Table 3.7. Activation energy values at various asphaltene decomposition weight loss .....	45
Table 4.1 Sensors specifications (Provided by manufacturer) .....	51
Table 4.2. Mass of asphaltene adsorbed from asphaltene in toluene solutions onto quartz crystal surfaces coated with different materials .....	57
Table 4.3. Contact angle of bare and asphaltene covered quartz crystal surfaces .....	58
Table 4.4. Mass of asphaltene adsorbed from asphaltene in heptol (1:1 volume ratio) solutions onto quartz crystal surfaces coated with different materials .....	60
Table 4.5. Atomic composition of bulk asphaltene, bare and asphaltene covered quartz crystal surfaces .....	65
Table 4.6. Atomic ratio of bulk asphaltene, bare and asphaltene covered quartz crystal surfaces .....	66

## List of Figures

Figure 3.1. UV-Vis absorbance spectra of asphaltene in toluene standard solutions .....	19
Figure 3.2. Calibration curve for asphaltene in toluene standard solutions .....	19
Figure 3.3. Asphaltene solubility in (a) Toluene; and (b) Heptol 1:1 volume ratio .....	22
Figure 3.4. Microscopic images of asphaltene solutions in (a) Toluene; and (b) Heptol (1:1 volume ratio) .....	22
Figure 3.5. Effect of mixing time and initial concentration on the adsorption of asphaltenes on untreated silica .....	25
Figure 3.6. Effect of particles to liquid (S/L) ratio on asphaltene concentration after the adsorption .....	26
Figure 3.7. Effect of particles to liquid (S/L) ratio on the amount of asphaltenes adsorbed on untreated silica and stainless steel .....	27
Figure 3.8. Adsorption isotherms of asphaltenes from toluene solutions (Solid lines are the best fit to Langmuir isotherms, dashed lines are the best fit to Freundlich isotherms) .....	29
Figure 3.9. Variation of $\Gamma_{\max}$ and K for solid particles of different surface properties .....	30
Figure 3.10. SEM micrographs of bare particles .....	32
Figure 3.11. DRIFT spectra of (a) nC <sub>5</sub> -iC <sub>5</sub> asphaltenes; (b) Bare and asphaltene covered untreated SiO <sub>2</sub> ; (c) Bare and asphaltene covered Untreated Al <sub>2</sub> O <sub>3</sub> ; and (d) Bare and asphaltene covered kaolinite .....	34
Figure 3.12. 3100-2700 cm <sup>-1</sup> DRIFT spectra regions obtained after subtracting the spectra of bare particles from that of asphaltene covered particles .....	35
Figure 3.13. Isotherms of asphaltene adsorption from solutions of toluene and heptol for: (a) Untreated SiO <sub>2</sub> ; (b) Untreated Al <sub>2</sub> O <sub>3</sub> ; and (c) Stainless steel .....	36
Figure 3.14. Asphaltene adsorption isotherms on (a) Untreated and thermally treated SiO <sub>2</sub> ; and (b) Untreated and thermally treated Al <sub>2</sub> O <sub>3</sub> .....	39
Figure 3.15. DRIFT spectra of (a) Untreated and thermally treated SiO <sub>2</sub> ; and (b) Untreated and thermally treated Al <sub>2</sub> O <sub>3</sub> .....	39

Figure 3.16. TGA curves obtained at 10 °C/min (a) Untreated SiO <sub>2</sub> case; and (b) Untreated Al <sub>2</sub> O <sub>3</sub> case .....	41
Figure 3.17. Normalized TGA curves of bulk asphaltenes at different heating rates .....	42
Figure 3.18. Log(heating rate) as function of the reciprocal of the temperature for constant weight loss: (a) Asphaltenes; (b) Asphaltenes adsorbed on untreated SiO <sub>2</sub> from toluene solutions; and (c) Asphaltenes adsorbed on untreated SiO <sub>2</sub> from heptol solutions .....	44
Figure 4.1. Frequency and dissipation change as a function of time for the adsorption of asphaltenes from asphaltene in toluene solutions on quartz crystal surfaces coated with: (a) Silicon dioxide; (b) Aluminum oxide; (c) Iron oxide; and (d) Stainless steel .....	56
Figure 4.2. Asphaltene adsorption kinetics onto quartz crystal surfaces coated with different materials from asphaltene in toluene solutions .....	58
Figure 4.3. Frequency and dissipation change as a function of time for the adsorption of asphaltenes from asphaltene in heptol (1:1 volume ratio) solutions on quartz crystal surfaces coated with: (a) Silicon dioxide; (b) Aluminum oxide; (c) Iron oxide, and (d) Stainless steel .....	60
Figure 4.4. Variation of the amount of asphaltenes adsorbed from 0.1 mg/mL asphaltene solutions in toluene and heptol (1:1 volume ratio) on quartz crystal surfaces coated with different materials .....	61
Figure 4.5 Asphaltene adsorption kinetics from heptol (1:1 volume ratio) solutions onto quartz crystal surfaces coated with different materials .....	62
Figure 4.6. XPS survey spectra of bulk asphaltenes and quartz crystal sensors before and after being exposed to asphaltene solutions in toluene or heptol: (a) SiO <sub>2</sub> ; (b) Al <sub>2</sub> O <sub>3</sub> ; (c) Stainless steel; and (d) Fe <sub>3</sub> O <sub>4</sub> .....	64
Figure 4.7. High resolution C1s XPS spectra of bulk asphaltenes, bare and asphaltene covered quartz crystal surfaces. (a) Silicon dioxide; (b) Aluminum oxide; (c) Stainless steel; and (d) Iron oxide .....	67
Figure 4.8. High resolution O1s XPS spectra of bulk asphaltenes, bare and asphaltene covered quartz crystal surfaces. (a) Silicon dioxide; (b) Aluminum oxide; (c) Stainless steel; and (d) Iron oxide .....	68

Figure 4.9. High resolution N1s XPS spectra of bulk asphaltenes, bare and asphaltene covered quartz crystal surfaces. (a) Silicon dioxide; (b) Aluminum oxide; (c) Stainless steel; and (d) Iron oxide ..... 69

Figure 4.10. High resolution S2p XPS spectra of bulk asphaltenes and asphaltene covered quartz crystal surfaces. (a) Silicon dioxide; (b) Aluminum oxide; (c) Stainless steel; and (d) Iron oxide ... .....70

# Chapter 1 Introduction

## 1.1 Introduction

Oil sands are naturally occurring sedimentary rocks that contain crude bitumen with high molar mass and high viscosity, unrecoverable in its natural state by conventional petroleum recovery methods. Canada's crude bitumen resource covers an area of 145000 km<sup>2</sup>, **(1)** which is mainly located in the northeastern part of the province of Alberta and is grouped into three geographic regions: Athabasca, Cold Lake and Peace River **(2)**. Alberta's oil sands represent the third largest proven crude oil reserve in the world, with established reserves of in situ and mineable crude oil around 167.2 billion barrels, **(3)** next to Saudi Arabia (265.8 billion barrels) and Venezuela (298.4 billion barrels). **(4)** In 2013 the average world oil demand increased by 1.4 percent from 2012, **(3)** and is expected to continue to rise. In this regard, Alberta's oil sands play an important and growing role in the global economy as a reliable source of crude oil.

There are two main methods used for the bitumen extraction from oil sands: in situ and open-pit mining. For deep deposits, where it is not economical to recover the bitumen by mining operations, in situ technology is used, which accounted for 53 percent of total bitumen production in Alberta in 2013. **(3)** Steam-assisted gravity drainage (SAGD) is currently used in commercial in situ operations, whereby the reservoir is heated using steam to induce the flow of bitumen under gravity through production wells. **(2)**

On the other hand, mining operations are used in relatively shallow oil sands formations (ores covered by less than 75 m of overburden), **(2)** and involves the application of the Clark Hot Water Extraction process (CHWE). In CHWE, the mined oil sand lumps are crushed and mixed with water and chemical additives, and sent through hydrotransport pipelines where lump size reduction, bitumen liberation from sand grains, bitumen-bitumen coalescence, and bitumen aeration take place. In current operations, the typical temperature used for the slurry is between 40-55 °C. The liberated and aerated bitumen aggregates are separated from the water-solids slurry using large gravity separation vessels, commonly referred to as primary separation vessels (PSV). The bitumen recovered in the form of froth, normally consisting of 60 wt. % bitumen, 30 wt. % water and 10 wt. % solids is then deaerated and diluted with solvents to facilitate solids and water removal by reducing the bitumen viscosity and providing sufficient density difference between

water and bitumen. There are two main methods for bitumen froth treatment, naphtha froth treatment and paraffinic froth treatment. When naphtha is used as solvent, asphaltenes do not precipitate, obtaining a diluted bitumen product that contains 1.5 wt. % to 2.5 wt. % water and 0.4 wt. % to 0.8 wt. % solids; however if a paraffinic solvent is added to the bitumen froth, asphaltenes precipitation occurs, leading to the formation of aggregates that trap water and solids, resulting in a diluted bitumen product with very small amounts of mineral solids and emulsified water (100 ppmw to 300 ppmw water and 500 ppmw to 800 ppmw solids). **(2, 5)** The by-product of the mining bitumen extraction process is composed of water, sand, fines, unrecovered solvent and residual bitumen. This tailings stream is discharged into a pond where coarse sands settle to the bottom rapidly. The fines (small clay particles under 44 microns in size) remain suspended within the water, forming the fluid fine tailings. Over time, excess water releases out of the fluid fine tailings and the solids sink down into the mature fine tailings layer. Untreated mature fine tailings with a very slow consolidation rate, raise a big concern since they can remain in a fluid-like state for decades. **(6-8)** Clear water rising to the top of the tailings pond is reused in the extraction process, allowing companies to recycle up to 90 % of process water, therefore using less fresh water from the Athabasca River.

Asphaltene are generally defined as the fraction of crude oil that is insoluble in short straight chain alkanes, such as pentane or heptane, but soluble in aromatic solvents, such as toluene. **(2, 9)** Changes in pressure, temperature, composition and shear rate may cause asphaltene precipitation and deposition. **(10, 11)** These changes may be induced by several current and potential applications in heavy oil and bitumen production and processing, including vapor extraction (VAPEX) method of heavy oil recovery, paraffinic oil sands froth treatment, and heavy oil dilution for transport by pipeline, all of which involve dilution of the oil to reduce its density and viscosity. Asphaltene adsorption in liquid-liquid and solid-liquid interfaces as well as their deposition on facilities' surfaces have adverse effects on the entire oil production chain. For example, at the well asphaltene adsorption on the formation rocks can reduce the oil recovery through changes in reservoir wettability and plugging of rock pores. **(10, 12, 13)** In addition, asphaltene adsorption on clay particles and at water-oil interfaces plays a critical role in the formation and stability of water-in-oil emulsions, **(14-16)** and can also stabilize solid particle suspensions, which complicates the oil separation process and removal of organic-contaminated solids.

Asphaltenes can also cause downstream issues, such as clogging of pipelines, surface facilities, pumps, safety valves, and fouling on refining and upgrading equipment, which hinders oil production and causes economic loss. **(10)** In the hot water oil sands extraction process, asphaltenes can be released into environment via tailings by adsorption on solid surfaces such as clays and silica. Furthermore, oil spills can cause asphaltene adsorption onto soil particles, which are difficult to recover, and would result in serious damage to the environment. Therefore, a better understanding of the mechanism of asphaltene adsorption and deposition on different surfaces and interfaces is of fundamental importance to prevent and mitigate the problems associated to this phenomena.

Asphaltene adsorption onto diverse surfaces has potential implications in heavy oil recovery and upgrading. By introducing substrates/sorbents with modified surfaces, asphaltenes could be selectively removed from petroleum streams, thus making the remaining fraction of oil more homogeneous, easier to upgrade and transport. **(17, 18)** Understanding sorbent-asphaltene interactions will help to find suitable sorbents, and design more efficient processes at industrial scale.

Several techniques have been used to study the adsorption of asphaltenes onto solid surfaces, including UV-Vis spectrophotometry and Quartz Crystal Microbalance (QCM). The adsorption of asphaltenes on mineral surfaces has been widely studied to determine the wettability changes of minerals, asphaltene adsorption isotherms, and the amount of asphaltenes adsorbed. Dean et al. **(19)** studied the adsorption of asphaltenes on two different clay minerals and concluded that the adsorption depends on the properties of the clay. In another study Dudasova et al. **(20)** investigated the adsorption of asphaltenes extracted from five different crude oils onto different inorganic mineral surfaces. They concluded that the adsorption of asphaltenes depends more on the particle type than on the origin of asphaltenes and that the amount of asphaltenes adsorbed increases with increasing the heteroatomic content in asphaltenes. In contrast, several authors reported asphaltene adsorption to be dependent on the source of asphaltenes. **(21, 22)**

Characterizing the adsorption of asphaltenes on different solid surfaces has been the subject of numerous studies, generally involving determination of adsorption isotherms. Several authors reported Langmuir type isotherms, indicating saturation adsorption of asphaltenes on the solid

surfaces investigated, (20-24) whereas others have shown a stepwise or continuous increase in adsorption and suggested a multilayer adsorption process of asphaltenes. (25-27)

Few studies have been conducted on the adsorption of asphaltenes on metal surfaces. (22, 28) Alboudwarej et al. (22) studied the adsorption of asphaltenes on stainless steel, iron and aluminum powders using the UV-Vis spectrophotometry. They observed Langmuir type of isotherms. Other researchers investigated the adsorption of asphaltenes on gold surfaces using Quartz Crystal Microbalance (QCM). (24, 25, 29) Both Langmuir type isotherms and continuous increase of adsorption with increasing asphaltene concentrations were observed.

Only a few investigators have characterized the chemical nature of adsorbed asphaltenes on different surfaces using X-ray photoelectron spectroscopy (XPS). According to reported XPS data, different functional groups are suggested to be present in the adsorbed asphaltene layer, including carboxylic, thiophenic, sulfide, sulfite, pyridinic and pyrrolic. (24, 28)

The kinetics of asphaltene adsorption has also been studied by Xie and Karan. (29) They investigated the kinetics of asphaltene adsorption on gold surface using Quartz Crystal Microbalance in a flow-cell system and found that the initial adsorption process is controlled by the diffusion of asphaltenes molecules from the bulk solution to the adsorption surface, as observed by Natarajan et al. (30) who studied the adsorption of asphaltenes on mica surfaces from toluene solutions using a surface forces apparatus (SFA).

From the literature, it is evident that asphaltene adsorption onto solid surfaces is a complex phenomenon that is sensitive to many variables. There remains no explanation for some inconsistencies found in literature, and molecular mechanisms of asphaltene adsorption on mineral and metallic surfaces from organic solvents remain unresolved. Furthermore, little is known about the kinetics of the asphaltene adsorption on metal surfaces other than on gold. Hence it is highly necessary to further investigate the adsorption of asphaltenes on inorganic and metallic surfaces in different solvents, in order to better understand the adsorption process and elucidate the source of interactions between asphaltenes and different solid surfaces.

## 1.2 Objectives and Thesis Outline

The main objective of this research is to study the adsorption of asphaltenes from organic solvents onto mineral and metallic surfaces. Two different techniques are used to investigate this phenomenon, Quartz Crystal Microbalance with Dissipation monitoring (QCM-D), which provides real time monitoring of interactions taking place between asphaltenes and solid surfaces, and UV-Vis spectrophotometry to quantify the amount of asphaltenes adsorbed onto different solid particles. Asphaltenes of different concentrations in toluene and heptane/toluene (1:1 volume mixture) solutions are used to investigate the adsorption of asphaltenes onto different solid surfaces. The current study highlights the influence of surface chemistry, morphology, and hydrophilicity of solids on asphaltene-solid interactions in the aforementioned systems. Furthermore, to gain insight into the chemical groups involved in the adsorption process, bulk asphaltenes and adsorbed asphaltenes are characterized through XPS analysis.

The following description outlines each chapter in this thesis:

**Chapter 1** is a general introduction on the problem and thesis objectives, along with the outline of the thesis.

**Chapter 2** contains a literature review on several topics covered in this study, including asphaltene chemical composition, molecular structure, and solubility characteristics. In addition, a particular focus is to review the literature to date on investigating the adsorption of asphaltenes on liquid-liquid interfaces, mineral surfaces, and metal substrates.

**Chapter 3** investigates the adsorption of  $nC_5$ - $iC_5$  asphaltenes onto different solid particles through UV-Vis spectrophotometry. The experimental protocol and the theory relevant to the methods employed in this study are presented along with the analysis and discussion of experimental results.

**Chapter 4** examines the adsorption kinetics of  $nC_5$ - $iC_5$  asphaltenes onto different materials using Quartz Crystal Microbalance with Dissipation (QCM-D). The theory, instrumentation and protocols used throughout the study are presented. In addition experimental results are discussed

**Chapter 5** contains general conclusions and recommendations for future work.

# Chapter 2 Literature Review

## 2.1 Bitumen

Bitumen, considered the heaviest form of petroleum, is a naturally occurring material immobile under reservoir conditions. With densities  $\geq 1000 \text{ Kg.m}^{-3}$  (API gravities  $\leq 10$ ) and viscosities  $\geq 10000 \text{ mPa.s}$ , bitumen is unrecoverable in its natural state by conventional oil well production methods. **(2, 31, 32)**

In general, bitumen is mainly composed of hydrocarbons with carbon and hydrogen content to the extent of 90-93 wt. %, and heteroatoms (nitrogen, oxygen and sulfur) in a combined amount of up to about 9.9 wt. %. The rest is made of metals, in the form of organometallic compounds (which contain metal-carbon bonds incorporated into the hydrocarbon molecules) such as vanadium and nickel porphyrins, carboxylic salts, oxides, carbonates, sulfides, silicates, clay particles, clay organics and heavy metals. **(32)** The hydrogen to carbon atomic ratio is an important parameter of the hydrocarbon fuel (the higher the ratio, the more valuable the crude). This ratio can be as high as 2.0 to 2.4 in very light crude oil and around 1.51 for Alberta bitumen. **(2, 32)**

SARA analysis is frequently used to characterize crude oils. This test method separates bitumen into four well defined fractions; saturates, aromatics, resins, and asphaltenes. The saturate fraction contains non-polar linear, branched, and cyclic hydrocarbons, the aromatic cut consists of molecules with one or more aromatic rings, whereas resins and asphaltenes contain aromatic rings and various polar groups. The SARA assay starts with the precipitation of asphaltenes in paraffinic solvents such as n-pentane or n-heptane at a solvent to bitumen ratio of 40:1 (vol/vol). The supernatant obtained is referred to as maltenes or de-asphalted oil, which is further separated into saturates, aromatics and resins by chromatographic methods. SARA analysis is completed by determining the weight of isolated fractions, after solvent removal from each eluted fractions. SARA composition of Alberta oil sand bitumen varies within the following ranges by weight: saturates 15-21 %, aromatics 18-19 %, resins 44-48 %, and asphaltenes 14-20 %. **(2, 33, 34)**

## 2.2 Asphaltene

### 2.2.1 Asphaltene Chemical Composition

Asphaltenes are generally defined as a solubility class that is insoluble in aliphatic alkanes, such as pentane or heptane, but soluble in aromatic solvents, such as toluene. (2, 9) Asphaltenes consist primarily of carbon, hydrogen, nitrogen, oxygen, and sulphur, with typical asphaltene elemental composition by weight being given in Table 2.1. They also contain a trace amount of vanadium, nickel and iron. The carbon and hydrogen content in asphaltene usually shows little variation (hydrogen-to-carbon atomic ratio of  $1.15 \pm 0.5$  %), while the amount of oxygen and sulfur is more variable. (31, 32)

**Table 2.1.** Elemental composition (wt. %) of typical Alberta oil sands asphaltene (32)

C	H	N	O	S
80.5± 3.5	8.1± 0.4	1.1± 0.3	2.5± 1.2	7.9± 1.1

### 2.2.2 Asphaltene Molecular Structure

Asphaltenes consist of a broad polydisperse range of organic compounds with diverse molecular weights and chemical structures, which makes it impossible to differentiate and characterize the size and the structure of each individual asphaltene molecule. Therefore, various techniques have been involved to study the average physicochemical properties of asphaltene. Taking the molecular weight of asphaltene for example, the reported molecular weight of asphaltene span a wide range, depending on the methods used to determine the molecular weight. Data obtained using vapour pressure osmometry (VPO) and gel permeation chromatography (GPC) can vary between 3000 Da to 10000 Da. It has been suggested that the very high molecular weight measured is probably due to the self-association of asphaltene. Currently, the accepted average molecular weight of asphaltene measured by mass spectrometry (2, 31) and molecular diffusion (35, 36) is about 750 g/mol, with the mass range from 300 to 1400 g/mol.

There is a long-standing debate on molecular structure of asphaltene. Two main models have been proposed to represent the average structure of asphaltene, known as archipelago and island models. The archipelago model proposes a flexible asphaltene molecular structure (molecular weight of about 2000 Da or more) composed of several small aromatic rings linked together by

aliphatic chains, or naphthenic moieties. (2, 37) In contrast, the island model states a smaller asphaltene molecule (molar mass in the range of 500-1000 Da) that has a single polyaromatic core, typically consisting of about seven fused aromatic rings, surrounded by several alkyl and naphthenic chains. (2, 38) Recently, Schuler and colleagues identified the “island” structures of more than one hundred asphaltene molecules from coal and petroleum by combining atomic force microscopy with scanning tunneling microscopy. (39)

### 2.2.3 Solubility Characteristics and Precipitation of Asphaltenes

The quantities and properties of the precipitated asphaltenes from bitumen depend on several factors including temperature, solvent type and solvent-to-bitumen (S/B) ratio. The solubility of asphaltenes in hydrocarbon solvents has been investigated and compared in previous studies. (38, 40, 41) Alboudwarej et al. (40) reported that the asphaltene yield increases as the carbon number in the n-alkane precipitant decreases. They also found that n-pentane precipitates more asphaltenes than n-heptane at the same S/B, and that for the same solvent, a higher S/B ratio leads to more asphaltene precipitation.

When a good solvent such as toluene is added to bitumen, asphaltene molecules completely dissolve or disperse in the solvent. In contrast, when a poor solvent, such as n-pentane or n-heptane is added, above the critical S/B ratio, asphaltenes precipitation takes place. Long et al. (38) stated that the threshold S/B value for the onset of asphaltene precipitation is around 1.0 (wt./wt.) for n-pentane, 1.35 (wt./wt.) for n-hexane, and 1.6 (wt./wt.) for n-heptane at 25 °C. Furthermore, if a mixture of n-heptane and toluene is used for asphaltenes precipitation, a critical volume fraction of n-heptane in the solvent mixture would be required for the initial formation of asphaltene precipitates. Alboudwarej et al. (40) found that the onset of precipitation of asphaltenes is about 0.35 n-heptane volume fraction in a mixture of n-heptane and toluene.

Andersen et al. (42) studied the precipitation of asphaltenes in mixtures of heptane and toluene from undiluted crude oil and from the heptane insoluble portion of the crude. They found that asphaltenes were more soluble in crude oil than in heptane–toluene blends that mimicked the crude composition.

The effect of temperature on the amount of asphaltenes precipitated from bitumen is an important thermodynamic property, essential to understanding phase separation of asphaltenes during refining and recovery operations. When n-C<sub>5-8</sub> solvents are used as the precipitants, previous

studies indicate that at a given solvent-to-bitumen ratio, the amount of asphaltene precipitates decreases as the temperature raises. (2, 43, 44)

#### **2.2.4 Asphaltene-Crude Oil System**

One important feature of asphaltenes is their propensity to self-associate and form nanoaggregates, even in the good solvents, such as toluene, and at very low concentrations. (45, 46) Wide research interests on asphaltenes focus on understanding the mechanism of asphaltene self-assembly in crude oil. In early studies, asphaltenes were proposed to form colloidal size aggregates in crude oil, which were considered to be similar in nature to the micelles formed by surfactants in aqueous solutions. This approach, known as the colloidal model, suggests that asphaltenes self-associate into the core of aggregates and resins adsorb onto the core via polar-polar interactions to form a steric shell, keeping the aggregates suspended in oil phase. (47-49) Later examination on the concept of resins peptizing asphaltene aggregates raised doubts about its validity. Compared with surfactants in aqueous systems, asphaltenes dissolved in an organic solvent represent a different system due to the lack of amphiphilic properties in the asphaltene molecules. (2, 32) Hence it is unlikely that asphaltene aggregates can actually resemble characteristic structures and shapes of well-defined micelles formed by amphiphilic surfactants. Moreover, several studies published in the literature suggest a different conception for asphaltene aggregation. Cimino et al. (9) reported that asphaltenes dissolved in toluene can form colloidal-size aggregates in the absence of resins. The resins were thought to be essential to suspend asphaltenes aggregates according to the colloidal model. In another study, it was found that resins do not desorb pre-adsorbed asphaltenes from the solid surface, neither do they associate onto the asphaltene adsorbed on the surface. This result contradicts the theory of stabilization effect of resins on asphaltenes. (25) Thus, resins are unlikely to coat on asphaltene nanoaggregates and do not provide the steric stabilizing layer that the colloidal model proposed.

Asphaltenes have also been considered to exist in a homogeneous liquid state as a physically solvated solute (asphaltene) in the solvent (oil). (50, 51) The solubility of asphaltenes in crude oil depends on a delicate balance between asphaltene fraction and the fractions of lighter components in the crude oil. Any unfavorable disturbance, such as the change in temperature, pressure, shear rate and solution composition, can induce precipitation of asphaltenes.

As evident from the foregoing discussion, the state of asphaltenes in crude oil is a complex topic, and there is still no conclusive understanding on the mechanism of asphaltene aggregation.

### **2.2.5 Interfacial Properties of Asphaltenes**

In petroleum industry, asphaltenes are well-known for causing multiple problems associated to their adsorption at liquid-liquid and solid-liquid interfaces in the extraction, upgrading and transportation operations during crude oil productions. Asphaltenes can change reservoir wettability, stabilize water-in-oil emulsions, plug wells and flowlines, and deactivate catalysts. These problems have motivated research studies focused on the adsorption of asphaltenes at liquid-liquid interfaces and onto different solid surfaces. The following discussion will highlight the major findings of these studies.

#### **2.2.5.1 Adsorption of Asphaltenes on Liquid-Liquid Interface**

The formation of stable water-in-crude oil emulsions is an ubiquitous phenomenon that contributes to several issues encountered in the petroleum industry. These emulsions normally cause environmental damage, corrosion to the downstream pipelines and plant equipment, creating operational and safety issues and additional operation costs. Resins, naphthenic acids, fine solids and more importantly asphaltenes are generally accepted to be components in crude oil that stabilize water-in-crude oil emulsion. A number of studies have focused on the adsorption of asphaltenes at liquid-liquid interfaces to understand the role of asphaltenes in stabilizing water-in-oil emulsions. These studies concluded that the irreversible adsorption of asphaltenes at the oil-water interface results in the formation of a rigid “skin like” layer that resists the deformation of the interface and acts as a barrier for the coalescence of water droplets, hindering removal of emulsified water droplets from the crude oil. **(52-55)** Some researchers claimed that the interfacial rigidity is due to the cross-linking of asphaltene aggregates. **(56, 57)**

Recently, several investigators studied the emulsification and interfacial properties of different asphaltene subfractions. In these studies asphaltenes were separated based on their solubility and polarity by precipitating different fractions of asphaltenes using solvents of different aromaticity and/or by increasing dilution ratios. Using such an approach, Spiecker et al. **(58)** proposed that the less soluble asphaltene fraction represents the major species responsible for asphaltene aggregation and emulsion stability. Czarnecki et al. **(59)** developed a model where water-in-oil petroleum emulsions are stabilized through the adsorption of two different chemical components, a

subfraction of asphaltenes and a surfactant-like material. Later in another study, (60) they used mass spectrometry to characterize the materials that emulsified water droplets and found that the composition of this material was different from that of asphaltenes, resins, and the parent oil. In both studies Czarnecki and co-workers suggested that the conventional belief that water-in-oil emulsions are almost exclusively stabilized by whole asphaltenes is an oversimplification. Furthermore, other researchers found that only a small fraction of asphaltenes is the real contributor to stabilizing water-in-oil emulsions. (61, 62) Recently, Yang et al. (63) developed a novel method for subfractionation of asphaltenes based on their interfacial activity. They found that the most interfacially active asphaltene subfraction represents less than 2 wt. % of whole asphaltenes and is the main contributor to emulsion stabilization and formation of rigid oil-water interfaces.

#### **2.2.5.2 Adsorption of Asphaltenes on Mineral Surfaces**

Asphaltene adsorption on the formation rock alters the wettability of rocks from water-wet to oil-wet (13) and reduces oil production from the reservoir.

The ability of asphaltenes to adsorb as monolayer (18, 20, 64) and multiple layers (23, 27, 65) on mineral surfaces has been reported in open literature. Acevedo et al. (21) studied the adsorption of asphaltenes obtained from three different crude oils onto silica particles by UV-Vis spectroscopy. They found that the shape of the adsorption isotherms of asphaltenes depends on the source of asphaltenes and suggested a possible correlation between these differences and the tendency for the asphaltenes to precipitate from the crude oil. Several other researchers (19, 23) examined the adsorption of asphaltenes on different clay minerals (kaolin, montmorillonite and illite) using UV-Vis spectroscopy. The results show that the adsorption capacity of asphaltenes depends on the properties of the clay. On the other hand, Dudasova et al. (20) reported that the adsorption of asphaltenes on minerals depends more on particle type than on the origin of the asphaltenes.

Asphaltene adsorption is also influenced by the aromaticity of the solvent used for the adsorption experiments. Studies have shown that increasing the solvent strength reduces the amount of asphaltenes adsorbed onto mineral surfaces due to the reduction in the size of asphaltene aggregates. (23, 66, 67)

A few studies showed the reverse trend of increased adsorption capacity with increasing solvent strength. The adsorption of vanadium-containing asphaltenes onto alumina was studied by Saint

and coworkers. (68) They found that the adsorption of asphaltenes was higher in toluene than in cyclohexane while very little adsorption occurred in pyridine. Another study, where Quartz Crystal Microbalance with Dissipation (QCM-D) was used to quantify the adsorption of asphaltenes extracted from different crude oils onto hydrophilic silica, alumina, titanium and FeO<sub>x</sub>, showed that depending on the source of asphaltenes alumina exhibited a higher asphaltene adsorption capacity in toluene solutions than in 1:1 heptol solutions. (69)

The presence of water can also affect the adsorption of asphaltenes on mineral surfaces. Exposure of solid surfaces subjected to the moisture prior to adsorption led to a reduction in the capacity of asphaltene adsorption. (19, 70) It is suggested that as the hydrophilicity of the mineral surface increases, water strongly competes with asphaltenes for surface adsorption sites, lowering the amount of asphaltenes adsorbed. (18, 71)

The effect of temperature on asphaltene adsorption has also been studied by several researchers. It has been reported that asphaltene adsorption onto mineral surfaces decreases with increasing temperature (exothermic process) due to a reduction in the size of asphaltene aggregates and self-association. (18, 72) In contrast, Dean et al. (19) claimed that the temperature does not affect the adsorption of asphaltenes onto clay surfaces.

### **2.2.5.3 Adsorption of Asphaltenes on Metal Surfaces**

The adsorption of asphaltenes on metal surfaces of transportation equipment and other facilities in crude oil production can have detrimental effects throughout the entire production and processing chain, which increases maintenance cost and causes a large economic loss. However, few studies have investigated adsorption of asphaltenes on metal surfaces. Ekholm et al. (25) studied the adsorption of asphaltenes onto a gold surface using QCM-D. They reported that asphaltenes redissolved in heptane-toluene mixtures were adsorbed on the gold surface by forming a rigid layer over an asphaltene concentration range of 25–1000 ppm. In toluene, the adsorption isotherm did not level off for asphaltene concentrations between 50 and 10000 ppm, suggesting a multilayer adsorption. Alboudwarej et al. (22) investigated the adsorption of asphaltenes on powdered metals (stainless steel, iron, and aluminum) from toluene solutions by UV-Vis spectrophotometry. In all cases, Langmuir isotherms were reported. The adsorption capacity of asphaltenes on these metals followed the order that stainless steel (2.7 mg/m<sup>2</sup>) > iron (1.35 mg/m<sup>2</sup>) > aluminum (0.25 mg/m<sup>2</sup>). The adsorption capacity was increased with increasing the heptane to toluene ratio. Other

researchers also used the quartz crystal microbalance to investigate the adsorption kinetics of asphaltenes on gold surface. Xie and coworkers, (29) for example, found that in toluene-heptane solutions (asphaltene concentration over 10-200 ppm) the adsorption of asphaltenes was slow and did not achieve equilibrium even after 700 minute. While in another QCM-D study, (24) adsorption experiments were conducted in toluene solutions containing asphaltenes from 50 to 1500 ppm. In this study, the adsorption isotherm was reported to follow the Langmuir isotherm model. Interestingly, both QCM-D work reported that the initial adsorption process was controlled by the diffusion of asphaltenes from the bulk solution to the metal surface.

In a more recent study (73) a combination of near-infrared (NIR) spectroscopy, Raman microscopy, and atomic force microscopy (AFM) was used to analyze the adsorption behavior of asphaltenes from benzene solutions on an iron (Fe) surface. Langmuir type isotherms were observed with a maximum adsorption amount at 4.9 mg/m<sup>2</sup>.

# Chapter 3 Adsorption of Asphaltenes on Silica, Alumina, Kaolinite and Stainless Steel Particles using UV-Vis Spectrophotometry

## 3.1 Introduction

It is generally agreed that asphaltenes do not constitute a chemically identifiable class of compounds. Asphaltenes are generally defined as the fraction of crude oil which is soluble in light aromatic hydrocarbons such as toluene, benzene or pyridine but insoluble in low molecular weight paraffins such as n-pentane or n-heptane. (2, 9) They comprise the heaviest and most polar portion of crude oils. The structure, composition and stability of asphaltenes depend upon the origin of crude oil and method of extraction. In addition to carbon and hydrogen, heteroatoms, such as nitrogen, oxygen and sulfur, and trace metals such as vanadium, iron and nickel are also present in the structure of asphaltene molecules. (2, 31, 32, 38) Asphaltene molecules are suggested to either contain small polyaromatic cores linked together via aliphatic chains and naphthenic moieties (archipelago model) or contain a single polyaromatic core with aliphatic chains or naphthenic moieties (island model). (2)

Asphaltenes are considered surface active due to their ability of adsorption on solid/liquid and liquid/liquid interfaces. Their interfacial activity has been attributed to the presence of polar functional groups, which are able to create a surface charge at the interface. (27, 64) The adsorption of asphaltenes onto solid/liquid surfaces has been associated to several process challenges commonly found in the petroleum industry, as it can reduce oil recovery through changes in reservoir wettability, plugging of rock pores and deposition within wells. (10) Upon adsorption at water/oil interface, asphaltenes stabilize undesirable water-in-oil emulsions, hindering the coalescence and removal of emulsified water droplets from the produced oil. (15, 74-76) These problems have led to research activities on asphaltene adsorption onto various surfaces using several techniques such as quartz crystal microbalance (QCM) and UV-Vis spectroscopy. Most of these studies concluded that asphaltene adsorption isotherms follow the Langmuir behavior, which have been associated to the saturation of the surface sites available for adsorption. (18-21, 23, 64, 73, 77) However, other researchers have observed stepwise asphaltene adsorption

isotherms and related this phenomenon to asphaltene aggregation, micellization and multilayer formation. (21, 23, 27, 65) There is still no satisfying explanation for this complex adsorption behavior.

In the present study, an effort to elucidate a probable mechanism for asphaltene adsorption onto different solid particles has been made. For this purpose, particles with different surface area and surface chemistry were employed for asphaltene adsorption. UV–Vis spectrophotometry was used to quantify asphaltene concentration. A fundamental understanding of asphaltene-solids interactions will lead to a deeper insight on the asphaltene adsorption behavior which can greatly help the modern petroleum industry.

## 3.2 Experimental

### 3.2.1 Materials

#### 3.2.1.1 Chemicals

The reagents used in the adsorption experiments are listed in Table 3.1. All these materials were used with no further purification.

**Table 3.1.** Chemicals used in the experiments

Chemical	Manufacturer	Grade
Toluene	Fisher Scientific	Certified ACS ( $\geq 99.5\%$ )
Heptane	Fisher Scientific	Certified ( $>99\%$ )
Pentane	Fisher Scientific	Certified ( $\geq 98\%$ )
Isopentane	Fisher Scientific	Certified ( $\geq 95\%$ )

#### 3.2.1.2 Asphaltenes Precipitation

Asphaltenes were precipitated from coker feed bitumen provided by Syncrude Canada, Ltd. The asphaltene content of this crude oil is about 16 wt. %. Asphaltenes were extracted by adding solvent (60 % pentane and 40 % isopentane) at a mass ratio of bitumen:solvent 1:1.7. The diluted bitumen was shaken for 24 h at room temperature. Then, the supernatant (mainly maltenes) was removed and the wet cake was re-dispersed in fresh solvent (60 % pentane and 40 % isopentane)

at a mass ratio of cake:solvent 1:1.7 and shaken for 2 h prior to removing washing solvent. This step was repeated until the supernatant did not change its color between washings. The precipitates were re-dissolved in toluene at a toluene to precipitates mass ratio 20:1. The solution was centrifuged at 14000 rpm for 20 min to remove fine mineral solids. Asphaltenes were then dried in a vacuum oven at 60 °C for 24 h until no obvious mass loss was observed. **(78)** Elemental analysis of the asphaltenes by the Thermo Scientific Flash 2000 CHNSO-organic elemental analyzer, showed the following composition in wt. %: C 72.8, H 7.4, N 1.1, S 5.7 and O 12.9. The H/C atomic ratio of the asphaltenes was 1.2.

### 3.2.1.3 Particles

Spherical silica gel (SiO<sub>2</sub>) and aluminum oxide (Al<sub>2</sub>O<sub>3</sub>) were purchased from Sigma Aldrich. Single mineral kaolinite was purchased from Acros Organics. Stainless steel nanoparticles were purchased from SkySpring Nanomaterials, Inc. These particles were used without further purification. The composition of the stainless steel particles provided by the manufacturer is presented in Table 3.2.

**Table 3.2.** Composition of stainless steel nanoparticles used in this study reported by SkySpring Nanomaterials, Inc.

C	P	S	Si	Mn	Cr	Ni	Mo	Fe
	ppm		wt. %					
300	450	300	0.750	2.000	16.0-18.0	10.0-14.0	2.0-3.0	Balance

## 3.2.2 Experimental Procedures

### 3.2.2.1 SEM Imaging

Scanning Electron Microscopy (SEM) was used to characterize the particles used in the asphaltene adsorption experiments. The SEM imaging was conducted by the Oil Sands and Coal Interfacial Engineering Facility (OSCIEF) Energy Innovation. The scanning electron microscope used was a Quanta 250 equipped with an Everhart Thornley Detector. The accelerating voltage for the SEM imaging was set between 10 and 15 kV. The working distance was 9 to 12 mm. Prior to the SEM measurements, silica, alumina and kaolinite particles were coated with a thin layer of carbon to make the samples conductive for the purpose of high quality images and

avoiding artifacts due to build-up of charges while being scanned with the electron beam. Stainless steel particles were measured without any previous pre-treatment.

### **3.2.2.2 Surface Area**

The specific surface area of particles was determined for quantitative comparison of adsorption results, by physical adsorption of nitrogen gas utilizing the Quantachrome Autosorb iQ instrument of two stations. Before measurements, the samples were degassed at 250 °C for 4.7 h with the exception of stainless steel particles which were degassed at 80 °C for 6.2 h to remove surface moisture. The surface areas were determined based on the standard 7 multipoint Brunauer–Emmet–Teller (BET) procedure.

### **3.2.2.3 FTIR-DRIFT Spectroscopy**

Asphaltenes, bare particles and asphaltene covered particles were characterized using a Cary 670 FTIR spectrometer equipped with a mercury cadmium telluride (MCT) detector and a diffuse reflectance infrared fourier transform (DRIFT) accessory. Spectra were recorded by accumulating 128 scans at 4 cm<sup>-1</sup> resolution and a MCT detector speed of 25 kHz. The instrument and the accessory were purged with dry air for 5 min before the analysis. A 5 % wt./wt. mixture of the sample and spectroscopic grade KBr was prepared using an agate mortar and pestle. Background KBr spectra were obtained and subtracted from sample spectra. The reflectance spectra expressed as Kubelka-Munk unit versus wavenumber curves are similar to absorbance spectra and can be evaluated accordingly.

### **3.2.2.4 UV-Vis Spectrophotometric Measurements**

UV-Vis spectrophotometry was used to study the asphaltene adsorption on solids by measuring the asphaltene concentration in bulk solutions before and after adsorption. Asphaltene solutions with concentration higher than 0.1 mg/mL were prepared by dissolving a known mass of asphaltenes in toluene or heptol (1:1 volume mixture of n-heptane and toluene), followed by sonication for 30 min to ensure that asphaltenes were completely dissolved. Asphaltene solutions with concentrations in the range of 0.01-0.1 mg/mL were prepared by diluting the concentrated standard-solution with the same solvent. The diluted solutions were sonicated for another 30 min. Fresh solutions were prepared daily.

The absorbance of asphaltene solutions was measured using a Shimadzu UV-3600 spectrophotometer. Before each set of measurements, the spectrophotometer was zeroed with either toluene or heptol (1:1 volume ratio) as the corresponding blanks.

Shown in Figure 3.1 are the UV-Vis spectra obtained for nC<sub>5</sub>-iC<sub>5</sub> asphaltene solutions with concentration range from 0.02 to 0.1 mg/mL in toluene. Within wavelength from 300 to 800 nm, there is a shoulder peak at wavelength 405 nm. The absorbance of asphaltenes at this wavelength increases with asphaltene concentration in solution. Therefore, absorbance of asphaltenes at wavelength 405 nm was used to build calibration curve and determine the asphaltene concentration in solution.

It is important to mention that for asphaltene concentrations higher than 0.1 mg/mL, the absorbance values exceeded the output range of the instrument. Therefore, the calibration curve (Figure 3.2) was built based on the absorbance readings obtained from the UV-Vis spectra at 405 nm for standard solutions within 0.01 and 0.1 mg/mL. As presented in Figure 3.2, the calibration curve shows a linear correlation between the absorbance and asphaltene concentration in toluene solutions, following the Beer-Lambert Law. Similar linear relationship was obtained for asphaltene in heptol solutions. After a linear fitting, an expression (Equation 3.1) that correlates asphaltene concentration with absorbance is obtained:

$$A = b + m * [Asp] \qquad \text{Equation 3.1}$$

where A is absorbance of asphaltenes at 405 nm, b is the intercept, m is the slope and [Asp] is asphaltene concentration in mg/mL. The b and m values measured from asphaltene solutions in toluene and heptol are listed in Table 3.3. For sample solutions, the absorbance of asphaltene solution can be measured. With the known b and m values, therefore, the concentration of asphaltenes in sample solution can be calculated from Eq. 3.1.

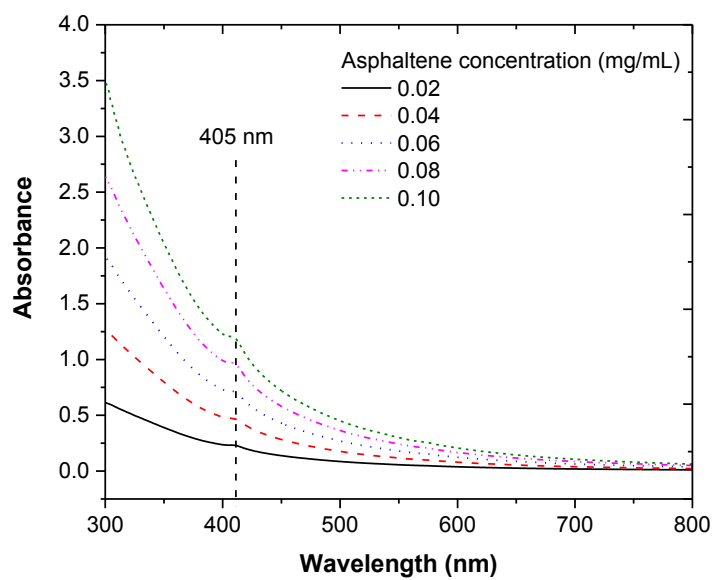


**Figure 3.1.** UV-Vis absorbance spectra of asphaltene in toluene standard solutions.

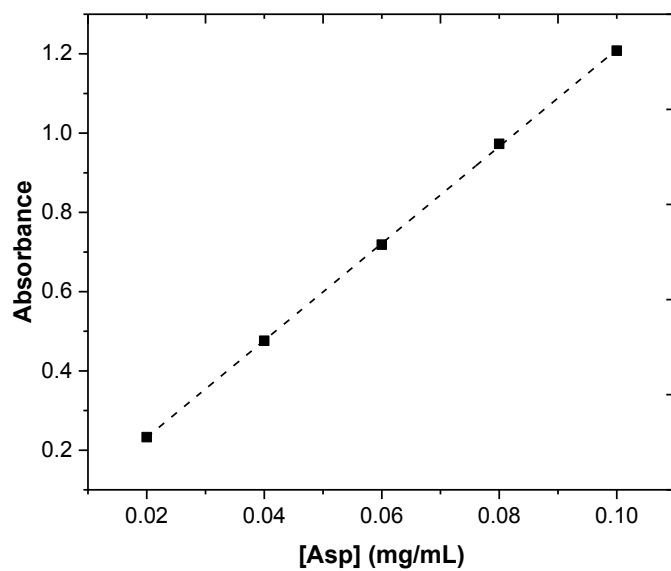


**Figure 3.2.** Calibration curve for asphaltene in toluene standard solutions.

**Table 3.3.** Intercept and slope values from linear fitting of calibration curves

<b>Solvent media</b>	<b>b</b>	<b>m</b>
Toluene	-0.0125	12.2358
Heptol (1:1 volume mixture)	-0.0040	11.2875

### 3.2.2.5 Asphaltene Solubility in Toluene and Heptol (1:1 volume ratio)

When studying the adsorption of asphaltenes onto solid surfaces any asphaltene precipitate can reduce the asphaltene concentration in bulk solution, and hence cause a positive bias for adsorption studies. Therefore, it is important to determine the concentration range in which asphaltenes remain dissolved and dispersed in both toluene and heptol solvents.

A combination of gravimetric and spectroscopic techniques was used for detection and quantification of asphaltene precipitation from toluene and heptol solutions. Asphaltene solutions were prepared by adding a desired amount of asphaltenes in the solvent of interest, followed by sonication for 30 min. Then all asphaltenes solutions were centrifuged at 14000 rpm for 20 min using the Sorvall WX Ultra Series centrifuge (Thermo Scientific) to remove any asphaltene precipitates. The concentration of asphaltenes in the supernatant was determined using the UV-Vis spectrophotometer explained in 3.2.2.4. The centrifugation of solution ensures true concentration of asphaltenes in bulk solution being used in adsorption study. However, when doing these experiments it was found that for asphaltene solutions with concentrations higher than 10 mg/mL in toluene and 8 mg/mL in heptol, even though sediment was observed after centrifugation, the concentration calculated by measuring the absorbance of the supernatant fluid was almost the same as the initial asphaltene concentration in fresh solutions. Therefore, in the case of asphaltene solutions with concentrations higher than 10 mg/mL in toluene and 8 mg/mL in heptol, a direct filtration method was used to detect the presence of particles in the system. Here, the sonicated solutions were left undisturbed for 30 min. Then precipitated asphaltenes were separated from the solution by filtration using a P5 Fisherbrand filter paper. The precipitates on filter paper were dried in the fume hood until no change in mass was observed. The amount of asphaltenes precipitated was determined by weighting the dried cake. The real asphaltene concentration in bulk solution can be calculated using Eq. 3.2:

$$[Asp]_{cal} = \frac{m_{Asp,i} - m_{Asp,p}}{V} \quad \text{Equation 3.2}$$

where  $[Asp]_{cal}$  is the real asphaltene concentration in bulk,  $m_{Asp,i}$  is the initial mass of asphaltenes,  $m_{Asp,p}$  is the mass of precipitated asphaltenes, and  $V$  is the initial volume of solvent used to prepare asphaltene solution. For asphaltene solution with initial concentration less than 10 mg/mL in toluene and 8 mg/mL in heptol, filtration method is also used to make sure no precipitation occurs in these solutions.

Shown in Figure 3.3 are plots of the real asphaltene concentration ( $[Asp]_{cal}$ ) versus the initial asphaltene concentration. The dashed line exhibits the ideal situation in which real asphaltene concentration in solution is equal to initial asphaltene concentration. As you can see, for initial asphaltene concentration between 0.02 to 10 mg/mL in toluene and 0.02 to 5 mg/mL in heptol,  $[Asp]_{cal}$  values fall in the dashed line, indicating no asphaltene precipitation. Whereas data points after 10 mg/ml in toluene and 5 mg/mL in heptol, show deviation from dashed line, which is due to precipitation and removal of asphaltene from bulk solution.

Furthermore, asphaltene solutions were observed under an Axioskop 40 Pol (Carl Zeiss) coupled with a microscope digital camera microscope. Figure 3.4 (a) shows the microscopic images obtained with 10X magnification lens for asphaltene solutions in toluene. No precipitates are observed in 0.5, 5 and 10 mg/mL solutions. However, as shown Figure 3.4 (b) for heptol solutions, the presence of asphaltene precipitates can be observed at 10 mg/mL asphaltene concentration.

Based on the solubility data, solutions with concentrations in the range 0.02 and 5 mg/mL are used to study the adsorption on solids in toluene. For heptol systems, adsorption experiments were performed at concentrations between 0.02 and 4 mg/mL.

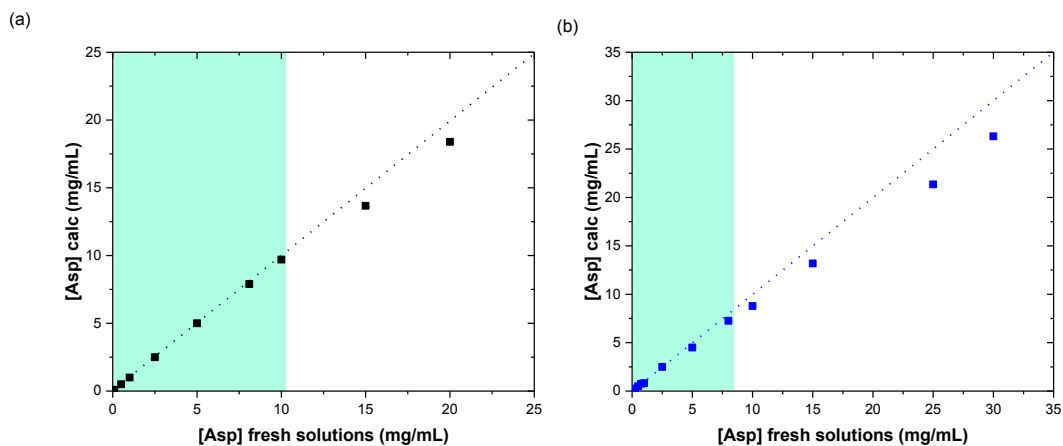


**Figure 3.3.** Asphaltene solubility in (a) Toluene; and (b) Heptol 1:1 volume ratio.

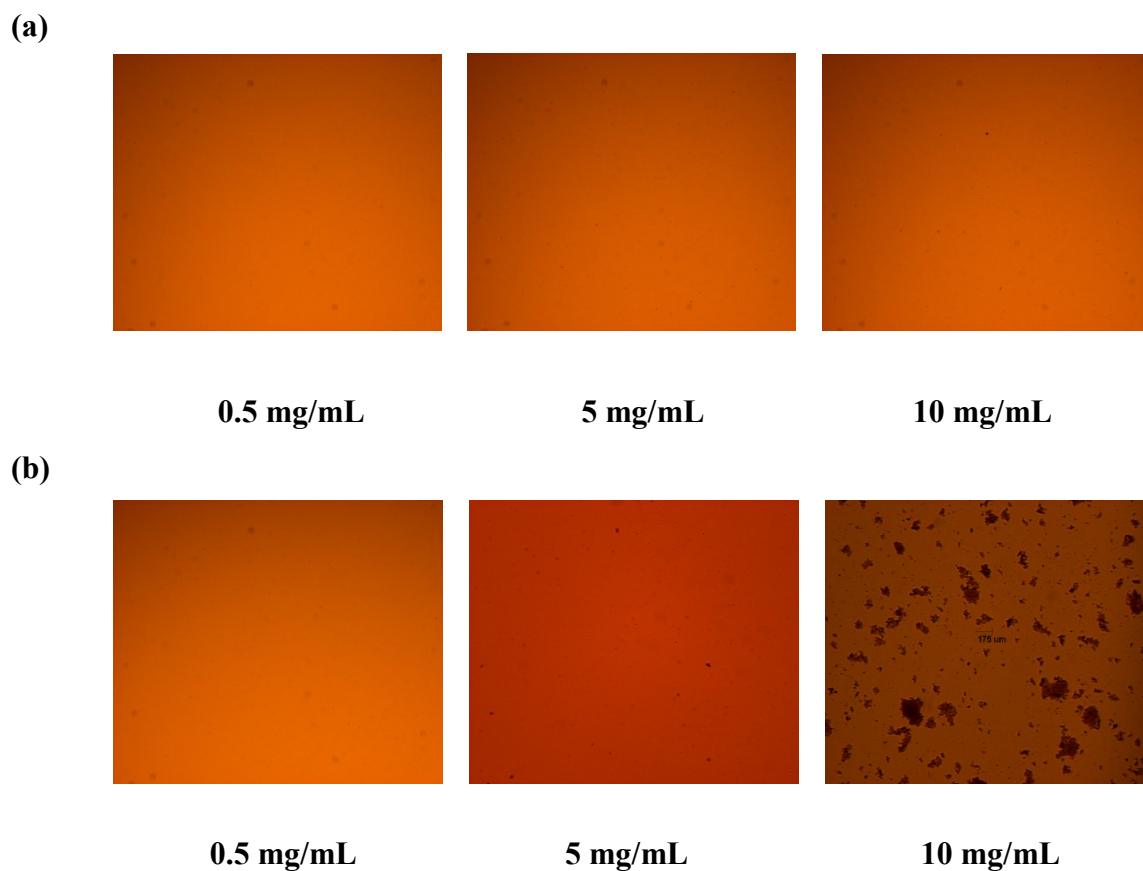


**Figure 3.4.** Microscopic images of asphaltene solutions in (a) Toluene; and (b) Heptol (1:1 volume ratio).

### 3.2.2.6 Adsorption Experiments

Adsorption experiments were conducted at different particle concentrations (300 and 500 mg in 10 mL solutions), depending on the surface area of particles (See Table 3.4). The particles were mixed with asphaltene solutions of different initial asphaltene concentrations in test tubes. The test tubes were sealed with paraffin tape wrapped around capped lid to reduce the loss of solvent by evaporation. Samples were continuously shaken on a magnetic stirring plate (Thermo Scientific Cimarec) at room temperature (22 °C) for 24 h, in order to allow the uniform distribution of all components and provide enough time to reach equilibrium of adsorption on surfaces of particles. After 24 h of contact, the particles were separated from asphaltene solutions by centrifugation for 20 min at 4000 rpm. A Hettich Rotanta 460R was used for this task. The asphaltene concentration was calculated from Equation 3.1, by measuring the UV absorbance of solution at 405 nm after adsorption. Asphaltene solutions with concentrations higher than 0.1 mg/mL were diluted prior the measurement to be in the range of the reliable calibration curve. Then, the real concentration of the asphaltene solution was calculated by taking into account the volumes of asphaltene solution and solvent used for dilution. The amount of asphaltene adsorbed was calculated from mass balance based on the difference of asphaltene solution concentrations before and after adsorption (equilibrium):

$$\Gamma \left( \frac{mg}{mg} \right) = \frac{([Asp]_0 - [Asp]_{eq}) * V}{m * 1000} \quad \text{Equation 3.3}$$

$$\Gamma \left( \frac{mg}{m^2} \right) = \frac{([Asp]_0 - [Asp]_{eq}) * V}{m * S} \quad \text{Equation 3.4}$$

where  $[Asp]_0$  is the initial asphaltene concentration (mg/mL),  $[Asp]_{eq}$  is the asphaltene concentration after the adsorption (mg/mL),  $\Gamma$  is the amount of asphaltene adsorbed (mg/mg or mg/m<sup>2</sup>),  $m$  is the mass of particles (g),  $V$  is the volume of asphaltene solution mixed with the particles (mL), 1000 is a conversion factor from grams to milligrams, and  $S$  is the specific surface area (m<sup>2</sup>/g) of particles.

**Table 3.4.** BET data and mass of particles used in the adsorption experiments

Particle	Surface area (m <sup>2</sup> /g)	Particle mass (mg)
Untreated SiO <sub>2</sub>	293.6± 10.5	300
Treated SiO <sub>2</sub> (950 °C)	188.8± 5.8	500
Untreated Al <sub>2</sub> O <sub>3</sub>	127.9± 0.2	300
Treated Al <sub>2</sub> O <sub>3</sub> (950 °C)	61.2± 1.7	300
Kaolinite	14.9± 2.6	300
Stainless steel	4.2± 0.6	500

### 3.2.2.7 Thermo-Gravimetric Analysis

Thermo-gravimetric analysis (TGA) is a technique for determination of thermal desorption/decomposition of materials while the sample is being heated at a controlled heating rate in a controlled atmosphere. TGA experiments were performed on a TGA Q500 (TA Instruments) equipped with a vertical thermobalance. Asphaltenes and asphaltene covered particles were analyzed in TGA to calculate the activation energy associated with the decomposition process of these materials. In order to remove loosely adsorbed asphaltenes, asphaltene covered particles were rinsed several times, with either toluene or heptol solvents before conducting the analysis. Then the solids were dried for 24 h at 60 °C with the purpose of removing the solvent. For TGA experiments, the samples (10-20 mg) were heated from room temperature to 700 °C at four different heating rates 5, 10, 15 and 20 °C/min under nitrogen atmosphere (100 mL/min).

## 3.3 Results

### 3.3.1 Optimization of Adsorption Experimental Conditions

#### 3.3.1.1 Kinetics of Asphaltene Adsorption on Different Particles

For the adsorption of asphaltenes on different particles, there are only a few reports on the effect of equilibration time on asphaltene adsorption. Alboudwarej et al. (22) found that asphaltene adsorption on stainless steel powder reaches a steady state within 24 h. Dudasova et al. (20)

reported that the amount of asphaltenes adsorbed on mineral particles and clays does not change with time after 12 h.

In this study, the asphaltene solution and solids were mixed at various mixing time. Untreated silica was selected as the model solid. Shown in Figure 3.5 are plots of the amount of asphaltenes adsorbed on untreated silica as a function of mixing time. In solutions at different initial asphaltene concentrations, the amount of asphaltenes adsorbed on untreated silica increases with mixing time and starts to reach a plateau after mixing for 24 h, indicating that asphaltene distribution between bulk solution and solid surface reached equilibrium after 24 h of adsorption. Since these experiments were performed at very high initial asphaltene concentration (highest concentration of the present work), equilibria for experiments at lower asphaltene initial concentration should be reached earlier. Therefore, mixing time of 24 h was used for the following adsorption experiments.

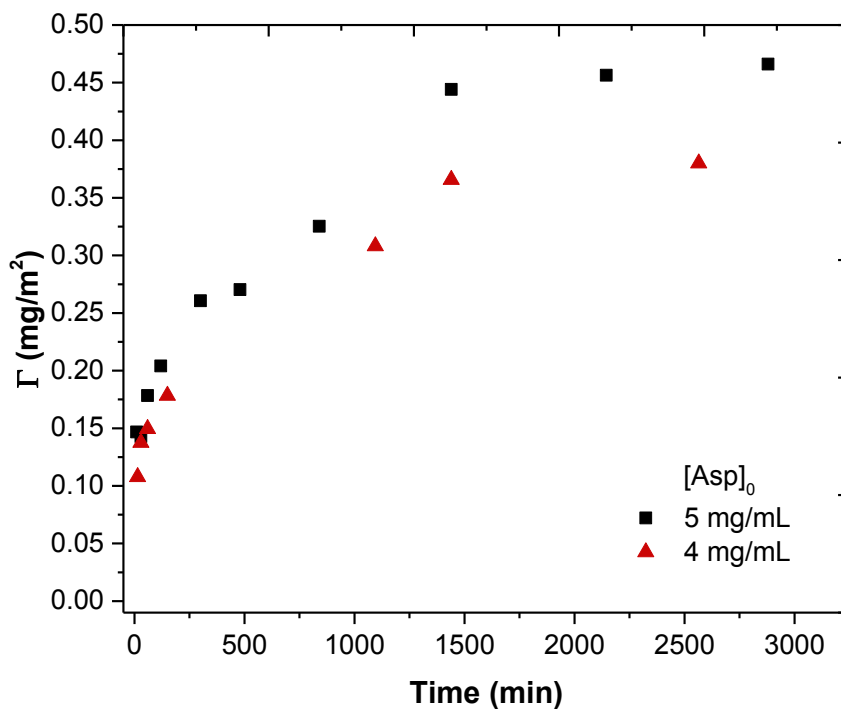


**Figure 3.5.** Effect of mixing time and initial concentration on the adsorption of asphaltenes on untreated silica.

### 3.3.1.2 Effect of Particles to Liquid Ratio (S/L)

Particles were added to 10 mL asphaltene solution in toluene at S/L ratios from 0.01 to 0.06 g/mL. Initial asphaltene concentration of 4 mg/mL and 1 mg/mL was used for this set of adsorption tests of asphaltenes on untreated silica, and on stainless steel particles, respectively. The samples were shaken for 24 h to ensure that solution equilibrium be reached. As shown in Figure 3.6, the asphaltene concentration at equilibrium ( $[\text{Asp}]_{\text{eq}}$ ) decreases with S/L ratio for both particles studied at a constant initial asphaltene amount, more so for untreated silica. The lower concentration of asphaltenes at equilibrium indicates a high adsorption due most likely to the increase in the available surfaces on solids that can adsorb more asphaltenes. However, when normalized by the surface area, the amount of asphaltenes adsorbed ( $\text{mg}/\text{m}^2$ ) on both silica and stainless steel decrease gradually with increased S/L ratio (Figure 3.7). This is because at a fixed amount of asphaltenes present in solution, we have more asphaltenes for the surface area available for adsorption at lower S/L ratios, resulting in a higher amount of asphaltenes adsorbed per  $\text{m}^2$  of particle. However, as we increase the S/L ratio, there is a point in which we have too many adsorption sites available for the same amount of asphaltenes present in solution, decreasing the amount of asphaltenes adsorbed per  $\text{m}^2$  of particles.

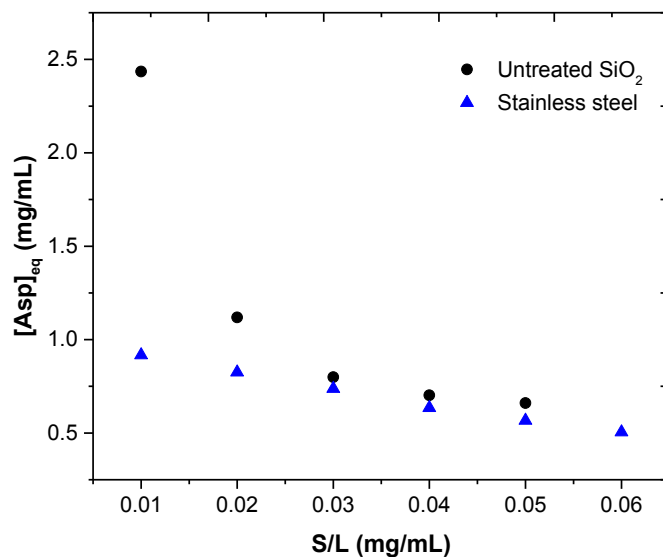


**Figure 3.6.** Effect of particles to liquid (S/L) ratio on asphaltene concentration after the adsorption.

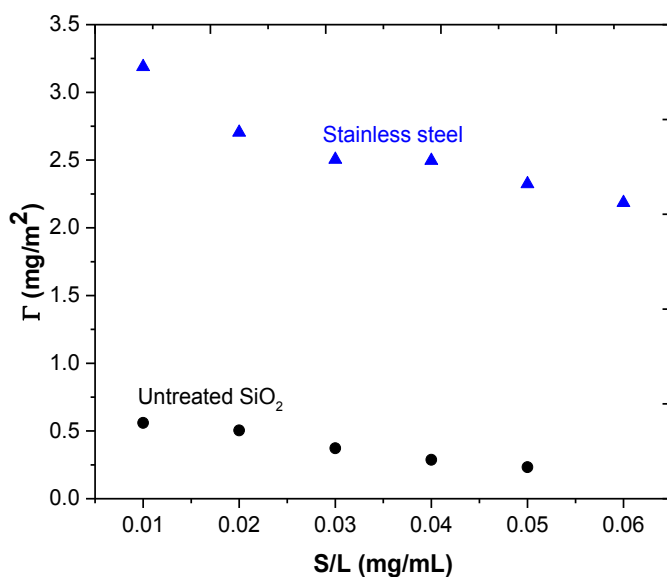


**Figure 3.7.** Effect of particles to liquid (S/L) ratio on the amount of asphaltenes adsorbed on untreated silica and stainless steel.

### 3.3.2 Effect of Types of Particles

The adsorption of asphaltenes from toluene solutions on untreated silica, untreated alumina, kaolinite and stainless steel particles was studied at an initial asphaltene concentrations within 0.01-5 mg/mL. Experiments were carried out at different S/L ratios (See Table 3.4), depending on the specific surface area of particles. Shown in Figure 3.8 are the plots of the amount of asphaltenes adsorbed as function of the equilibrium asphaltene concentration in toluene solutions. As you can see, at low asphaltene concentrations, there is a sharp increase in the adsorbed amount of asphaltenes on particles studied. When further increasing initial asphaltene concentration in solution, the isotherms reach a plateau, which indicates an equilibrium saturation point in the adsorption process that could be attributed to the presence of a dynamic balance between the asphaltene concentration in the bulk solution and at the solid/liquid interface. (79)

Adsorption isotherms give important information on the affinity and capacity of asphaltene adsorption on solid particles. In general, two different types of adsorption behavior of asphaltenes onto solid surfaces have been reported. For some systems Langmuir type isotherms have been reported, indicating that asphaltene molecules form a single layer on the solid surface. (18, 20, 64) Other researchers concluded that isotherms of asphaltene adsorption were of Freundlich type and

proposed a multilayer adsorption. **(21, 23, 27, 65)** To investigate the adsorption behavior, the isotherms of asphaltene adsorption on the particles obtained in this study, were fitted using the Langmuir (Equation 3.5) and Freundlich (Equation 3.6) models:

$$\Gamma = \frac{K * \Gamma_{max} * [Asp]_{eq}}{1 + K * [Asp]_{eq}} \quad \text{Equation 3.5}$$

$$\Gamma = K_f * [Asp]_{eq}^{1/n} \quad \text{Equation 3.6}$$

where  $\Gamma$  is the amount of asphaltene adsorbed onto the particles ( $\text{mg}/\text{m}^2$ ),  $\Gamma_{max}$  is the saturation amount of asphaltene adsorbed ( $\text{mg}/\text{m}^2$ ),  $[Asp]_{eq}$  is the asphaltene equilibrium concentration ( $\text{mg}/\text{mL}$ ),  $K$  is the Langmuir adsorption equilibrium constant related to the affinity of binding sites ( $\text{mL}/\text{mg}$ ), **(80)**  $K_f$  is the Freundlich adsorption equilibrium constant related to the adsorption capacity  $[(\text{mg}/\text{m}^2)(\text{mL}/\text{mg})^{1/n}]$  and  $1/n$  (dimensionless) is the intensity factor of adsorption which is a function of the adsorption strength in the adsorption process. **(81)**

Figure 3.8 reveals that all adsorption isotherms are fitted much better with Langmuir model than with Freundlich model, with correlation coefficients in the range from 0.95 to 1.0. Such finding is in good agreement with previously published data in literature. **(20, 22, 64, 82)** Table 3.5 summarizes the values of  $\Gamma_{max}$ ,  $K$ ,  $K_f$  and  $1/n$ , obtained after fitting the adsorption data. It can be seen that stainless steel shows the highest adsorption capacity ( $2.32 \text{ mg}/\text{m}^2$ ), followed by kaolinite ( $1.85 \text{ mg}/\text{m}^2$ ), while untreated  $\text{SiO}_2$  ( $0.84 \text{ mg}/\text{m}^2$ ) and untreated  $\text{Al}_2\text{O}_3$  show the least adsorption capacity ( $0.52 \text{ mg}/\text{m}^2$ ). These results indicate that the adsorption capacity strongly depends on the surface type and area. The adsorption capacity of asphaltene on stainless steel particles is on the same order of magnitude as the amount of asphaltene adsorbed on minerals. Metals and mineral particles are alike in terms of their hydrophilic properties, hence similar amounts of asphaltene adsorption are to be expected. **(22)**

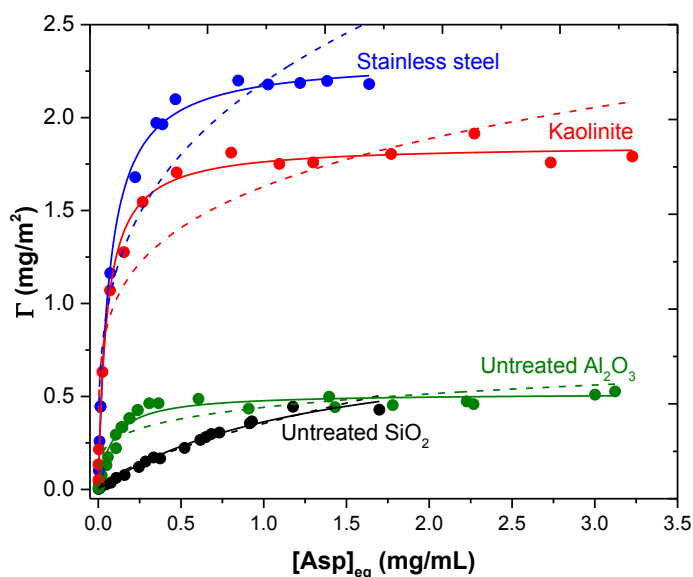


**Figure 3.8.** Adsorption isotherms of asphaltenes from toluene solutions (Solid lines are the best fit to Langmuir isotherms, dashed lines are the best fit to Freundlich isotherms).

**Table 3.5.** Model parameters of asphaltenes adsorption on different particles from toluene solutions

Particle	Langmuir model				Freundlich model		
	$\Gamma_{\max}$ mg/m <sup>2</sup>	$\Gamma_{\max}$ mg/mg	K	R <sup>2</sup>	K <sub>f</sub>	n	R <sup>2</sup>
Untreated SiO <sub>2</sub>	0.84	0.25	0.77	0.98	0.35	1.50	0.96
Untreated Al <sub>2</sub> O <sub>3</sub>	0.52	0.07	11.82	0.95	0.44	4.58	0.77
Kaolinite	1.85	0.03	19.10	0.99	1.63	4.74	0.87
Stainless steel	2.32	0.01	14.63	1.00	2.19	3.55	0.89

The adsorption of asphaltenes on solid surfaces in toluene depends on the type and strength of interactions between asphaltenes and the surface. In the following discussion, Langmuir parameters ( $\Gamma_{\max}$  and K) will be further analyzed to better understand the observed difference in asphaltene adsorption between the solids investigated. Figure 3.9 illustrates the variation on  $\Gamma_{\max}$

and K values for various solid particles. Interestingly, the ranking of  $\Gamma_{\max}$  and K appears to be different.  $\Gamma_{\max}$  followed the order of stainless steel > kaolinite > untreated SiO<sub>2</sub> > untreated Al<sub>2</sub>O<sub>3</sub>, whereas the quality of adsorption measured by K values has the following order: kaolinite > stainless steel > untreated Al<sub>2</sub>O<sub>3</sub> > untreated SiO<sub>2</sub>. The differences in adsorption affinity (K) can be attributed to a different degree of interaction between the solids and asphaltenes. **(12, 83)** The observed difference between the ranking of  $\Gamma_{\max}$  and K could be related to the fact that the  $\Gamma_{\max}$  and K by definition refer to different but linked phenomena.  $\Gamma_{\max}$  mainly depends on number of adsorption sites on solid surfaces, the interactions between the surface and asphaltenes, and the conformation of asphaltenes at the interface, while K denotes the affinity of binding sites which depends on how strong the interactions between the surface and asphaltene are. **(20)** These differences in ranking have been reported by other researchers for adsorption of asphaltenes onto different minerals and clays. **(12, 20, 83)**

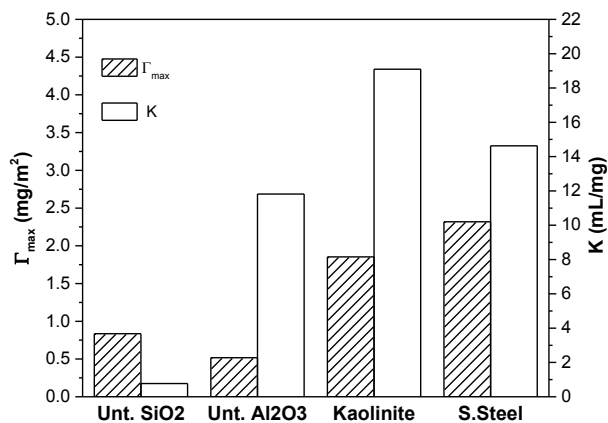


**Figure 3.9.** Variation of  $\Gamma_{\max}$  and K for solid particles of different surface properties.

For a given solvent, adsorption of asphaltenes onto solid surfaces is governed by the chemical and physical characteristics of the solid (sorbent) and the structural and chemical properties of asphaltenes, the latter are determined by their source and how they were isolated. **(17)** To further understand the adsorption of asphaltenes on solid surfaces, SEM and FT-IR were used to characterize the solid surface properties and chemical properties of adsorbed asphaltenes, respectively.

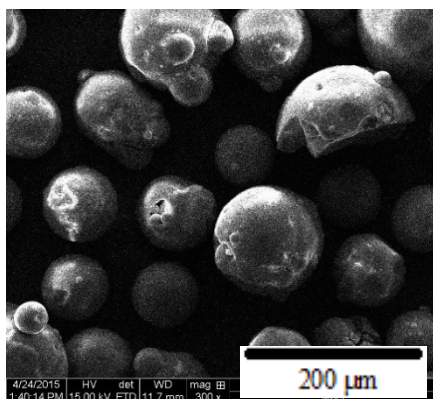
SEM images of untreated SiO<sub>2</sub>, untreated Al<sub>2</sub>O<sub>3</sub>, kaolinite and stainless steel were obtained to identify the role of surface morphology on the adsorption of asphaltenes. From the image analysis of the SEM micrographs (Figure 3.10), the particle size was found to be larger for untreated Al<sub>2</sub>O<sub>3</sub> followed by untreated SiO<sub>2</sub>, kaolinite and stainless steel. The surface of stainless steel appears to be rougher with many small particles. In the case of kaolinite, a mixture of particles of different sizes can be observed. Untreated SiO<sub>2</sub> appears to be spherical in shape and similar in sizes, whereas untreated Al<sub>2</sub>O<sub>3</sub> presents a peculiar shape with an uneven surface. These differences in the surface morphology may affect the nature of the asphaltene-surface adsorption.

Stainless steel is a steel alloy that have a high content of chromium and nickel along with other elements such as manganese, phosphorus, sulfur, silicon, molybdenum and carbon, although present in a less amount (Table 3.2). The existence of heteroatoms, such as metals, silicon and carbon in the structure of stainless steel could provide a good environment for a better covalent bonding between asphaltenes and stainless steel particles. **(22)** In addition, the formation of metal-oxygen bond between asphaltenes and stainless steel particles may aid the adsorption process.

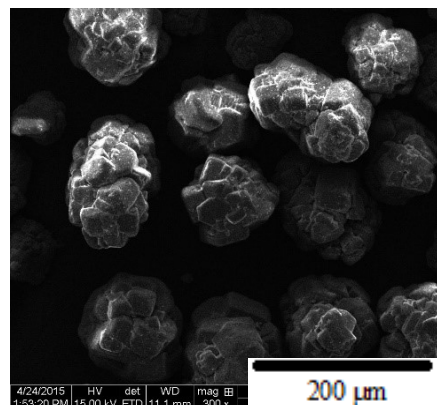
Kaolinite is a two-layered structured clay, composed of a silicon-oxygen tetrahedron sheet (T) and an aluminum-oxygen-hydroxyl octahedron sheet (O). This arrangement of tetrahedron and octahedron basic sheets is commonly referred to as 1:1 or –TO-TO- layer structure. The 1:1 layer structure of kaolinite features basal oxygen on the tetrahedral surface sheet and hydroxyls on the octahedral aluminous sheet. Kaolinite has polar sites, mainly octahedral Al–OH and tetrahedral Si–OH groups, located at the broken edges and exposed hydroxyl-terminated planes, **(84)** which have been proposed to be active sites for asphaltene adsorption. **(20, 71, 85)**

Regarding alumina particles, the nature of the intermolecular interactions in the asphaltene-alumina system may be associated to the aluminol (Al–OH) groups present on the alumina surface. **(86-88)**

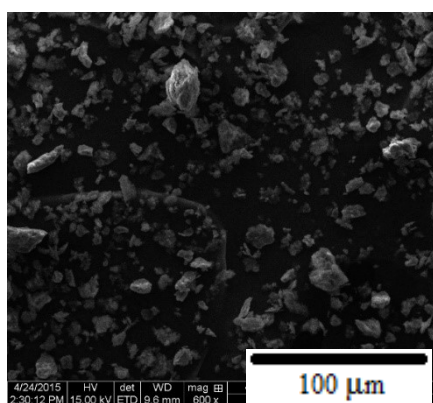
Silica particles contain silanol groups (Si–OH) that gives some hydrophilicity to its surface and make it able to form hydrogen bonding with suitable molecules. The –OH density on silica has been reported to be between 2.5-3.5 OH/nm<sup>2</sup>. **(89)** Besides silanol, silica particles contain surface siloxane (Si–O–Si) groups that may be weaker adsorption sites due to their less hydrophilic nature, when compared to silanol groups. Hence, it is more likely that the adsorption of asphaltenes on silica particles to be strongly mediated by surface silanol groups (Si–OH). **(20, 89)**



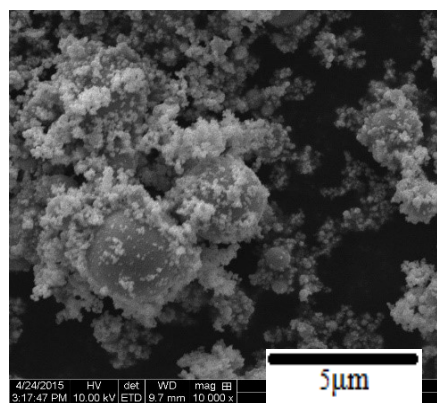
(a) Untreated SiO<sub>2</sub>



(b) Untreated Al<sub>2</sub>O<sub>3</sub>



(c) Kaolinite



(d) Stainless steel

**Figure 3.10.** SEM micrographs of bare particles.

The adsorption of asphaltenes onto solid surfaces is also influenced by the chemical and structural properties of asphaltenes. Asphaltene molecules consist of several fused aromatic rings surrounded by various alkyl and naphthenic chains containing nitrogen, oxygen, sulphur and trace amounts of metals. Some studies showed that the presence of heteroatoms and functional groups in the asphaltene molecules plays a significant role in asphaltene-solid interactions. (20, 27, 64, 71) The influence of the structure of asphaltenes on their adsorption properties will be further discussed in Chapter 4.

Diffuse reflectance infrared fourier transform (DRIFT) spectroscopy was used to assess the structural modifications induced by the asphaltene adsorption process.

The IR spectrum for nC<sub>5</sub>-iC<sub>5</sub> asphaltenes (Figure 3.11 (a)) shows that asphaltene molecules primarily consist of aliphatic groups (1376, 1456, 2852, 2924 cm<sup>-1</sup>) and low amounts of condensed aromatic rings (3048 cm<sup>-1</sup>). **(23, 71)** Bands in the range of 3694-3620 cm<sup>-1</sup> are attributed to the presence of O-H groups. The peak at 1598 cm<sup>-1</sup> corresponds to the vibration of C=C aromatic double bond. Signals between 1032 cm<sup>-1</sup> and 1011 cm<sup>-1</sup> appear in the region for heteroatom vibrations such as sulphur and nitrogen. **(90)** Figures 3.11 (b-d) show the DRIFT spectra of bare and asphaltene covered particles.

For untreated silica particles (Figure 3.11 (b)), the broad band in the interval 3700-3000 cm<sup>-1</sup> corresponds to the overlapping of the stretching modes in hydrogen-bonded hydroxyl bands produced by O-H bonds in water and Si-OH. **(91)** The strong absorption band at 1097 cm<sup>-1</sup> has been reported to appear due to the asymmetric stretching of Si-O-Si bonds. The peak at 974 cm<sup>-1</sup> is due to the bending stretching of Si-OH. A peak due to bending vibrations of Si-O-Si bonds also appeared at 804 cm<sup>-1</sup>. **(92)** Further, a series of peaks can be observed in the lower frequency region from 495 to 424 cm<sup>-1</sup>, which have been reported to appear due to the combination of bending and rocking modes of Si-O-Si or O-Si-O bonds. **(92, 93)** The DRIFT spectra of untreated alumina particles are shown on Figure 3.11 (c) A very broad band centered at around 3407 cm<sup>-1</sup> arises due to the presence of hydroxyl groups stretching on the alumina surface. **(94)** The bands in the range of 723-496 cm<sup>-1</sup> correspond to Al-O stretching frequency. **(86)** Figure 3.11 (d) presents the DRIFT spectra of kaolinite particles. The bands at 3620, 3653, 3668 and 3695 cm<sup>-1</sup> have been referred to as the hydroxyl stretching region, which is related to the presence of silanol and aluminol surface groups. **(95, 96)** Si-O stretching vibrations are observed between 1010 and 1112 cm<sup>-1</sup>. The peaks at 914 and 937 cm<sup>-1</sup> correspond to the hydroxyl deformation vibration mode of the inner surface hydroxyl groups. The spectral region between 700 and 800 cm<sup>-1</sup> presents bands associated with hydroxyl translation vibration modes. Also, peaks in the range of 417-538 cm<sup>-1</sup> correspond to the O-Si-O and O-Al-O bending modes. **(97)**

As can be observed, the IR spectra of asphaltene covered particles are quite similar to the corresponding bare particles. By subtraction of IR spectrum of bare particle from that of asphaltene covered particles, the characteristic peaks of asphaltenes, located at 2924 and 2852 cm<sup>-1</sup> can be observed, indicating that asphaltenes are adsorbed on the surface of the particles. The 3100-2700 cm<sup>-1</sup> region of the IR spectra obtained after subtraction of bare particles spectra is shown in Figure 3.12. Another notable result from the spectra of asphaltene covered particles is the absence of the

asphaltene bands attributed to the C=C aromatic double bond and heteroatom vibrations, which might be due to their interaction with the particles surface groups. (71)

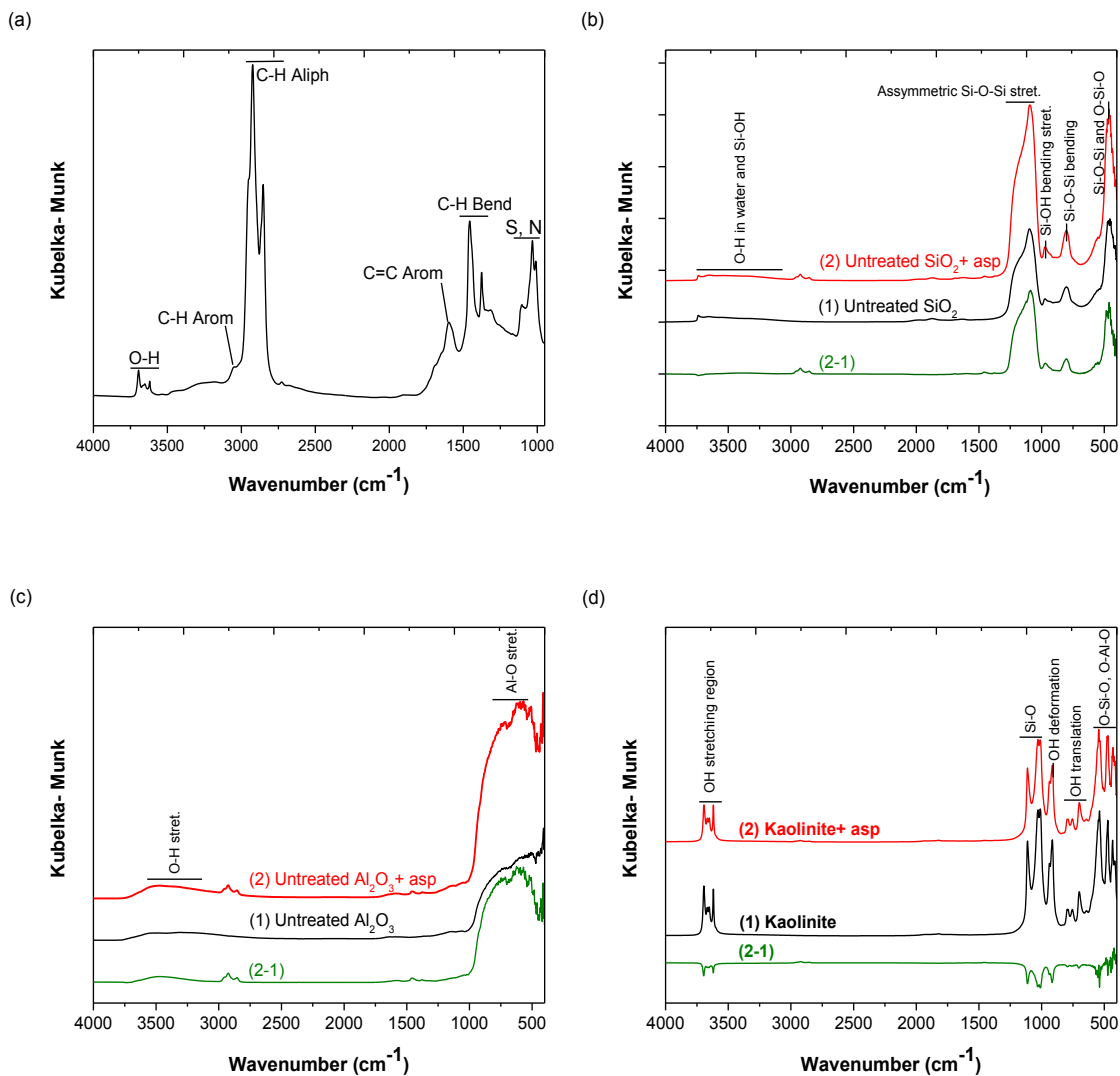


**Figure 3.11.** DRIFT spectra of (a) nC<sub>5</sub>-iC<sub>5</sub> asphaltenes; (b) Bare and asphaltene covered untreated SiO<sub>2</sub>; (c) Bare and asphaltene covered Untreated Al<sub>2</sub>O<sub>3</sub>; and (d) Bare and asphaltene covered kaolinite.

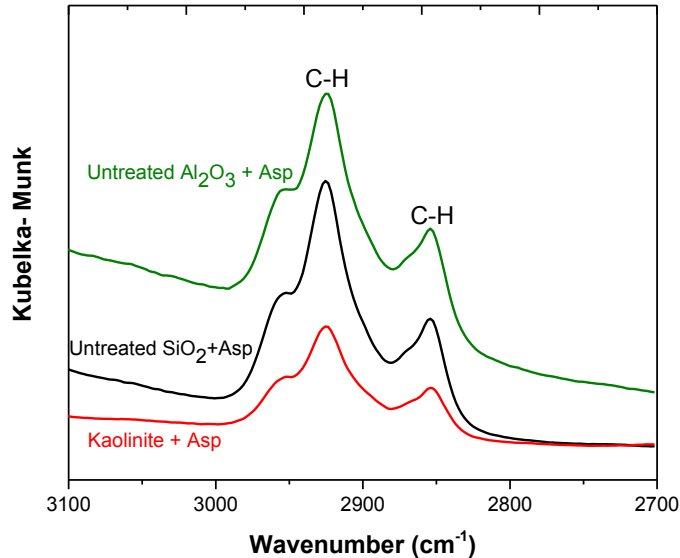


**Figure 3.12.** 3100-2700  $\text{cm}^{-1}$  DRIFT spectra regions obtained after subtracting the spectra of bare particles from that of asphaltene covered particles.

### 3.3.3 Effect of Solvents Properties

The effect of the solvent properties on asphaltene adsorption was assessed through a series of experiments performed using an n-heptane and toluene mixture at 1:1 volume ratio (heptol) as the liquid medium. The adsorption experiments were carried out on three different particles, untreated  $\text{SiO}_2$ , untreated  $\text{Al}_2\text{O}_3$  and stainless steel powder, using the procedures explained in section 3.2.2. The results of the adsorption measurements from heptol and toluene solutions are presented together in Figure 3.13 for comparison. As can be seen, a different adsorption behavior was observed in heptol system, showing a continuous increase in the amount of asphaltenes adsorbed within the concentration range studied. Noticeably the amount of asphaltenes adsorbed from heptol is consistently higher than that from toluene. Since heptane is a poor solvent for asphaltenes, adding heptane into solution lowers asphaltene solubility and enhances the degree of asphaltene aggregation. Therefore, larger asphaltene aggregates adsorb on the surface, resulting in a larger amount of asphaltenes adsorbed, and possibly also in multilayers. Furthermore, a poor solvent may cause the adsorption of asphaltenes on weaker adsorption sites that were not adsorbed on in a good solvent such as toluene. **(22)**

Different from the results in toluene, the adsorption isotherms in heptol were fitted better with the Freundlich model, which is expressed in Equation 3.6. This result suggests a multilayer adsorption of asphaltenes from heptol solutions, less dependent on the distribution of adsorption affinities over the heterogeneous surface. (98, 99) Table 3.6 lists the Freundlich fitted parameters. The values of the Freundlich adsorption equilibrium constant ( $K_f$ ), related to the adsorption capacity followed the order of stainless steel > untreated  $\text{Al}_2\text{O}_3$  > untreated  $\text{SiO}_2$ , whereas the quality of the adsorption measured by the  $n$  factor has the order of untreated  $\text{Al}_2\text{O}_3$  > stainless steel > untreated  $\text{SiO}_2$ . This different ranking order in  $K_f$  and  $n$  indicates that a high adsorption capacity is not necessarily related to a high strength in the interactions between the adsorption sites and asphaltene aggregates.

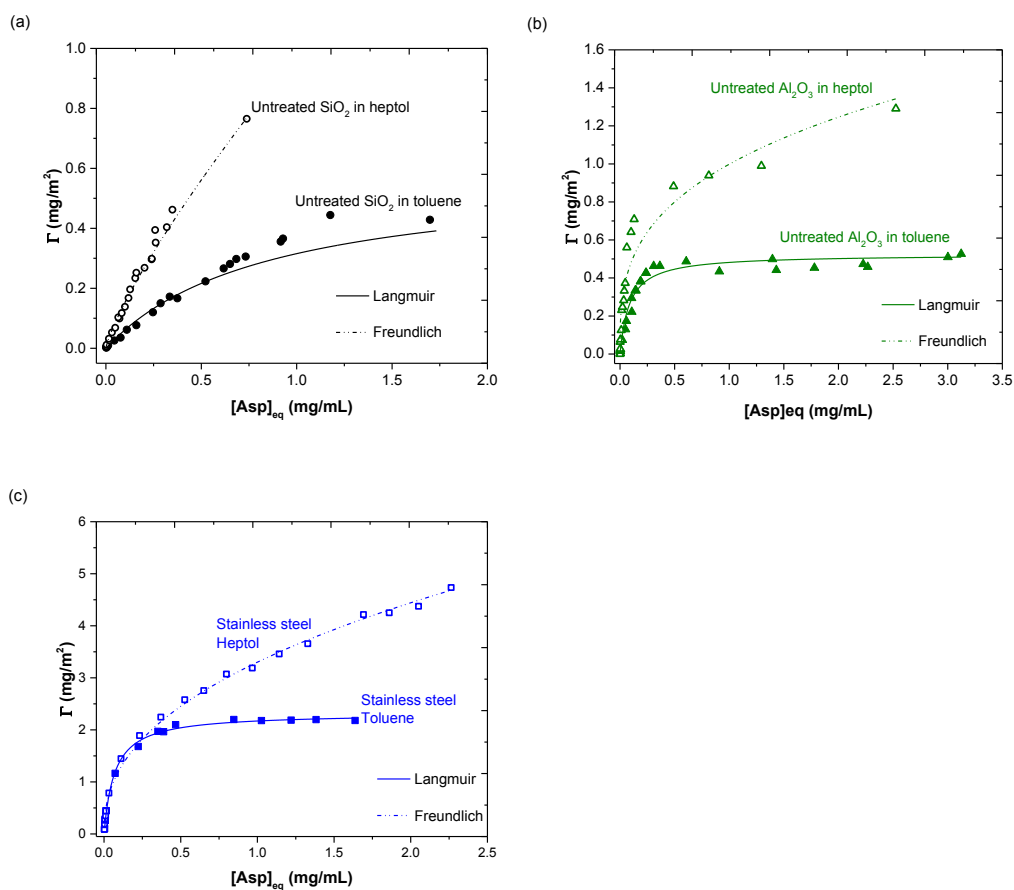


**Figure 3.13.** Isotherms of asphaltene adsorption from solutions of toluene and heptol for: (a) Untreated  $\text{SiO}_2$ ; (b) Untreated  $\text{Al}_2\text{O}_3$ ; and (c) Stainless steel.

**Table 3.6.** Freundlich model parameters for adsorption of asphaltenes on different particles from heptol solutions

Particle	Freundlich model		
	$K_f$	$n$	$R^2$
Untreated SiO <sub>2</sub>	0.98	1.24	0.99
Untreated Al <sub>2</sub> O <sub>3</sub>	1.00	3.13	0.94
Stainless steel	3.30	2.33	1.00

### 3.3.4 Thermally Treated Particles

In order to gain further insight into the nature of the surface groups responsible for the adsorption of asphaltenes, silica and alumina particles were conditioned in a furnace at 950 °C for 1 hour before being used in asphaltene adsorption experiments. The purpose of thermally treating these two samples is to reduce surface –OH groups and hence hydrophilic nature of particle surfaces. The thermal treatment of silica and alumina particles resulted in a reduction in their specific surface area (See Table 3.4). Figure 3.14 shows the adsorption isotherms of asphaltenes on thermally treated silica and alumina in toluene system. Data for untreated particles in toluene are also included in this figure for comparison. Same as untreated particles, the amount of asphaltenes adsorbed on the treated silica and alumina increases first with increasing asphaltene concentrations and levels off at high  $[Asp]_{eq}$ , reaching an equilibrium saturation point where no possible active site is available for asphaltene adsorption. The adsorption isotherms were fitted to the Langmuir model (Equation 3.5), obtaining correlation coefficients of 0.99 and 0.96 for the thermally treated silica and alumina particles, respectively. From Figure 3.14 (a), it is clear that the thermally treated silica shows a much lower adsorption capacity than untreated silica. A possible explanation is that calcination of silica particles at 950 °C reduced the density of surface silanol groups (Si-OH), resulting in less number of active adsorption sites for asphaltenes. Fritschy et al. (85) reported a decrease in the density of hydroxyl groups on silica with increasing thermal treatment temperature, to about 1 -OH/nm<sup>2</sup> after pyrolysis at 1000 °C. Hence it is expected to have a drop in the adsorption capacity on silica, after its heat treatment, which underlines the significance of the presence of surface silanol groups for asphaltene adsorption. In addition, strained siloxane bridges, present

after calcination may play a role in the adsorption capacity shown by thermally treated silica particles. **(85)**

SEM images of untreated and thermally treated silica particles (Images not shown) do not present any difference in surface morphology that could help us to better explain our data.

Untreated and thermally treated silica particles were also characterized by diffuse reflectance infrared fourier transform (DRIFT) spectroscopy (Figure 3.15 (a)). After the thermal treatment of silica particles at 950 °C, the broad band at about 3700-3000  $\text{cm}^{-1}$  and the peak at 1626  $\text{cm}^{-1}$  associated to physically adsorbed water molecules disappeared. Adsorption bands at 3740  $\text{cm}^{-1}$  and 804  $\text{cm}^{-1}$  originated from hydrogen-bonded OH groups of silica and bending vibrations of Si-O-Si bonds, respectively, are still present on the spectrum of treated silica particles. The peak at 1097  $\text{cm}^{-1}$  attributed to the asymmetric stretching of Si-O-Si bonds is less sharp after the thermal treatment. Furthermore, the signal at 974  $\text{cm}^{-1}$  related to the bending stretching of Si-OH is absent from the spectrum of treated silica, which suggests a reduction in the silanol groups as consequence of the high temperature treatment, resulting in the reduced adsorption of asphaltenes on the treated silica particles.

In contrast to the silica particles, thermally treated alumina presents a higher adsorption capacity than the untreated alumina (Figure 3.14 (b)). Unfortunately, SEM images (not shown), do not exhibit any morphological change after the alumina calcination. Furthermore, the DRIFT spectra of untreated and thermally treated alumina as shown in Figure 3.15 (b) do not indicate any chemical modification induced by the calcination process.

However, it is important to mention that as a result of high temperature treatment of alumina particles, neighboring hydroxyl groups from the surface of alumina may react with each other forming strained oxygen bridges (Lewis base) and Lewis acid sites ( $\text{Al}^+$ ), which may play an important role in the adsorption of asphaltenes on thermally treated alumina surfaces. **(100, 101)** Therefore, it could be suggested that thermal treatment of alumina may enhance the exposure of active sites, consequently increasing its adsorption capacity.

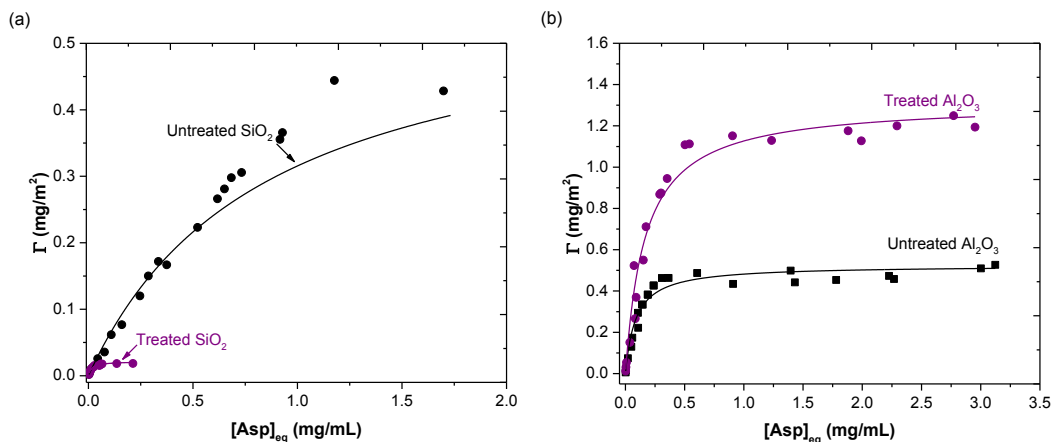


**Figure 3.14.** Asphaltene adsorption isotherms on (a) Untreated and thermally treated SiO<sub>2</sub>; and (b) Untreated and thermally treated Al<sub>2</sub>O<sub>3</sub>.

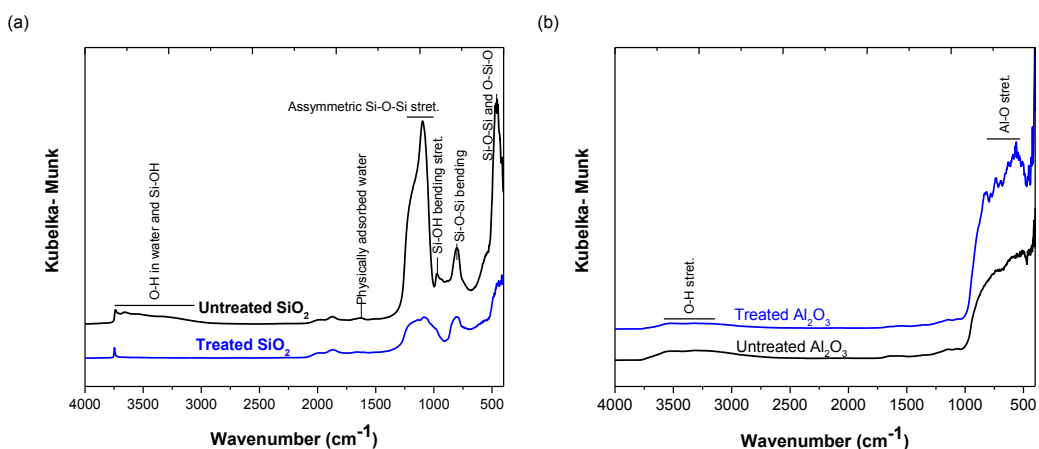


**Figure 3.15.** DRIFT spectra of (a) Untreated and thermally treated SiO<sub>2</sub>; and (b) Untreated and thermally treated Al<sub>2</sub>O<sub>3</sub>.

### 3.3.5 Thermo-Gravimetric Analysis of Asphaltenes Adsorbed on Solid Particles

The decomposition kinetics of nC<sub>5</sub>-iC<sub>5</sub> asphaltenes adsorbed on particles were obtained by thermo-gravimetric analysis. For comparison, decomposition kinetics of nC<sub>5</sub>-iC<sub>5</sub> asphaltenes, mixture of asphaltenes-untreated SiO<sub>2</sub> and a mixture of asphaltenes-untreated Al<sub>2</sub>O<sub>3</sub> were also studied. In general kinetic studies are conducted isothermally at different temperatures. However, non-isothermal techniques are used when working with complex samples, such as asphaltenes to avoid problems associated with the interpretation of chemical changes occurring during the thermal-heating period. (102, 103) Non-isothermal kinetic experiments were carried out on each sample using four

different heating rates 5, 10, 15 and 20 °C/min, respectively. Shown in Figure 3.16 are thermograms obtained at 10 °C/min. The TGA curves corresponding to the untreated silica and untreated alumina particles show a small weight loss below 100 °C, which may be related to the evaporation of physically adsorbed water present on solid surfaces. Asphaltenes do not show any appreciable change in their weight up to about 250 °C, indicating that the structure of asphaltenes remains almost intact below 250 °C. A small weight loss between 250 and 350 °C is observed for asphaltenes due to the elimination of alkyl groups located in peripheral sites of asphaltenes. **(104)** At higher temperatures (> 350 °C) the stronger chemical bonds of asphaltenes are broken and molecular skeletons are decomposed, which is evident by more significant weight loss between 350-600 °C. **(104)** Particles with adsorbed asphaltenes show a similar decomposition characteristics to bare particles under 350 °C and similar decomposition characteristics to asphaltenes at T > 350 °C.

For the particles with adsorbed asphaltenes, the weight loss at T < 350 °C is attributed to the loss of physically adsorbed water, which is not seen in the decomposition of asphaltenes. In order to facilitate the analysis of the data, each curve was normalized within the decomposition temperatures of asphaltenes (250-550 °C, Eq. 3.7).

$$\text{NormalizedWt\%} = \frac{Wt\% - Wt\%_{550\text{ }^{\circ}\text{C}}}{Wt\%_{250\text{ }^{\circ}\text{C}} - Wt\%_{550\text{ }^{\circ}\text{C}}} \quad \text{Equation 3.7}$$

The normalized TGA curves of asphaltenes at four different heating rates (5, 10, 15 and 20 °C/min) are shown in Figure 3.17. At faster heating rate, decomposition of asphaltenes occurs at higher temperature, as predicted from kinetic theory. **(105)**

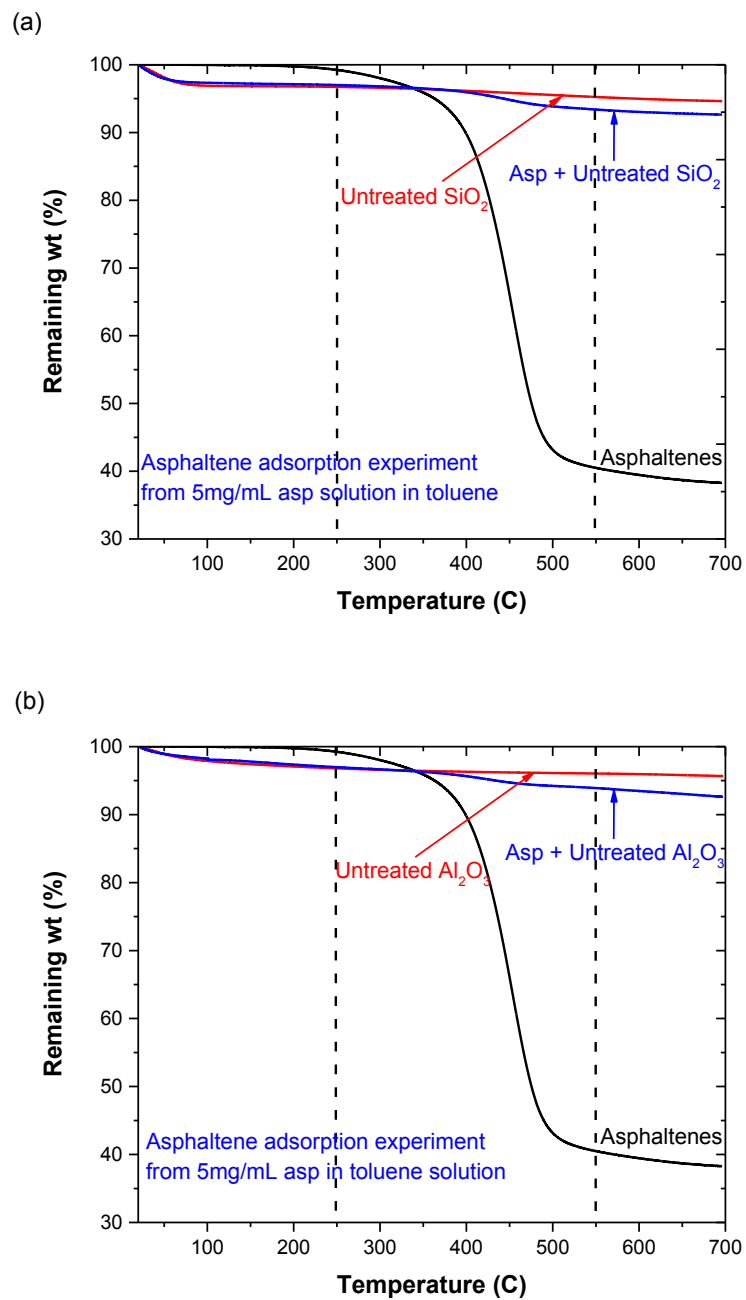


**Figure 3.16.** TGA curves obtained at 10 °C/min (a) Untreated  $\text{SiO}_2$  case; and (b) Untreated  $\text{Al}_2\text{O}_3$  case.

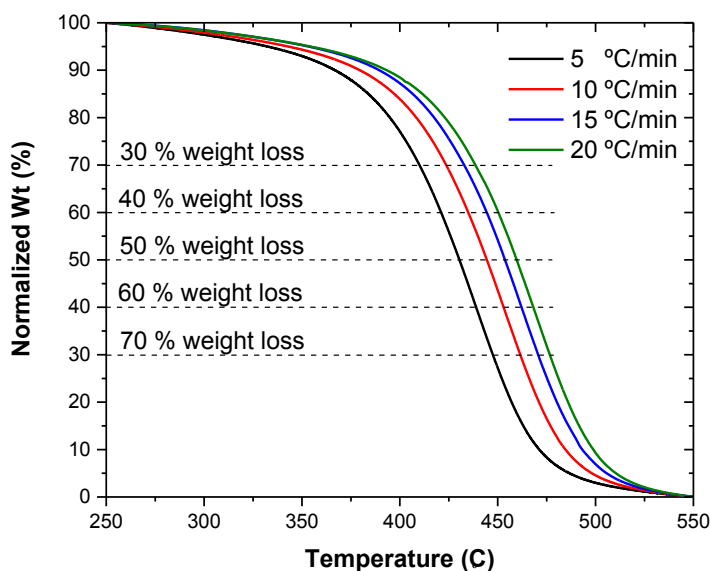


**Figure 3.17.** Normalized TGA curves of bulk asphaltenes at different heating rates.

As shown in Figure 3.17 for each normalized % weight loss shown by horizontal dashed lines, there are four intersects at four temperatures for decomposition at four different heating rates. The activation energy of decomposition was calculated using the method developed by Flynn and Wall, for well-resolved single step decompositions and first order decomposition kinetics, which is a rearrangement of the Arrhenius equation: **(106)**

$$E_a = - \frac{R}{b} * \frac{d(\text{Log } k)}{d(1/T)} \quad \text{Equation 3.8}$$

where  $E_a$  is the activation energy of decomposition (Kcal/mol),  $R$  is the gas constant (8.314 J/mol K),  $T$  is the temperature (K),  $k$  is the heating rate (°C/min) and  $b$  is a constant, which is a function of  $E/R \cdot T$  and has been reported to be between 0.457 and 0.494 for complex mixtures of hydrocarbon molecules such as pitch materials. **(107-109)**

Shown in Figure 3.18 are plots of the  $\log(\text{heating rate})$  as a function of the reciprocal of the absolute temperatures recorded (intercepts of Figure 3.17) at different weight loss values obtained for asphaltenes and asphaltenes adsorbed on silica. The data exhibit a linear behavior. According to

Flynn-Wall equation (Equation 3.8), the weight-loss-dependent decomposition activation energy can be calculated from the slope of Figure 3.18.

The values of decomposition activation energy obtained for the main stage of asphaltenes decomposition are shown in Table 3.7. Only  $E_a$  values corresponding to weight loss within 30-70 % are shown. Since the data were fitted by simple linear regression, the statistical goodness of fit ( $r^2$ ) is an indication of the quality of the data. **(103)** The  $r^2$  values obtained ranged from 0.981 to 0.999, indicating a good correlation and high quality of data.

Overall, an increase in  $E_a$  is observed as weight loss increases from 30 to 70 %. Differences in  $E_a$  values suggest a change in decomposition mechanism with weight loss. The increase in the  $E_a$  with weight loss, likely reflects more energetic processes when desorbing/decomposing stronger bonding species at high desorbing temperatures. **(103, 104, 107)** Collett et al. **(107)** performed thermo-gravimetric measurements of asphaltenes from heavy vacuum residuum oil. They also observed increase in the activation energy with temperature and suggested that the increase in the activation energy reflected a change in the nature of the rate-controlling step. In a similar study Trejo et al. **(104)** claimed that the increase in  $E_a$  as a function of reaction reflects changes in the strength of the bonds.

In the case of bulk asphaltenes the activation energy increases slightly during the course of decomposition, with values between 44 and 48 Kcal/mol. These  $E_a$  values for the decomposition of asphaltenes agree well with reported data. **(102-104)**

On the other hand, the  $E_a$  values for asphaltenes adsorbed on the untreated silica/ alumina particles in toluene are consistently lower (37-46 Kcal/mol for untreated silica and 37-48 Kcal/mol for untreated alumina) than that of bulk asphaltenes, suggesting that the asphaltenes adsorbed onto these particles were the ones with a lower chemical bond strength. In contrast, asphaltenes adsorbed on untreated silica/alumina particles in heptol show a higher activation energy (48-62 Kcal/mol for untreated silica and 52-60 Kcal/mol for untreated alumina) than that of bulk asphaltenes. This result indicates a difference in the chemical structure of the asphaltene molecules that were adsorbed from toluene and heptol solutions, when compared to the bulk asphaltenes. It is well known that the degree of asphaltene aggregation increases in poor solvents such as heptol. Hence the higher activation energies could be related to the stronger aggregation of asphaltenes that are adsorbed on the particle surfaces, reducing the selectivity of the adsorption process. As

anticipated, the decomposition activation energy values for the mixtures of bulk asphaltenes and untreated silica or alumina particles are very close to those of bulk asphaltenes.

From the foregoing discussion, it is demonstrated that thermo-gravimetric analysis can provide further insights on the decomposition kinetics of asphaltenes adsorbed on solid particles. Care should be taken, however, not to attempt to extract too much structural information from these data. Rather they should be used as supplement information.

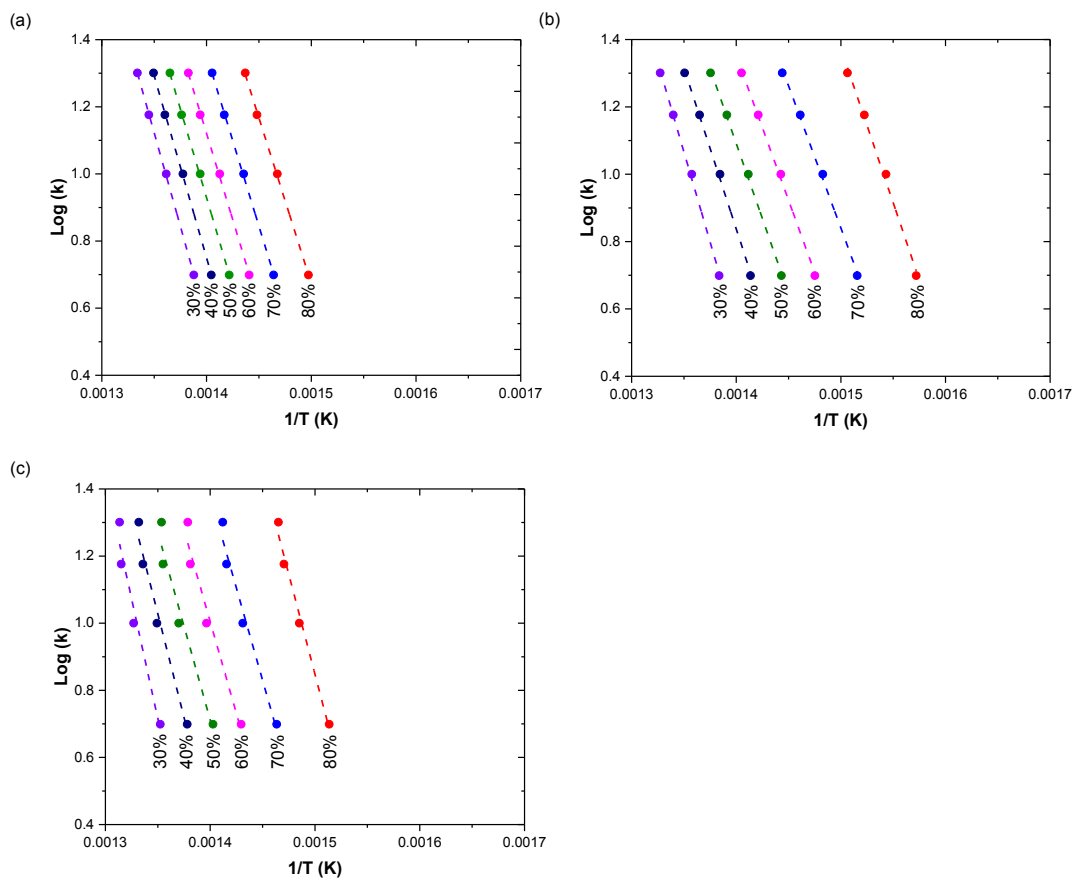


**Figure 3.18.** Log(heating rate) as function of the reciprocal of the temperature for constant weight loss: (a) Asphaltenes; (b) Asphaltenes adsorbed on untreated  $\text{SiO}_2$  from toluene solutions; and (c) Asphaltenes adsorbed on untreated  $\text{SiO}_2$  from heptol solutions.

**Table 3.7.** Activation energy values at various asphaltene decomposition weight loss

Weight loss (%)	$E_a$ (Kcal/ mol)						
	Asp	Asp-Unt.SiO <sub>2</sub> Tol	Asp-Unt.SiO <sub>2</sub> heptol	Mix Asp-Unt.SiO <sub>2</sub>	Asp-Unt.Al <sub>2</sub> O <sub>3</sub> Tol	Asp-Unt.Al <sub>2</sub> O <sub>3</sub> heptol	Mix Asp-Unt.Al <sub>2</sub> O <sub>3</sub>
30	44	37	48	41	37	52	41
40	45	37	48	42	38	54	42
50	46	39	49	44	40	52	44
60	47	42	54	46	43	56	47
70	48	46	62	49	48	60	50

### 3.4 Conclusions

The adsorption of asphaltenes on the surface of different particles was quantified using UV–Vis spectrophotometry. For the solid particles investigated, the adsorption of asphaltenes from toluene solution exhibits Langmuir type adsorption isotherms. The adsorption of asphaltenes was found to be strongly dependent on the type of particle, as shown by the saturation amount of asphaltenes adsorbed varying from 2.32 mg/m<sup>2</sup> on stainless steel to 0.52 mg/m<sup>2</sup> on untreated Al<sub>2</sub>O<sub>3</sub> particles. Such drastic difference was attributed to the differences in the surface morphology and chemical characteristics of the solids, which affects the nature of asphaltene adsorption.

Asphaltene adsorption was found to be significantly increased in heptol systems, suggesting that the adsorption process is highly dependent on the quality of the solvent. Heptol is a poor solvent that drives asphaltenes to form larger aggregates, leading to larger adsorption capacities of the particles studied in heptol. In contrast to the adsorption of asphaltenes from toluene solutions, asphaltene adsorption data from heptol solutions were fitted very well by the Freundlich model.

Thermally treated silica particles showed a lower asphaltene adsorption capacity than the untreated silica. From analysis of DRIFT spectroscopy it appears that asphaltene adsorption on silica particles is strongly mediated by surface silanol groups. In the case of thermally treated alumina particles the affinity towards asphaltene adsorption was enhanced by the thermal treatment of the surface. Unfortunately SEM imaging and DRIFT spectroscopy did not provide any information to

better explain the results. However, it was speculated that a higher adsorption capacity could be a consequence of changes in the configuration of the alumina particles, which may expose more Brønsted acid sites (Al–OH) or Lewis acid centres (Al<sup>3+</sup>) to enhance the adsorption.

Furthermore, the thermogravimetry was found to be a useful technique to study the decomposition kinetics of nC<sub>5</sub>-iC<sub>5</sub> asphaltenes adsorbed on solid particles. The observed difference in the decomposition activation energies of asphaltene and asphaltenes adsorbed on solid particles suggests structural differences among the asphaltene molecules adsorbed.

# Chapter 4 Adsorption of Asphaltenes on Silica, Alumina, Stainless Steel and Iron Oxide QCM-D Sensors

## 4.1 Introduction

Asphaltenes in bitumen and crude oil are defined as a solubility class, which is soluble in aromatic solvents, e.g. toluene, but insoluble in n-alkane, typically n-heptane. **(2, 9)** The undesirable adsorption of asphaltenes onto mineral and metallic surfaces has been considered as the source of severe issues found along the entire production chain of petroleum from the reservoir to the refinery. For instance, adsorption of asphaltenes on solids can lead to reduction in oil recovery, changes in wettability, plugging within pipelines, wells, reservoirs, fluid flow lines and surface facilities as well as catalyst fouling, which increases maintenance cost and causes a large economic loss. **(10)** However, taken advantage of the ability of asphaltene adsorption removal of undesirable asphaltene fractions from petroleum become feasible by selectively choosing suitable adsorbents. Therefore, understanding the adsorption kinetics of asphaltenes on various surfaces is of fundamental importance for understanding these issues encountered in oil industry.

In Chapter 3 we studied the adsorption of asphaltenes onto different solid particles using UV-Vis spectroscopy. The adsorption of asphaltenes was found to be dependent on the solvent type, morphology and chemical characteristics of the solids. Although the UV-Vis spectroscopy was found to be a useful technique to quantify the adsorption of asphaltenes on the surface of solid particles, it is also important to investigate the adsorption kinetics of asphaltenes and the structural (viscoelastic) properties of the adsorbed layer. Hence, in this study Quartz Crystal Microbalance with Dissipation (QCM-D) is used to elucidate the adsorption kinetics along with the state of the adsorbed asphaltene layer(s) on different solid surfaces.

QCM-D is a highly sensitive equipment that has been widely used to characterize bio-interfaces in the fields of biomaterials, molecular biology, cellulose, polymers, lipids, pharmaceuticals, proteins, and nanoparticles. **(110-118)** The use of QCM-D has been extended to studying the adsorption of asphaltenes onto different materials. **(24-26, 29, 69, 119, 120)** In an effort to improve

understanding of asphaltene-metal interactions, studies were carried out on gold surfaces. **(24-26, 29)** Studies with hydrophilic gold surfaces using QCM-D technique, although not practical in commercial applications, have provided valuable insights into the characteristics of asphaltene adsorption and desorption at various solution conditions. For example, Ekholm et al. **(25)** were among the first to investigate the adsorption of asphaltenes and resins on a gold surface using QCM-D techniques. They found that the adsorbed amount of asphaltenes from toluene and heptol (1:1 volume ratio of toluene and n-heptane) solutions was  $7.1 \text{ mg/m}^2$  and  $4.8 \text{ mg/m}^2$ , respectively. Moreover, they reported that asphaltenes from toluene solutions were adsorbed as small aggregates onto the surface at low concentrations. When injecting solutions of higher concentrations, further adsorption occurred, which was attributed to the strong tendency for aggregation of concentrated asphaltenes in bulk solution. Different from resins, asphaltenes were adsorbed irreversibly in multilayers onto the surface from toluene solutions. In another study, **(24)** the adsorption of asphaltenes onto gold surface was investigated using Quartz Crystal Microbalance (QCM) and X-ray photoelectron spectroscopy (XPS). The adsorption isotherms obtained exhibited characteristics of a single layer adsorption (Langmuir type I) over the concentration range investigated. The free energy of asphaltene adsorption and the thickness of the adsorbed layers were also estimated from QCM-D and XPS. Tavakkoli et al. **(26)** used QCM-D to investigate the adsorption kinetics and deposition tendency of asphaltenes from model oil systems in different depositing environments onto gold sensor crystals. The adsorbed layers showed a viscoelastic behavior and the adsorption isotherms were successfully fitted by the Langmuir type I model. Moreover, the results showed that increasing the ratio of n-heptane/toluene as a solvent increases the amount of asphaltenes deposited from the corresponding heptol solutions up to the onset of precipitation and decreases beyond that. They also studied the effect of the type of surfaces on the amount of asphaltenes adsorbed. Their results showed a higher adsorption capacities of asphaltenes on carbon steel and iron oxide surfaces than on gold surfaces.

The adsorption of asphaltenes onto other hydrophilic surfaces has also been assessed by the QCM-D technique. **(69, 119, 120)** Hannisdal et al. **(120)** studied the adsorption of asphaltenes and resins onto silica surfaces from asphaltene (1 wt. %), resin (1 wt. %) and asphaltene-resins (0.5 wt. % asphaltene + 0.5 wt. % resin) solutions in toluene. Frequency and dissipation responses were in the same range for asphaltenes and asphaltene-resins mixtures, with an adsorbed mass of  $5.6 \text{ mg/m}^2$  and  $6.4 \text{ mg/m}^2$ , respectively. In addition, resins showed a low degree of adsorption over

the timescale of the experiment. Later, Dudasova et al. (69) studied the adsorption of asphaltenes onto silica, titanium, alumina and FeOx coated quartz crystals in n-heptane-toluene and toluene solutions for concentrations in the range of 0.01–1.0 g/L. The amounts of asphaltenes adsorbed were in the range of 1.5–9.8 mg/m<sup>2</sup> for n-heptane-toluene solutions (50:50 vol %) and 1.7–9.1 mg/m<sup>2</sup> for toluene solutions. In another study, Farooq and coworkers (119) used QCM to study the adsorption of asphaltenes onto a silica surface from 1 g/L asphaltene solutions in toluene. They found that the amount of asphaltenes adsorbed was  $5.3 \pm 0.8$  mg/m<sup>2</sup>. They also investigated desorption of asphaltenes upon exposure to various low salinity aqueous solutions of variable salt concentrations and valency of cations.

As can be seen, within the published studies of asphaltene adsorption kinetics using the QCM-D technique, work has been carried out mainly on gold and silica surfaces, while asphaltenes generally adsorb on different minerals, catalysts, pipeline steels, etc. in oil industry. Investigation on the adsorption behaviour of asphaltenes on surfaces similar to what is used in industry would provide more insights into the asphaltene-surface interactions and mechanism of asphaltenes deposition during oil production.

This clear link needed has motivated the present work to systematically study the adsorption of asphaltenes from their solutions onto surfaces with diverse chemistry and hydrophilicity using QCM-D techniques, allowing real time monitoring of interactions taking place at solution-solid interfaces. To understand the effect of concentration on asphaltene adsorption kinetics, solutions of 0.01 and 1 mg/mL asphaltene concentrations were used for the adsorption experiments. Furthermore, to study the effect of the solubility state of asphaltenes (aromaticity of the solvent) on the amount of asphaltenes adsorbed, asphaltenes in n-heptane-toluene (1:1 ratio by volume) mixture solutions were also utilized. Results are discussed and compared with the adsorption of asphaltenes onto particles studied by UV–Vis spectrophotometry presented in Chapter 3.

## **4.2 Experimental**

### **4.2.1 Quartz Crystal Microbalance with Dissipation (QCM-D)**

#### **4.2.1.1 Principle**

QCM-D is an extremely sensitive technique, consisting of a thin piezoelectric quartz crystal disc sandwiched between two electrodes. One side of the disc is coated with a thin gold film. Upon excitation by AC voltage, the crystal oscillates at its main resonance frequency and its odd-order

overtone. In addition to adsorbed mass (ng/cm<sup>2</sup> sensitivity), measured as changes in the resonance frequency of the oscillation of the quartz crystal, the dissipation parameter provides novel insights on structural (viscoelastic) properties of adsorbed layers as they build up or change on the sensor surface. Dissipation occurs when the external driving voltage to the crystal is turned off and the energy from the oscillating crystal dissipates from the system. **(121)**

According to literature, when the quartz crystal is exposed to a liquid, there is a decrease in frequency that is dependent upon the viscosity and density of the liquid. Kanazawa et al. **(122)** derived an expression that estimates the frequency change ( $\Delta F$ ) induced by immersing the crystal in a liquid medium:

$$\Delta F = -f_0^{3/2} * \sqrt{\frac{\mu_L * \rho_L}{\rho_q * \mu_q * \pi}}$$

**Equation 4.1**

where  $f_0$  is the resonant frequency of unloaded crystal (Hz),  $\mu_L$  is the viscosity of the liquid in contact with the electrode (N·s/m<sup>2</sup>),  $\rho_L$  is the density of the liquid in contact with the electrode (Kg/m<sup>3</sup>),  $\rho_q$  is the density of quartz (2648 Kg/m<sup>3</sup>) and  $\mu_q$  is the shear modulus of quartz (2.947× 10<sup>10</sup> Pa).

When something is adsorbed onto the crystal, the frequency decreases. In the case of rigid films, well known Sauerbrey equation, that establishes a linear relationship between the added (deposited) mass on the crystal surface and the resonance frequency shift of the crystal, can be used to calculate the mass of the adhering layer: **(123)**

$$\Delta m = -\frac{C * \Delta f}{n}$$

**Equation 4.2**

where  $\Delta m$  is the adsorbed mass or mass uptake (mg/m<sup>2</sup>),  $n$  is the number of harmonic overtones of the crystal sensor ( $n= 1, 3, 5... 13$ ),  $\Delta f$  is the shift in frequency signal and  $C$  is the sensitivity constant of the crystal. For the 5 MHz quartz crystals used in this study,  $C= 0.177$  mg/ (Hz·m<sup>2</sup>).

The Sauerbrey relation is valid under the following conditions: (a) the mass adsorbed is evenly distributed over the crystal, and (b)  $\Delta m$  is much smaller than the mass of the sensor crystal itself

(<1 %). However, in some situations the adsorbed film is not rigid and the Sauerbrey relation becomes invalid. A “soft” (viscoelastic) film will not fully couple to the oscillatory motion of the crystal and the oscillation of crystals will be dampened. A loosely adsorbed layer leads to an increase in dissipation due to the frictional energy created when the adsorbed film slips on the electrode and internal friction in the film which is characteristic of viscous layers. **(25)** With a substantial change in the sensor dissipation, usually considered to be > 5 % of the frequency shift, the apparent mass of the deposited viscoelastic film can be modeled using Voigt equation. **(124, 125)**

#### 4.2.1.2 Instrumentation and QCM-D Crystals

A dissipative quartz crystal microbalance device, Q-Sense E4 (Biolin Scientific AB, Sweden) was used to study the adsorption behavior of asphaltenes onto quartz crystals coated with different materials. The Q-Sense E4 unit is a temperature controlled chamber equipped with removable flow modules made of aluminum (shell) and titanium (liquid contact surfaces). Solvent resistant o-rings and sealing gaskets were used in the experiments. Sensor quartz crystals used in this study were of AT-cut family, top coated with different materials through physical vapor deposition method by the manufacturer. Sensors have a diameter of 14 mm and fundamental frequency of 5 MHz. The specifications of crystal sensors used in this study are given in Table 4.1.

**Table 4.1.** Sensors specifications (Provided by manufacturer)

Top coating material	Description	Thickness of coating (nm)
Silicon dioxide (SiO <sub>2</sub> )	QSX 303	50
Aluminum oxide (Al <sub>2</sub> O <sub>3</sub> )	QSX 309	100
Stainless Steel (SS2343)	QSX 304	100
Iron oxide (Fe <sub>3</sub> O <sub>4</sub> )	QSX 326	100

#### 4.2.2 Asphaltene Solutions

Asphaltenes were extracted from coker feed bitumen, following the procedure shown in section 3.2.1.2. Prior to preparation of asphaltene solutions, toluene and heptol (1:1 by volume n-

heptane:toluene mixture) solvents were degassed using the sonicator bath for 30 min. To prepare the asphaltene stock solution, a known amount of asphaltenes was added to the degassed solvent. The mixture was sonicated for 30 min and then centrifuged at 14000 rpm for 30 min using the Sorvall WX Ultra Series centrifuge (Thermo Scientific). Undissolved asphaltene particles, if any, were removed by filtering the supernatant using a P5 Fisherbrand filter paper. Thereafter the filtered solution was sonicated for 30 min. The asphaltene stock solution was then diluted to the required concentrations for the experiments. Diluted solutions were further sonicated for 30 min to reduce the risk of forming air bubbles in the measurement system.

#### **4.2.3 Asphaltene Adsorption Experiments**

Before each experiment all contaminants were removed from the surface of new quartz crystal sensors by following the conventional cleaning protocol suggested by the manufacturer, with the exact procedures varying depending on the top coating material.

Before experiments, flow modules were sonicated for 1 hour in 1 wt. % Hellmanex III (Hellma Analytics) solution and subsequently rinsed with excess Milli-Q water and blow-dried with nitrogen gas. O-rings and sealing gaskets were immersed in the solvent of interest, either toluene or heptol (1:1 volume mixture), at least 24 h before the experiment. Electrodes were kept in a desiccator, when not in use. They were not subjected to any cleaning procedure, as recommended by the vendor, since there were no direct contacts of the electrodes with any fluid during the experiments.

The system was assembled by mounting a clean sensor in the flow module, with its active surface down, resting on the o-ring. The flow module was then connected to the tubing and the peristaltic pump, and placed inside the chamber. The Q-Sense E4 unit was inverted in order to eliminate concern of asphaltene deposition due to gravity. To make sure that the sensor is correctly mounted and not damaged, the resonance frequencies of the sensors were first measured in air. In air, the frequency of the 1st overtone should be very close to the fundamental resonance frequency (5 MHz). For all the experiments the fluid temperature was maintained at  $22\text{ }^{\circ}\text{C} \pm 0.02\text{ }^{\circ}\text{C}$  and the flow rate at  $80\text{ }\mu\text{L}/\text{min}$ .

Asphaltene adsorption experiments were performed with the following procedures: Initially the chamber was flushed with solvent (toluene or heptol, depending on the experiment) in order to establish a baseline. The baseline was considered to be stable when the fluctuations in the

frequencies were less than  $\pm 1$  Hz for 10 min. To test the accuracy of the QCM-D before each measurement, the frequency shift obtained when changing the sensor environment from air to liquid was verified and compared with the estimated values from equation 4.1, -472 Hz and -535 Hz for toluene and heptol (1:1 by volume n-heptane:toluene mixture) solvents, respectively.

After a stable baseline in pure solvent was reached, asphaltene solutions were injected into the chamber in a stepwise manner, from low to high concentrations with an injection time of 60 min for each solution. Desorption study was done by injecting pure solvent after the most concentrated asphaltene solution was introduced into the flow cell. To minimize sensor disturbance, the peristaltic pump was stopped temporarily while changing the fluids, making sure the absence of air bubbles in the system.

Data of frequencies and energy dissipations for all overtones ( $n= 1, 3, 5, 7, 9, 11$  and  $13$ ) were collected. It is pertinent to mention that different overtones have different surface sensitivities. The higher order overtones ( $n= 3, 5, 7$ ) are more sensitive to changes in the film properties close to the surface than the fundamental frequency ( $n= 1$ ). Therefore in subsequent discussions, the frequency and dissipation values based on the average of 3<sup>rd</sup>, 5<sup>th</sup> and 7<sup>th</sup> overtones are reported. Also, only the results corresponding to the 5<sup>th</sup> overtone are shown in Figures 4.1-4.5.

#### **4.2.4 Wettability of Quartz Crystals-Contact Angle**

The wettability changes on the quartz crystal surfaces upon asphaltene adsorption were determined by contact angle measurements. The contact angle of bare and asphaltene covered quartz crystals was measured using sessile drop method on an Attension Theta Optical Tensiometer (Biolin Scientific AB, Sweden) equipped with a high-resolution digital camera. The images were recorded after placing a water drop (Millipore milli-Q system,  $\Omega= 18.2$  M<sub>cm</sub>) on the quartz crystal surface with a syringe. The captured images were analyzed with a drop profile fitting method in order to determine the contact angle through the Young–Laplace equation. **(98)** The contact angle reported corresponds to the mean value of left and right three-phase contact points of the water droplet. For each sample, at least three measurements were performed at three different locations on a sensor surface.

#### 4.2.5 X-ray Photoelectron Spectroscopy (XPS)

nC<sub>5</sub>-iC<sub>5</sub> asphaltenes and quartz crystal sensors before and after being exposed to asphaltene solutions in toluene or heptol (n-heptane-toluene mixtures of 1:1 ratio by volume) were analyzed by XPS at the Alberta Centre for Surface Engineering and Science (ACSES), University of Alberta.

The XPS technique was used to investigate the elemental composition and chemical state of elements present on the surface of these samples, in order to identify key functional groups from asphaltenes interacting with the solid surfaces studied.

The XPS data was processed using Casa XPS software. Peak deconvolution of high resolution scans was done to obtain peak positions and intensities. Depending on the nature of the spectrum Shirley type or linear background was subtracted and the photoemission features were fitted using the Gaussian-Lorentzian functions. The energy scale was calibrated using the binding energy of C1s photoelectron peak at 284.8 eV as the reference.

### 4.3 Results

#### 4.3.1 Adsorption of Asphaltenes on Solid Surfaces using QCM-D Technique

##### 4.3.1.1 Effect of Type of Surfaces

Shown in Figure 4.1 are plots of the frequency and dissipation as a function of time for the adsorption of asphaltenes on four different solid surfaces (silicon dioxide, aluminum oxide, iron oxide and stainless steel) from asphaltene in toluene solutions with concentrations in the range of 0.01–0.3 mg/mL. Overall, when the solid surfaces are exposed to 0.01 mg/mL asphaltene in toluene solutions, there is a sharp decrease in the resonance frequency, suggesting a rapid adsorption of asphaltenes onto the solid surfaces studied. For silicon dioxide the frequency signal is stabilized after few min and no further shift in the resonance frequency seems to occur upon injection of 0.05 and 0.1 mg/mL asphaltene in toluene solutions, indicating saturation adsorption of asphaltenes on the silica surface. (119) Interestingly, injection of 0.3 mg/mL asphaltene solution in toluene leads to a slight increase in the frequency shift, suggesting that a part of the adsorbed asphaltenes was released from the surface. A possible explanation is that 0.3 mg/mL asphaltene solution in toluene could solubilize part of the adsorbed asphaltene molecules, resulting in less mass of asphaltenes adsorbed onto this surface. Regarding aluminum oxide, it is worth noting that a decrease in the resonance frequency is observed when 0.01 and 0.05 mg/mL asphaltene in toluene

solutions were injected. The injection of 0.1 and 0.3 mg/mL asphaltene in toluene solutions leads to a slight decrease in the frequency signal, indicating more or less asphaltene saturation adsorption of asphaltenes on the alumina surface.

Unlike the silicon dioxide and aluminum oxide surfaces, changes in the resonance frequency for the adsorption of asphaltenes onto iron oxide and stainless steel surfaces do not level off within the concentration range investigated. This result suggests that the adsorption sites of these surfaces were not saturated with asphaltenes or that a multilayer asphaltene adsorption occurred to some extent. **(25)** The multilayer adsorption of asphaltenes onto iron oxide and stainless steel surfaces from toluene solutions could be explained by the metal-oxygen bonds that may be formed between these surfaces and asphaltene molecules. Metal-oxygen compounds could form large associated asphaltene structures that may block part of the adsorption sites of these surfaces which will lead to a multilayer adsorption.

The corresponding dissipation factor is also shown in Figure 4.1. As can be seen, very small increase in dissipation ( $2 \times 10^{-6}$  at most) occurred as asphaltenes adsorbed onto the surfaces tested. Moreover, there were small increases in frequency and slight drops in dissipation during the toluene injection performed at the end of the experiment. The result indicates that weakly bounded asphaltenes were removed and remaining asphaltenes formed a more compact layer on the crystal surface. Since the resonance frequency values showed a negligible spreading at different overtones,  $n=3,5,7$  (raw data not shown) and dissipation changes were small, indicating the formation of a rigid layer, **(126)** the Sauerbrey equation (Equation 4.2) was used to determine the mass of asphaltenes adsorbed onto the surfaces studied (Table 4.2). Iron oxide showed the highest adsorption capacity at  $5.7 \text{ mg/m}^2$ . This value was slightly higher than the adsorption capacity of asphaltenes on iron ( $4.9 \text{ mg/m}^2$ ) observed by Balabin et al. **(73)** They used a combination of near-infrared (NIR) spectroscopy, Raman microscopy, and atomic force microscopy (AFM) to investigate the adsorption of asphaltenes on an iron (Fe) surface from asphaltene solutions in benzene.

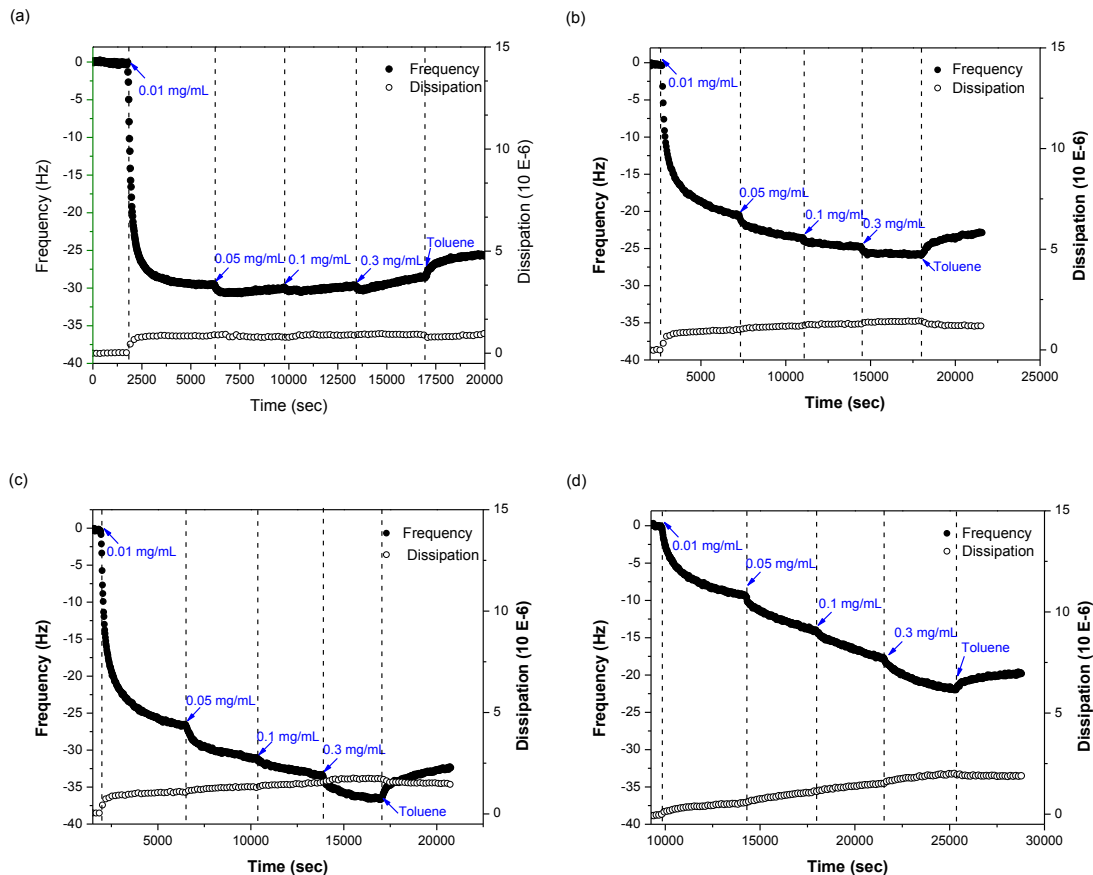


**Figure 4.1.** Frequency and dissipation change as a function of time for the adsorption of asphaltenes from asphaltene in toluene solutions on quartz crystal surfaces coated with: (a) Silicon dioxide; (b) Aluminum oxide; (c) Iron oxide; and (d) Stainless steel.

The amount of asphaltenes adsorbed on silicon dioxide and aluminum oxide surfaces was found to be  $4.6 \text{ mg/m}^2$  and  $4.0 \text{ mg/m}^2$ , respectively. Such finding is in good agreement with previously published data in literature. Dudasova et al. (69) studied the adsorption of asphaltenes extracted from six different crude oils onto silicon dioxide and aluminum oxide surfaces from asphaltene in toluene solutions. They reported that the maximum amount of asphaltenes adsorbed was in the range of  $2\text{-}9 \text{ mg/m}^2$  for silicon dioxide and  $2.3\text{-}8.7 \text{ mg/m}^2$  for aluminum oxide. In another QCM study, the amount of asphaltenes adsorbed onto silica surface from  $1 \text{ g/L}$  asphaltene solution in toluene was found to be  $5.3 \pm 0.8 \text{ mg/m}^2$ . (119)

Furthermore, stainless steel showed the least adsorption capacity at  $3.4 \text{ mg/m}^2$ . This value is slightly higher than the amount of asphaltenes adsorbed on stainless steel powder from toluene

solutions (2.7 mg/m<sup>2</sup>), obtained using UV-Vis spectrophotometry, reported by Alboudwarej et al. (22) The observed difference in the amount of asphaltenes adsorbed onto the surfaces studied, suggest that the adsorption capacity of asphaltene on the surfaces investigated strongly depends on the surface type. As can be seen in Table 4.2, less than 10 % of asphaltenes were desorbed after toluene rinsing, which suggests that the binding of the asphaltene adsorbed layer to the surface is very strong. (69)

**Table 4.2.** Mass of asphaltenes adsorbed from asphaltene in toluene solutions onto quartz crystal surfaces coated with different materials

Substrate	Mass of asphaltenes adsorbed (mg/m <sup>2</sup> )				
	0.01 mg/mL	0.05 mg/mL	0.1 mg/mL	0.3 mg/mL	After toluene rinsing
SiO <sub>2</sub>	5.4	5.4	5.4	5.2	4.6
Al <sub>2</sub> O <sub>3</sub>	3.6	4.1	4.3	4.5	4.0
Fe <sub>3</sub> O <sub>4</sub>	4.6	5.4	5.8	6.4	5.7
Stainless Steel	1.6	2.4	3.1	3.8	3.4

The modification of the surfaces studied upon asphaltene adsorption is evident by considering the changes in surface wettability. As shown in Table 4.3, asphaltene covered quartz crystal surfaces exhibit higher contact angle values than bare quartz crystal surfaces, suggesting that the surfaces investigated became more hydrophobic due to the adsorption of asphaltenes from toluene solutions. However, no evident correlation between the hydrophobicity of the substrates studied and their adsorption properties was found.

Shown in Figure 4.2 are the plots of the amount of asphaltenes adsorbed onto the surfaces studied as a function of time. It is important to mention that the data corresponding to the toluene baseline was ignored since we were interested in observing the asphaltene adsorption kinetics. As can be seen, there was a sharp increase in the amount of asphaltenes adsorbed upon switching to asphaltene in toluene solutions. This was followed by a gradual increase in the adsorbed mass as solutions of higher asphaltene concentration were injected. The adsorption of asphaltenes onto

silicon dioxide and aluminium oxide appeared to approach an equilibrium state. However, steady state adsorption over the tested period of time and concentrations was not reached on both iron oxide and stainless steel surfaces, which was evident by the trajectory of the plots.

**Table 4.3.** Contact angle of bare and asphaltene covered quartz crystal surfaces

Substrate	Contact angle (degree)		
	Blank	After adsorption from toluene solutions	After adsorption from heptol solutions
SiO <sub>2</sub>	21± 3	81± 1	85± 2
Al <sub>2</sub> O <sub>3</sub>	35± 5	85± 2	73± 8
Fe <sub>3</sub> O <sub>4</sub>	62± 3	92± 3	89± 4
Stainless Steel	57± 1	84± 1	86± 6

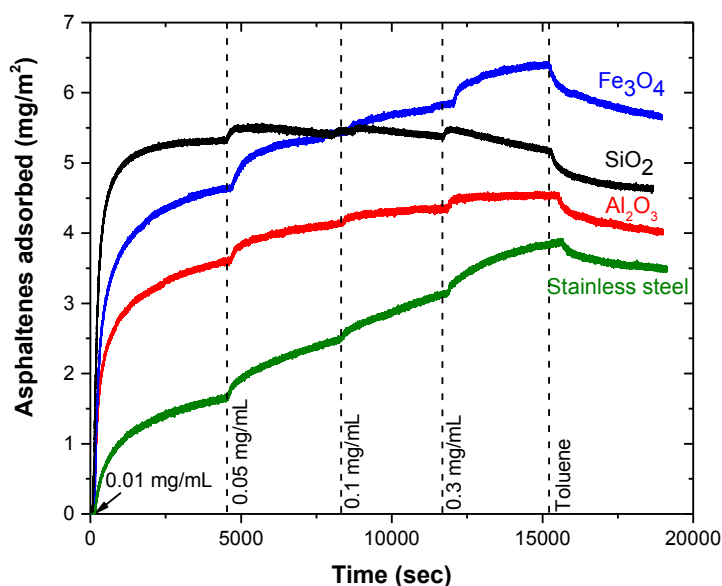


**Figure 4.2.** Asphaltene adsorption kinetics onto quartz crystal surfaces coated with different materials from asphaltene in toluene solutions.

#### 4.3.1.2 Effect of Solvents Properties

In order to evaluate the effect of the aromaticity of the solvent on asphaltene adsorption kinetics, the adsorption of asphaltenes from heptol (1:1 volume mixture of n-heptane and toluene) solutions

onto quartz crystals with different coating materials (silicon dioxide, aluminum oxide, iron oxide and stainless steel) was studied. Figure 4.3 shows the QCM-D response for the adsorption of asphaltenes from heptol solutions on solid surfaces studied. Overall, there is an immediate initial response featured by a drop in the resonance frequency, which is an indication of a very rapid adsorption of asphaltenes onto the surfaces tested. Furthermore, aluminum oxide, iron oxide and stainless steel surfaces show a gradual decrease in the frequency response with subsequent additions of asphaltene solutions. For silicon dioxide surface, the adsorption behavior shows negligible shifts in the resonance frequency after the injection of 0.05 mg/mL, suggesting saturation of asphaltene adsorption on the silica surface. **(119)**

Although, the adsorption of asphaltenes onto stainless steel surface was performed within a higher asphaltene concentration range (0.01-1 mg/mL) no leveling off in the frequency shift with increasing asphaltene concentration was observed. The fact that the frequency signal does not reach equilibrium for iron oxide, stainless steel and aluminum oxide suggests a multilayer adsorption of asphaltenes from heptol solutions. The multilayer adsorption of asphaltenes from n-heptane-toluene solutions has been reported in previous investigations. **(27, 127, 128)**

From Figure 4.3, it is also seen that the dissipation shift increases slightly by increasing asphaltene concentration of solutions injected, but decreases and stabilizes around a constant value upon rinsing the surface of the crystals tested with heptol. The adsorbed films show a rigid behavior due to the small dissipation changes (lower than  $6 \times 10^{-6}$ ) and the overlapping of all the overtones in frequency responses (raw data not shown). Hence the mass of the adsorbed asphaltene layer(s) was also calculated using the Sauerbrey equation (Equation 4.2) which is summarized in Table 4.4.

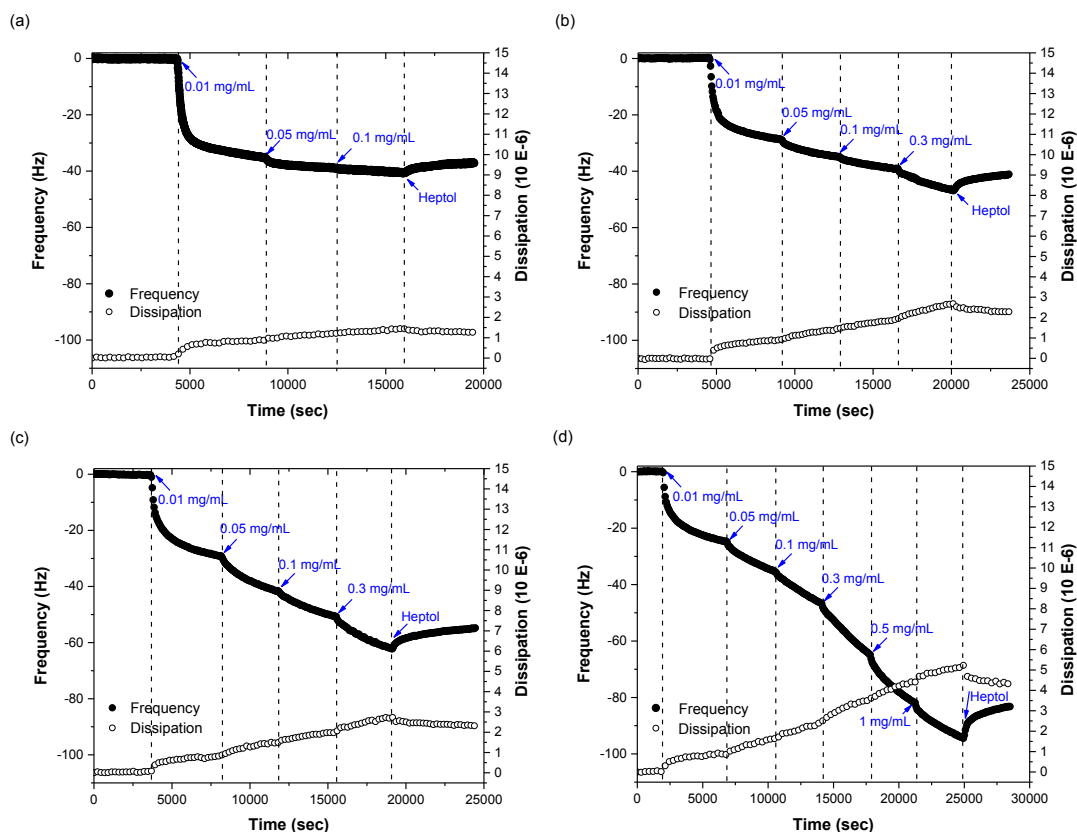


**Figure 4.3.** Frequency and dissipation change as a function of time for the adsorption of asphaltenes from asphaltene in heptol (1:1 volume ratio) solutions on quartz crystal surfaces coated with: (a) Silicon dioxide; (b) Aluminum oxide; (c) Iron oxide, and (d) Stainless steel.

**Table 4.4.** Mass of asphaltenes adsorbed from asphaltene in heptol (1:1 volume ratio) solutions onto quartz crystal surfaces coated with different materials

Substrate	Mass of asphaltenes adsorbed (mg/m <sup>2</sup> )						After heptol rinsing
	0.01 mg/mL	0.05 mg/mL	0.1 mg/mL	0.3 mg/mL	0.5 mg/mL	1.0 mg/mL	
SiO <sub>2</sub>	6.1	6.8	7.1	-	-	-	6.5
Al <sub>2</sub> O <sub>3</sub>	4.9	6.0	6.6	7.8	-	-	6.9
Fe <sub>3</sub> O <sub>4</sub>	5.0	7.1	8.6	10.5	-	-	9.3
Stainless Steel	4.2	5.9	7.8	10.8	13.7	15.7	13.9

For comparison, the amount of asphaltenes adsorbed after the injection of 0.1 mg/mL asphaltene solutions in toluene and heptol solvents is shown in Figure 4.4. As can be seen, the amount of asphaltenes adsorbed is higher in heptol solutions than in toluene solutions. Such difference in the adsorption capacity of the surfaces studied could be related to the dispersive state of asphaltenes in the liquid medium. Heptane is a poor solvent that can enhance the aggregation of asphaltenes in bulk solution. (71) In n-heptane-toluene mixtures the degree of asphaltene self-association is expected to be significantly higher than that in toluene. (129) Therefore, it is very plausible that the asphaltene adsorbed layer is formed by asphaltenes in aggregate state which will lead to higher mass of asphaltenes adsorbed. (29)

Similar to the results in toluene, the adsorbed asphaltene layers from heptol solutions led to an increase in the hydrophobicity of solid surfaces studied, as shown by increase in the contact angle (Table 4.3). Nonetheless, we did not find any correlation between the amount of asphaltenes adsorbed and the wettability of the quartz crystal surfaces investigated.

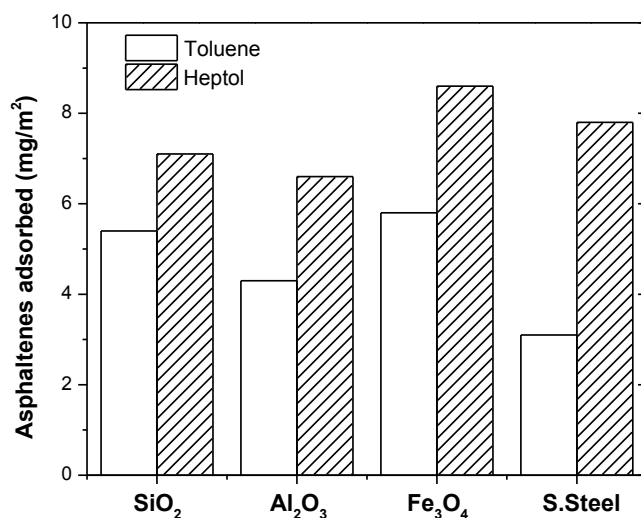


**Figure 4.4.** Variation of the amount of asphaltenes adsorbed from 0.1 mg/mL asphaltene solutions in toluene and heptol (1:1 volume ratio) on quartz crystal surfaces coated with different materials.

Shown in Figure 4.5 are plots of the mass of asphaltenes adsorbed onto the surfaces studied as a function of time. It can be seen that the mass of asphaltenes adsorbed increases dramatically with the injection of more concentrated asphaltene solutions. Unlike silicon dioxide surface, which seems to become saturated, the other solid surfaces tested (aluminum oxide, iron oxide and

stainless steel) exhibit a continuous increase in the amount of asphaltenes adsorbed over the time range investigated, which has been attributed to a multilayer adsorption of asphaltenes. (29, 130)

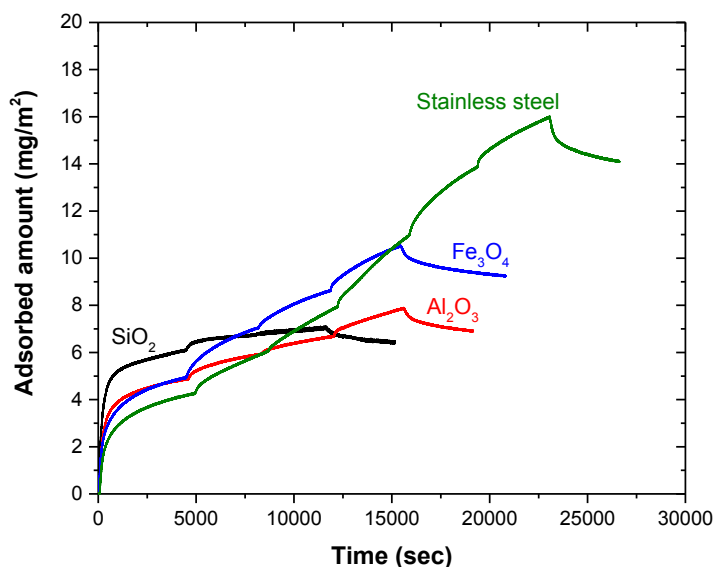


**Figure 4.5** Asphaltene adsorption kinetics from heptol (1:1 volume ratio) solutions onto quartz crystal surfaces coated with different materials.

This study demonstrates that QCM-D is a suitable technique to investigate the adsorption of asphaltenes onto different solid surfaces. However, comparison between the amount of asphaltenes adsorbed on different solid surfaces from toluene solutions, obtained by QCM-D and UV-Vis spectroscopy (Chapter 3), shows that the adsorption capacities of asphaltene on silicon dioxide, aluminum oxide and stainless steel surfaces using QCM-D (3.4-4.6 mg/m<sup>2</sup>) are consistently higher than the adsorption capacities of asphaltene on silica, alumina and stainless steel particles obtained by UV-Vis spectroscopy (0.5-2.3 mg/m<sup>2</sup>). Such finding is in good agreement with reported data by Dudasova et. al. (20, 69) who investigated the adsorption of asphaltenes (of different source) from toluene solutions onto hydrophilic silica, alumina, FeOx, and titanium surfaces using UV-Vis spectroscopy and QCM-D technique. The amount of asphaltenes adsorbed by QCM-D and UV-Vis spectroscopy were in the range of 1.7-9.1 mg/m<sup>2</sup> and 0.26-3.78 mg/m<sup>2</sup>, respectively.

QCM-D and UV-Vis spectroscopy techniques have their advantages and limitations. Although both techniques are suitable for quantitative measurements, QCM-D as used in this study does not account for effects of porosity, layers typically found in clays, surface chemistry and morphology

that can be studied using UV-Vis spectroscopy. However, QCM-D is a powerful tool that enables to track the adsorption kinetics at various solution conditions and viscoelastic properties of the adsorbed layer. To our knowledge, there is still no explanation in the available literature for the differences observed in the mass of asphaltenes adsorbed obtained using these techniques.

### **4.3.2 XPS Spectral Analysis**

Although the study of the adsorption kinetics of asphaltenes onto different solid surfaces is a key step in understanding the mechanism of adsorption, it is equally important to analyze the surface chemical composition of both asphaltenes and solid materials to identify the chemical groups involved in asphaltene-surface interactions. A few investigators have examined the chemical groups in asphaltenes that mediate their adsorption onto different surfaces through X-ray photoelectron spectroscopy (XPS). Rudrake et al. (24) analyzed bulk and adsorbed asphaltenes on gold surfaces used for QCM adsorption experiments. Abdallah et al. (28) used XPS to characterize the adsorbed asphaltene layer on a stainless steel surface. Both studies identified the presence of C1s, O1s, S2p and N1s peaks which were linked to the presence of different types of functional groups such as carboxylic, pyrrolic, pyridinic and thiophenic on the asphaltenes adsorbed on solid surfaces, and suggested polar interaction forces to be responsible for the adsorption of asphaltenes. (24, 28) In this study, XPS is used to characterize the surface chemistry of the quartz crystal sensors before and after the adsorption of asphaltenes.

#### **4.3.2.1 Survey Spectra**

Shown in Figure 4.6 are the XPS survey scan spectra for bare and asphaltene covered quartz crystal surfaces. As can be seen, the intensity of the oxygen peak decreases with the adsorption of asphaltenes, whereas the carbon signal grows in intensity upon the adsorption of asphaltenes on the solid surfaces studied. It is worth noting that the spectra for blank substrates contain weak signals in the C1s region, related to either environment carbons of XPS instrument and/or organic residue that cannot be removed by the solvent-cleaning step. In addition, the presence of O Auger feature (OKLL) on the spectra is attributed to the relaxation of the excited ions remaining after photoemission. (131)

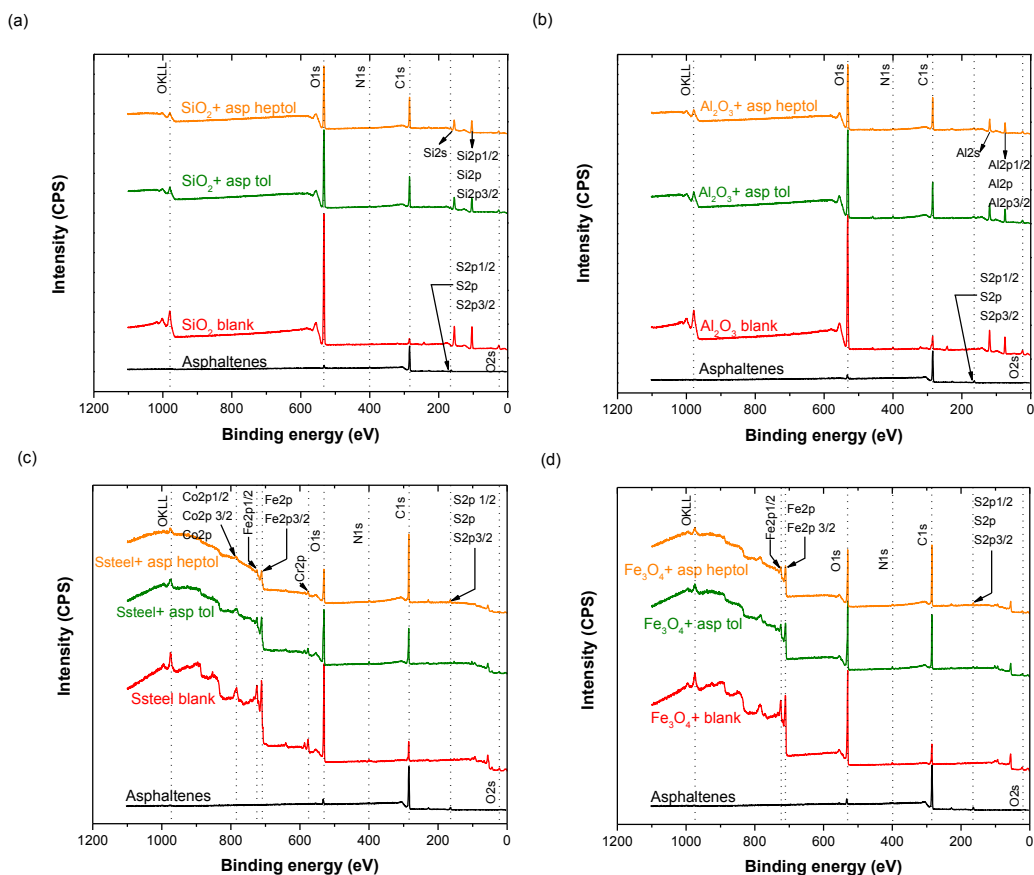


**Figure 4.6.** XPS survey spectra of bulk asphaltenes and quartz crystal sensors before and after being exposed to asphaltene solutions in toluene or heptol: (a)  $\text{SiO}_2$ ; (b)  $\text{Al}_2\text{O}_3$ ; (c) Stainless steel; and (d)  $\text{Fe}_3\text{O}_4$ .

The atomic surface elemental composition of bulk asphaltenes, bare and asphaltene covered quartz crystal surfaces is summarized in Table 4.5. Iron oxide surface shows the highest atomic concentration of O. As anticipated, asphaltenes show the highest C content. The adsorption of asphaltenes is evident by higher atomic concentration of C and lower atomic concentration of O on asphaltene covered surfaces, when compared to bare quartz crystal surfaces.

Furthermore, the Si/O, Al/O and Fe/O atomic ratios (Table 4.6) do not change after the adsorption of asphaltenes onto silicon dioxide, aluminum oxide and iron oxide surfaces, respectively. Such finding suggests that the adsorbed asphaltene layers are sufficiently thin (lower than penetration depth) or adsorbed in patches that allowed substrate surface to be probed.

However, the Fe/O atomic ratio decreased by 70 % in the asphaltene covered stainless steel surfaces, suggesting that the iron sites were preferentially covered by the asphaltenes adsorbed. Another notable result is that the Co/O atomic ratio reaches zero values after the adsorption of asphaltenes onto stainless steel surface, while the Cr/O atomic ratio does not change, indicating that the asphaltene layer was able to cover all the cobalt sites present on this surface

**Table 4.5.** Atomic composition of bulk asphaltenes, bare and asphaltene covered quartz crystal surfaces

	<b>O1s</b>	<b>N1s</b>	<b>C1s</b>	<b>S2p</b>	<b>P2p</b>	<b>Si2p</b>	<b>Al2p</b>	<b>Cr2p</b>	<b>Co2p</b>	<b>Fe2p</b>
SiO <sub>2</sub> blank	51	0	7	0	0	41	-	-	-	-
SiO <sub>2</sub> + asp tol	34	1	38	1	0	27	-	-	-	-
SiO <sub>2</sub> + asp heptol	32	1	40	1	0	26	-	-	-	-
Al <sub>2</sub> O <sub>3</sub> blank	48	1	12	1	0	-	39	-	-	-
Al <sub>2</sub> O <sub>3</sub> + asp tol	34	1	33	2	0	-	30	-	-	-
Al <sub>2</sub> O <sub>3</sub> + asp heptol	30	1	38	2	0	-	29	-	-	-
Ssteel blank	52	1	25	0	-	-	-	2	3	17
Ssteel+ asp tol	39	2	54	0	-	-	-	1	0	4
Ssteel+ asp heptol	20	1	74	3	-	-	-	1	0	2
Fe <sub>3</sub> O <sub>4</sub> blank	56	2	31	0	0	-	-	-	-	12
Fe <sub>3</sub> O <sub>4</sub> + asp tol	33	2	59	2	0	-	-	-	-	5
Fe <sub>3</sub> O <sub>4</sub> + asp heptol	25	1	67	2	0	-	-	-	-	4
Asphaltenes	4	1	92	4	0	0	0	0	0	0

**Table 4.6.** Atomic ratio of bulk asphaltenes, bare and asphaltene covered quartz crystal surfaces

	Si/O	Al/O	Fe/O	Co/O	Cr/O
SiO <sub>2</sub> Blank	0.81	0	0	0	0
SiO <sub>2</sub> + Asp Tol	0.82	0	0	0	0
SiO <sub>2</sub> + Asp heptol	0.82	0	0	0	0
Al <sub>2</sub> O <sub>3</sub> Blank	0	0.80	0	0	0
Al <sub>2</sub> O <sub>3</sub> + Asp Tol	0	0.90	0	0	0
Al <sub>2</sub> O <sub>3</sub> + Asp Heptol	0	0.95	0	0	0
Ssteel Blank	0	0	0.33	0.06	0.04
Ssteel+ Asp Tol	0	0	0.09	0	0.03
Ssteel+ Asp Heptol	0	0	0.11	0	0.04
Fe <sub>3</sub> O <sub>4</sub> Blank	0	0	0.21	0	0
Fe <sub>3</sub> O <sub>4</sub> + Asp Tol	0	0	0.16	0	0
Fe <sub>3</sub> O <sub>4</sub> + Asp Heptol	0	0	0.17	0	0
Asphaltenes	0	0	0	0	0

### 4.3.2.2 High Resolution Spectra

#### 4.3.2.2.1 Carbon Spectra

Shown in Figure 4.7 are the C1s high resolution scans of bulk asphaltenes, bare and asphaltene covered quartz crystal surfaces. Two peaks were fitted to all the C1s XPS spectra (labeled as A and B in Figure 4.7). Overall, the C1s region presents a significant feature at 284.8 eV (labeled as A) that represents C in an aliphatic or aromatic C–H environment. **(24)** Also a sub-peak at a higher binding energy between 285.0 and 286.5 eV (labeled as B) is attributed to carbon bonded with nitrogen, sulfur or oxygen. **(28, 132)** Another notable result is that asphaltene covered surfaces show a drop in the area ratio of peak A to peak B, when compared to blank surfaces. This result, suggests that species containing C-N, C-S or C-O groups are preferentially adsorbed on the surfaces studied. It is worth noting that, except for aluminum oxide, all other three substrates exposed to asphaltene in heptol solutions show that the sub-peak labeled as B shifts to slightly lower binding energy values, when compared to bulk asphaltenes; suggesting that the bonding environment of C has changed after the adsorption of asphaltenes on this surfaces. The relatively

lower binding energy values could be explained by the presence of C associated to less electronegative elements such as Cr, Fe, Co or Si which are present on the surfaces investigated. **(133)** Interestingly, for silicon dioxide, aluminum oxide and iron oxide substrates exposed to asphaltene in toluene solutions, the sub-peak B is located between the binding energies of the sub-peak B of bulk asphaltenes and blank surfaces or at the same position of sub-peak B of blank surfaces. Such finding could be explained by the lower amount of asphaltenes adsorbed from toluene solutions and consequently less number of metal-polar bonds in the adsorbed layer.

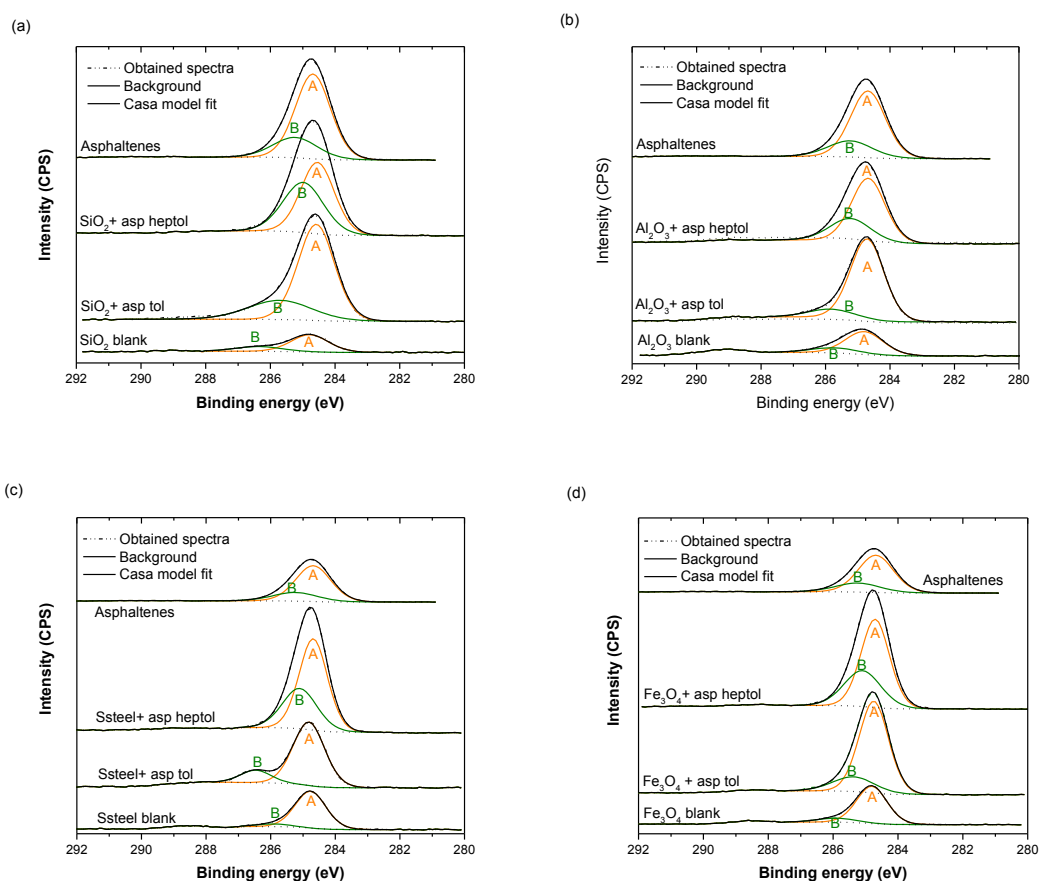


**Figure 4.7.** High resolution C1s XPS spectra of bulk asphaltenes, bare and asphaltene covered quartz crystal surfaces. (a) Silicon dioxide; (b) Aluminum oxide; (c) Stainless steel; and (d) Iron oxide.

#### 4.3.2.2.2 Oxygen Spectra

Shown in Figure 4.8 are the O1s spectra of bulk asphaltenes, bare and asphaltene covered quartz crystal surfaces. Bulk asphaltenes present a peak at 532.6 eV, attributed to O-C bonds. **(28)** Peaks

in the spectra from silicon dioxide and aluminum oxide correspond well with the binding energies expected for  $\text{SiO}_2$  (532.5-533.3 eV) and  $\text{Al}_2\text{O}_3$  (529.9-531.8) compound types. **(131)** Regarding the iron oxide and stainless steel surfaces, the O1s peaks show an asymmetrical band, which was fitted into two different peaks. A main peak appears between 529.5 and 530 eV (labeled as A), which indicates the presence of  $\text{Fe}_2\text{O}_3$  compounds on both surfaces and other metal oxides (chromium and cobalt content) on the stainless steel surface. **(131)** The other shoulder peak located in the range 530.9–532.0 eV (labeled as B) could be attributed to C-O and C=O bonds. **(24, 28)** When comparing iron oxide and stainless steel blank surfaces with asphaltene covered surfaces, it can be observed that the area ratio of peak A to peak B is not altered after the adsorption of asphaltenes, suggesting that these oxygen chemical groups are present in the same proportion even after the adsorption of asphaltenes.

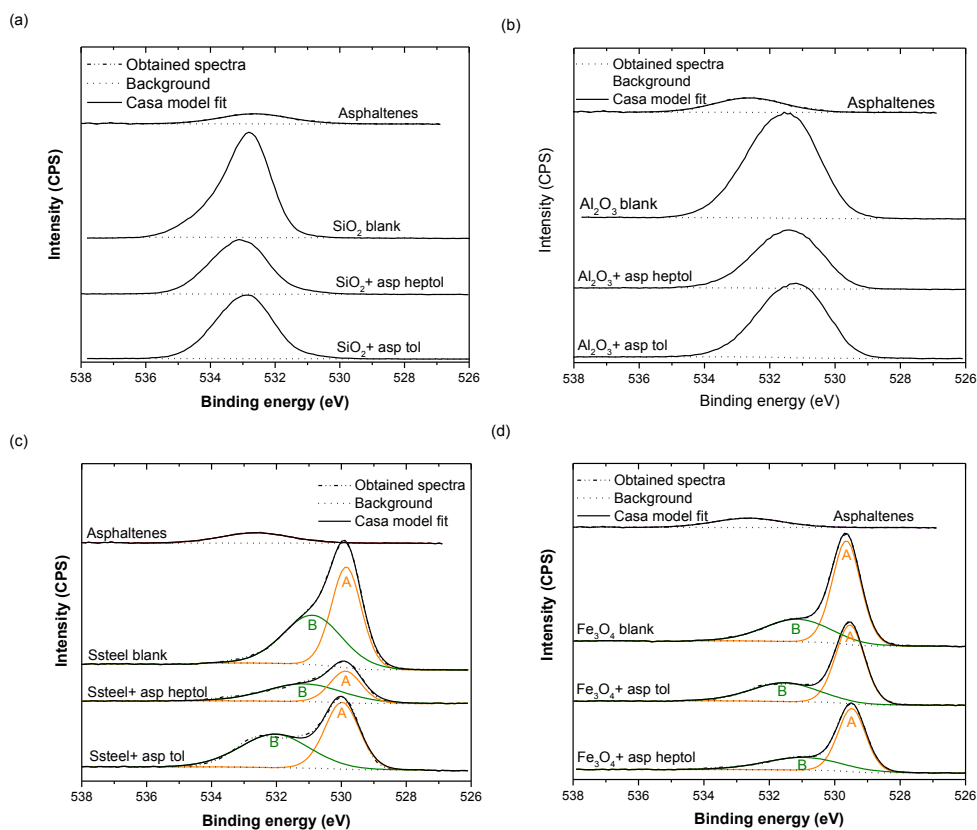


**Figure 4.8.** High resolution O1s XPS spectra of bulk asphaltenes, bare and asphaltene covered quartz crystal surfaces. (a) Silicon dioxide; (b) Aluminum oxide; (c) Stainless steel; and (d) Iron oxide.

### 4.3.2.2.3 Nitrogen Spectra

The high resolution N1s spectra of bulk asphaltenes, bare and asphaltene covered quartz crystal surfaces are shown in Figure 4.9. The N1s spectrum of bulk asphaltenes indicates the presence of pyridinic (398.1 eV) and pyrrolic (399.8 eV) nitrogen compounds. However, the surfaces exposed to asphaltene solutions in toluene and heptol only show a main peak at binding energy values between 399.6-400 eV, characteristic of pyrrolic nitrogen. These results suggest that pyrrolic compounds, present in the bulk asphaltenes, may be the only nitrogen form directly involved in the adsorption of asphaltenes on the surfaces studied.

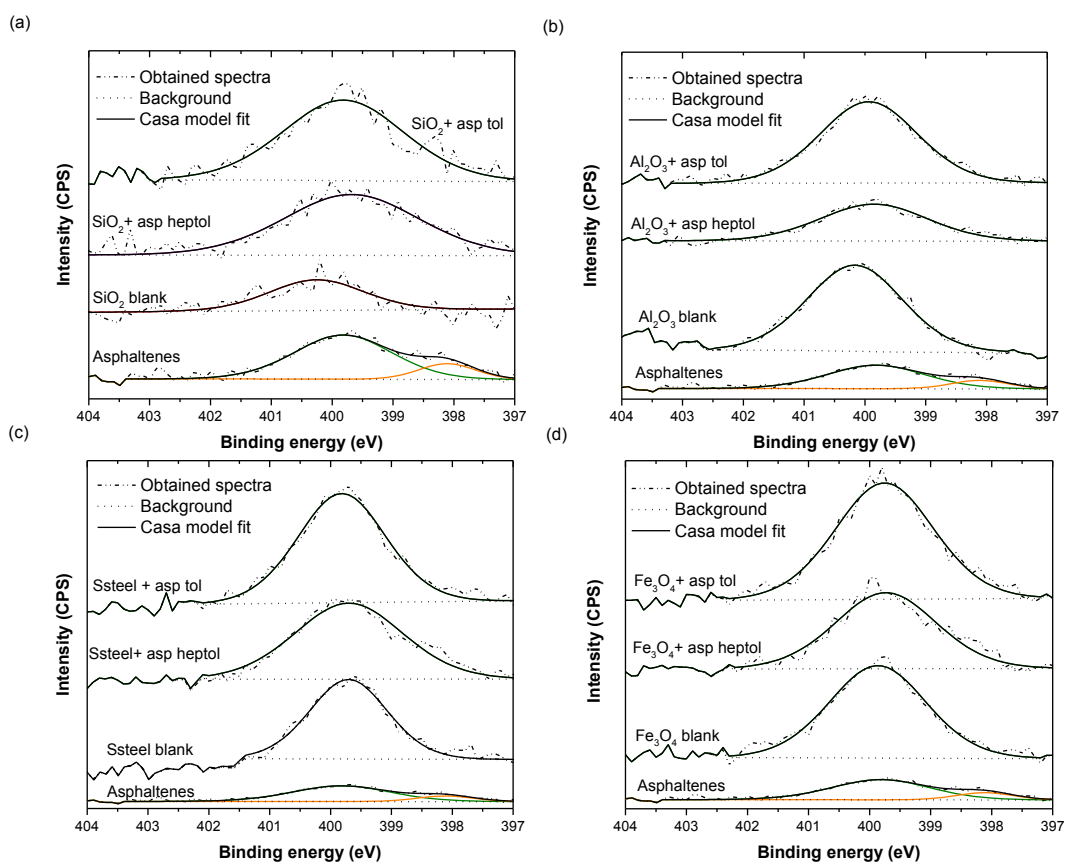


**Figure 4.9.** High resolution N1s XPS spectra of bulk asphaltenes, bare and asphaltene covered quartz crystal surfaces. (a) Silicon dioxide; (b) Aluminum oxide; (c) Stainless steel; and (d) Iron oxide.

#### 4.3.2.2.4 Sulfur Spectra

The high resolution S2p spectra of bulk asphaltenes and asphaltene covered quartz crystal surfaces are shown in Figure 4.10. The S2p photoemission spectrum was fitted with two peaks, corresponding to the 2p<sub>3/2</sub> and 2p<sub>1/2</sub> components which are separated in energy by 1.2 eV. **(131, 134)** The peak between 163.4-164.4 eV (labeled as A) corresponds to non-aromatic sulfur form. **(134)** The other sub-peak binding energy at 164.6-165.6 eV (labeled as B) is consistent with thiophenic sulfur. **(24, 134)** It is worth noting that after the adsorption of asphaltenes the area ratio of peak A to peak B decreased from 1.9 in bulk asphaltenes to values between 0.2-1.7, indicating preferential adsorption of higher binding energy sulfur (thiophene) than lower binding energy sulfur (non-aromatic S) on the surfaces investigated.

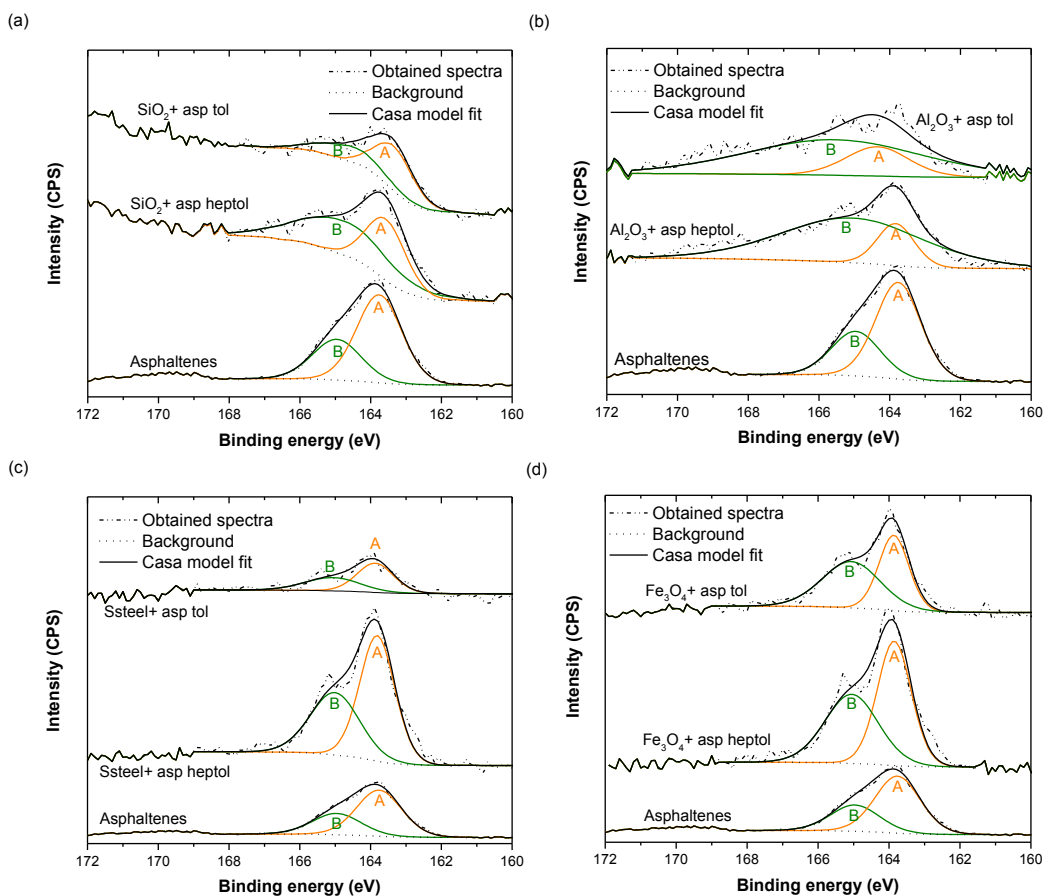


**Figure 4.10.** High resolution S2p XPS spectra of bulk asphaltenes and asphaltene covered quartz crystal surfaces. (a) Silicon dioxide; (b) Aluminum oxide; (c) Stainless steel; and (d) Iron oxide.

#### 4.3.2.3 Summary and Further Discussion

The chemical composition changes on the quartz crystal surfaces due to the adsorption of asphaltenes were assessed by XPS analysis.

Interestingly, XPS data show that asphaltenes were preferentially adsorbed onto the cobalt sites present on the stainless steel surface, which is reflected by a 100 % reduction on the Co/O ratio of the asphaltene covered surfaces when compared with the blank substrate.

Although the atomic concentration of the key components present in the coating materials studied (Al, Si and Fe) decreased after the adsorption of asphaltenes onto the solid surfaces investigated, when compared with the blank substrates, it is very difficult to determine if the surfaces studied were completely covered by the asphaltenes adsorbed, since it is possible to have a thin asphaltene layer that is below the X-ray and photo-electron penetration depth.

The analysis for C1s, N1s, O1s and S2p photoelectron peaks suggests the presence of certain functional groups of the asphaltenes adsorbed, including carboxylic, pyrrolic and thiophenic, and in some cases with slight differences in their binding energies. Hence, it could be said that the mechanism of asphaltene adsorption might be highly mediated by the asphaltene polar entities represented by these functional groups, which have been found to produce significant chemical interactions. **(135)** Studies using asphaltene model molecules concluded that the heteroatom content, in particular N and O is more important for modeling Athabasca asphaltene adsorption behavior than the overall chemical composition of the molecules. **(136, 137)**

In addition, hydrogen bonding forces are likely to participate in the interactions between the polar groups of asphaltenes and the surfaces investigated, leading to adsorption. Dubey et al. **(138)** proposed hydrogen bonding as the major mechanism for adsorption of asphaltenes on kaolin and other clays from toluene solutions. This force has also been reported to be important in directing asphaltene aggregation. **(139, 140)** Van der Waals forces could also play a role in asphaltene-solid and asphaltene-asphaltene interactions, promoting the adsorption of asphaltene aggregates. Several studies have reported van der Waals forces to be important for asphaltene aggregation **(139, 141, 142)** and precipitation. **(143)** In a recent study, Gray et al. **(144)** proposed a supramolecular assembly model for asphaltene aggregation that includes different cooperative intermolecular interactions such as hydrogen bonding, metal coordination, acid-base interactions and van der Waals forces.

#### 4.4 Conclusions

In the current study, QCM-D and XPS techniques were used to develop a fundamental understanding on the adsorption of asphaltenes from model oil systems on various solid surfaces.

For the solid surfaces investigated, the adsorption of asphaltenes was found to be a rapid process featured by the formation of rigid film(s). The interactions between the asphaltenes and surfaces investigated were found to be strong, as shown by the amount of asphaltenes desorbed that represents less than 10 % of asphaltenes adsorbed, when rinsing with toluene or heptol (1:1 volume mixture n-heptane and toluene) solvents.

The adsorption of asphaltenes onto silicon dioxide and aluminum oxide surfaces from toluene solutions, reached an equilibrium state, suggesting saturation of the adsorption sites on these surfaces. However, the amount of asphaltenes adsorbed on iron oxide and stainless steel surfaces from toluene solutions, did not level off within the concentration range investigated, which points towards a multilayer adsorption of asphaltenes on these surfaces or no saturation of the adsorption sites of these surfaces. It was speculated that a multilayer adsorption on iron oxide and stainless steel surfaces could be due to the presence of large associated asphaltene molecules which could be a consequence of the metal-oxygen bonds formed between asphaltene molecules and these surfaces. Interestingly, with the exception of silicon dioxide, the adsorption of asphaltenes from heptol solutions onto all other surfaces studied also exhibits multilayer adsorption.

The adsorption of asphaltenes was found to be strongly dependent on the nature of the solvent, as shown by an increase in the amount of asphaltenes adsorbed on the solid surfaces from heptol solutions (7.1-8.6 mg/m<sup>2</sup>), when compared to adsorption capacity obtained in toluene solutions (3.4-5.7 mg/m<sup>2</sup>). Asphaltenes dissolved in heptol have a higher degree of aggregation. Hence, the adsorbed layer(s) was(were) suggested to be formed by asphaltenes in associated state, which translates to a higher mass of asphaltenes adsorbed.

Although all the solid surfaces studied showed changes in wettability (more hydrophobic) after the adsorption of asphaltenes; there is no correlation between the wettability of the surfaces investigated and their adsorption capacity of asphaltene.

XPS analysis of adsorbed and bulk asphaltene surfaces revealed the presence of carboxylic, pyrrolic and thiophenic functional groups, responsible for the polar interactions that aided the

adsorption of asphaltenes on the solid surfaces investigated. These results agree with the functional groups identified in the chemical analysis of asphaltene reported in the literature. **(24, 28, 132)**

# Chapter 5 General Conclusions and Future Work

## 5.1 General Conclusions

The present study focuses on investigating the adsorption of asphaltenes on different solid surfaces from organic solvents using two different techniques: UV-Vis spectrophotometry and Quartz Crystal Microbalance with Dissipation (QCM-D), in an attempt to better understand the adsorption process and elucidate the molecular mechanism involved in the interactions between asphaltenes and different solid surfaces. A systematic study on the impact of the solvent type and surface chemistry of solids on the asphaltene adsorption capacity of solids investigated is carried out. The major findings of this work are summarized as follows:

- Asphaltene adsorption tests on different solid particles from toluene solutions using UV-Vis spectrophotometry showed that the adsorption of asphaltenes is highly dependent on the surface morphology and chemical characteristics of the solids.
- Thermal treatment of silicon dioxide and aluminum oxide particles before being used in asphaltene adsorption experiments is a good approach to study the nature of the surface groups responsible for the adsorption of asphaltenes on these solids. A decrease in the surface silanol groups on silicon dioxide particles resulted in a lower asphaltene adsorption capacity. In contrast, a decrease in the surface aluminol groups on aluminum oxide particles enhanced the asphaltene adsorption capacity. When thermally treating aluminum oxide particles, strained oxygen bridges are formed along with Lewis sites  $Al^+$  that may increase the adsorption capacity. This experiment showed that asphaltene adsorption capacity of silicon dioxide and aluminum oxide particles is strongly mediated by the surface hydroxyl groups.
- Thermo-gravimetric analysis was found to be a useful technique to study the decomposition kinetics of asphaltenes adsorbed on solid particles. Structural differences in the asphaltene molecules adsorbed on silicon dioxide and aluminum oxide particles from toluene and heptol solutions were evident by differences in the decomposition activation energies of asphaltenes and asphaltenes adsorbed on solid particles from toluene and heptol solvents.

- Adsorption experiments using QCM-D technique showed that the nature of the adsorption process and the asphaltene adsorption capacity is strongly dependent on the chemistry of the solid surfaces investigated. In toluene solutions, asphaltene adsorption curves for silicon dioxide and aluminum oxide surfaces reached equilibrium, which indicates saturation of the adsorption sites on these surfaces. In contrast, asphaltene adsorption curves for iron oxide and stainless steel materials showed a continuous increase in the amount of asphaltenes adsorbed, indicating a multilayer adsorption of asphaltenes or absence of saturation adsorption on these surfaces.
- The frequency and dissipation changes because of the adsorbed asphaltenes showed that asphaltenes are strongly adsorbed as a rigid film(s).
- The effect of the aromaticity of the solvent on asphaltene adsorption on solid surfaces was clearly identified by using UV-Vis spectrophotometry and QCM-D techniques. The adsorption of asphaltenes was found to be strongly dependent on the nature of the solvent as evident by higher asphaltene adsorption capacities of the solids investigated when using heptol (1:1 volume mixture of n-heptane and toluene) solutions.
- The adsorption of asphaltenes on the solid surfaces investigated is highly mediated by polar interactions occurred between solid surface active sites and different functional groups (carboxylic, pyrrolic and thiophenic) present in asphaltene molecules.

## 5.2 Future Work

To gain a better understanding of the adsorption of asphaltenes on solid surfaces from organic solvents, more work needs to be conducted as listed below:

- Considering the complex nature of asphaltenes, a study on the adsorption of model compounds with well-defined structure and similar properties to real asphaltenes on different solid surfaces from organic solvents would provide further insights into the mechanism of asphaltene adsorption.
- It may be interesting to use Quartz Crystal Microbalance with Dissipation (QCM-D) technique to study the effect of non-asphaltenic components of bitumen, e.g., resins and naphthenic acids, on adsorption of asphaltenes on different substrates. This approach could shed some light on the contributions of asphaltene-resins and asphaltene-naphthenic acids interactions to the adsorption process.

- It is well-known that asphaltene composition and structure depend on the origin of crude oil and the method of extraction. In some studies a specific asphaltene subfraction was reported to be primarily responsible for stabilizing water-in-oil (W/O) emulsions. Therefore, a study on the adsorption of different asphaltene sub-fractions onto different solid surfaces is proposed. This would help to elucidate particular asphaltenic structures which could be critically important to better understand the asphaltene adsorption phenomenon.
- QCM-D experiments performed in this work evidenced that desorbed asphaltenes corresponds to around 10 % of the adsorbed layer on the solid surfaces investigated. Several investigators have reported the ability of strong amphiphilic molecules in dissolving precipitated asphaltenes and stabilizing asphaltene suspensions in non-polar media. Hence, a study on the influences of the chemical structure of different alkyl benzene-derived amphiphiles, (e.g., dodecyl benzene sulfonic acid) on the effectiveness of asphaltene desorption using QCM-D is proposed.
- Study the impact of thermal dehydration of quartz crystal surfaces coated with silicon dioxide and aluminum oxide on the adsorption of asphaltenes from toluene solutions. Comparison with the UV-Vis data reported in Chapter 3 for the adsorption of asphaltenes on thermally treated silicon dioxide and aluminum oxide particles will help to better understand the relation between the hydroxyl groups present on these materials and their adsorption capacity.
- Temperature programmed desorption with quantitative mass spectrometry analysis (TPD-MS) of asphaltene covered surfaces will allow the quantitative analysis of the released gases as a function of temperature, which would provide further insight into the surface chemistry and binding energy of the bound species.
- In this study the adsorption of asphaltenes onto different solid surfaces from toluene and heptol (1:1 volume mixture of heptane and toluene) solutions was investigated. Research focusing on real oil systems is an important next step in this work to evaluate more accurately the adsorption of asphaltenes in industrial processes.

# References

1. Honarvar A, Rozhon J, Millington D, Walden T, Murillo C, Walden Z. Economic Impacts of New Oil Sands Projects in Alberta (2010-2035). Calgary, Alberta: Canadian Energy Research Institute, 2011.
2. Masliyah JH, Xu Z, Czarnecki JA, Dabros M. Handbook on Theory and Practice of Bitumen Recovery from Athabasca Oil Sands: Kingsley Knowledge Pub., c2011-2013, Cochrane, Alberta; 2011.
3. Teare M, Cruickshank R, Miller S, Overland S, Marsh R, Willwerth A, et al. Alberta's Energy Reserves 2013 and Supply/Demand Outlook 2014–2023. Calgary, Alberta: Alberta Energy Regulator, 2014.
4. OPEC Annual Statistical Bulletin. Vienna, Austria: Organization of the Petroleum Exporting Countries, 2014.
5. Masliyah J, Zhou Z, Xu Z, Czarnecki J, Hamza H. Understanding water-based bitumen extraction from Athabasca oil sands. *The Canadian Journal of Chemical Engineering*. 2004;82(4):628-54.
6. (GOA) GoA. Environmental Management of Alberta's Oil Sands. Edmonton: 2009.
7. Scott JD, Dusseault MB, Carrier WD. Behaviour of the clay/bitumen/water sludge system from oil sands extraction plants. *Applied Clay Science*. 1985;1(1-2):207-18.
8. Small CC, Cho S, Hashisho Z, Ulrich AC. Emissions from oil sands tailings ponds: review of tailings pond parameters and emission estimates. *Journal of Petroleum Science and Engineering*. 2014.
9. Sheu EY, Mullins OC. *Asphaltenes : Fundamentals and Applications* / edited by Eric Y. Sheu and Oliver C. Mullins: Plenum Press, c1995., New York; 1995.
10. Akbarzadeh K, Hammami A, Kharrat A, Zhang D, Allenson S, Creek J, et al. Asphaltenes - problematic but rich in potential. *Oilfield Review*. 2007;19(2):22-43.
11. Aske N, Kallevik H, Johnsen EE, Sjoblom J. Asphaltene aggregation from crude oils and model systems studied by high-pressure NIR spectroscopy. *Energy & Fuels*. 2002;16(5):1287-95.

12. Franco CA, Nassar NN, Ruiz MA, Pereira-Almao P, Cortes FB. Nanoparticles for inhibition of asphaltene damage: adsorption study and displacement test on porous media. *Energy & Fuels*. 2013;27(6):2899-907.
13. Buckley JS. Wetting alteration of solid surfaces by crude oils and their asphaltene. *Revue de l'Institut Francais du Petrole*. 1998;53(3):303-12.
14. Kokal S. Crude-oil emulsions: a state-of-the-art review. *SPE Production and Facilities*. 2005;20(1):5-12.
15. McLean JD, Kilpatrick PK. Effects of asphaltene aggregation in model heptane-toluene mixtures on stability of water-in-oil emulsions. *Journal of Colloid and Interface Science*. 1997;196(1):23-34.
16. Ese MH, Sjöblom J, Førdedal H, Urdahl O, Rønningsen HP. Ageing of interfacially active components and its effect on emulsion stability as studied by means of high voltage dielectric spectroscopy measurements. *Colloids and Surfaces A: Physicochemical and Engineering Aspects*. 1997;123-124:225-32.
17. Adams JJ. Asphaltene adsorption, a literature review. *Energy & Fuels*. 2014;28(5):2831-56.
18. Nassar NN. Asphaltene adsorption onto alumina nanoparticles: kinetics and thermodynamic studies. *Energy & Fuels*. 2010;24(4):4116-22.
19. Dean KR, McAtee Jr JL. Asphaltene adsorption on clay. *Applied Clay Science*. 1986;1(4):313-9.
20. Dudášová D, Simon S, Hemmingsen PV, Sjöblom J. Study of asphaltene adsorption onto different minerals and clays. Part 1. Experimental adsorption with UV depletion detection. *Colloids and Surfaces A: Physicochemical and Engineering Aspects*. 2008;317:1-9.
21. Acevedo S, Ranaudo MA, Escobar G, Gutiérrez L, Ortega P. Adsorption of asphaltene and resins on organic and inorganic substrates and their correlation with precipitation problems in production well tubing. *Fuel*. 1995;74(4):595-8.
22. Alboudwarej H, Pole D, Y. Svrcek W, W. Yarranton H. Adsorption of asphaltene on metals. *Industrial & Engineering Chemistry Research*. 2005;44(15):5585.
23. Pernyeszi T, Patzkó Á, Berkesi O, Dékány I. Asphaltene adsorption on clays and crude oil reservoir rocks. *Colloids and Surfaces A: Physicochemical and Engineering Aspects*. 1998;137:373-84.

24. Rudrake A, Karan K, Horton JH. A combined QCM and XPS investigation of asphaltene adsorption on metal surfaces. *Journal of Colloid & Interface Science*. 2009;332(1):22-31.
25. Ekholm PA, Blomberg EA, Claesson PMA, Auflem IHA, Sjöblom JA, Kornfeldt AA, et al. A quartz crystal microbalance study of the adsorption of asphaltenes and resins onto a hydrophilic surface. *Journal of Colloid and Interface Science*. 2002:342.
26. Tavakkoli M, Panuganti SR, Vargas FM, Taghikhani V, Pishvaie MR, Chapman WG. Asphaltene deposition in different depositing environments: part 1. Model oil. *Energy & Fuels*. 2014;28(2):1617.
27. Marczewski AW, Szymula M. Adsorption of asphaltenes from toluene on mineral surface. *Colloids and Surfaces A: Physicochemical and Engineering Aspects*. 2002;208:259-66.
28. Abdallah WA, Taylor SD. Surface characterization of adsorbed asphaltene on a stainless steel surface. *Nuclear Instruments and Methods in Physics Research, Section B: Beam Interactions with Materials and Atoms*. 2007;258(1):213-7.
29. Xie K, Karan K. Kinetics and thermodynamics of asphaltene adsorption on metal surfaces: a preliminary study. *Energy and Fuels* 2005;19(4):1252-60.
30. Natarajan A, Kuznicki N, Harbottle D, Masliyah J, Zeng H, Xu Z. Understanding mechanisms of asphaltene adsorption from organic solvent on mica. *Langmuir: The ACS Journal Of Surfaces And Colloids*. 2014;30(31):9370-7.
31. Speight JG. *The Chemistry and Technology of Petroleum*: CRC Press, Hoboken; 2014.
32. Strausz OP, Lown EM. *The Chemistry of Alberta Oil Sands, Bitumens and Heavy Oils*: Alberta Energy Research Institute, c2003, Calgary, Alberta; 2003.
33. ASTM. D4124-09 Standard Test Method for Separation of Asphalt into Four Fractions. 2009.
34. Meléndez LV, Lache A, Orrego-Ruiz JA, Pachón Z, Mejía-Ospino E. Prediction of the SARA analysis of Colombian crude oils using ATR–FTIR spectroscopy and chemometric methods. *Journal of Petroleum Science and Engineering*. 2012;90–91(0):56-60.
35. Andrews AB, Guerra RE, Mullins OC, Sen PN. Diffusivity of asphaltene molecules by fluorescence correlation spectroscopy. *Journal of Physical Chemistry A*. 2006(26):8093.
36. Groenzin H, Mullins OC. Molecular size and structure of asphaltenes from various sources. *Energy and Fuels*. 2000;14:677-84.

37. Strausz OP, Mojelsky TW, Lown EM. The molecular structure of asphaltene: an unfolding story. *Fuel*. 1992;71(12):1355-63.
38. Mullins OC. *Asphaltenes, Heavy Oils, and Petroleomics* [electronic resource] / edited by Oliver C. Mullins, Eric Y. Sheu, Ahmed Hammami, Alan G. Marshall: Springer, c2007., New York; 2007.
39. Schuler B, Meyer G, Pena D, Mullins OC, Gross L. Unraveling the molecular structures of asphaltenes by atomic force microscopy. *Journal of the American Chemical Society*. 2015(31):9870.
40. Alboudwarej H, Akbarzadeh K, Beck J, Svrcek WY, Yarranton HW. Regular solution model for asphaltene precipitation from bitumens and solvents. *AIChE Journal*. 2003;49(11):2948.
41. Mitchell DL, Speight JG. The solubility of asphaltenes in hydrocarbon solvents. *Fuel*. 1973;52(2):149-52.
42. Andersen SI, Keul A, Stenby E. Variation in composition of subfractions of petroleum asphaltenes. *Petroleum Science and Technology*. 1997;15(7-8):611-45.
43. Andersen SI. Effect of precipitation temperature on the composition of n-heptane asphaltenes. *Fuel Science and Technology International*. 1994;12(1):51-74.
44. Fuhr BJ, Cathrea C, Coates L, Kalra H, Majeed AI. Properties of asphaltenes from a waxy crude. *Fuel*. 1991;70(11):1293-7.
45. Acevedo S, Zuloaga C, Rodríguez P. Aggregation-dissociation studies of asphaltene solutions in resins performed using the combined freeze fracture-transmission electron microscopy technique. *Energy and Fuels*. 2008;22(4):2332-40.
46. Derakhshesh M, Bergmann A, Gray MR. Occlusion of polyaromatic compounds in asphaltene precipitates suggests porous nanoaggregates. *Energy and Fuels*. 2013;27(4):1748-51.
47. Dickie JP, Yen TF. Macrostructures of the asphaltic fractions by various instrumental methods. *Analytical Chemistry*. 1967;39(14):1847-52.
48. Pfeiffer JP, Saal RNJ. Asphaltic bitumen as colloid system. *The Journal of Physical Chemistry*. 1940;44(2):139-49.
49. Nellensteyn FJ. *Bereiding en constitutie van asphalt (Manufacture and constitution of asphaltic bitumen)*. Netherlands: Technische Hoogeschool, Delft; 1923.

50. Hirschberg A, de Jong LNJ, Meijers JG, Schipper BA. Influence of temperature and pressure on asphaltene flocculation. SPEJ, Soc Pet Eng J; (United States). 1984:283.
51. Kawanaka S, Park SJ, Mansoori GA. Organic deposition from reservoir fluids; A thermodynamic predictive technique. SPE (Society of Petroleum Engineers) Reservoir Engineering; (United States). 1991:185.
52. Jeribi M, Almir-Assad B, Langevin D, Hénaut I, Argillier JF. Adsorption and deposition: adsorption kinetics of asphaltenes at liquid interfaces. Journal of Colloid And Interface Science. 2002;256:268-72.
53. Carlos da Silva Ramos A, Haraguchi L, Notrispe FR, Loh W, Mohamed RS. Interfacial and colloidal behavior of asphaltenes obtained from Brazilian crude oils. Journal of Petroleum Science and Engineering. 2001;32:201-16.
54. Ese MH, Yang X, Sjöblom J. Film forming properties of asphaltenes and resins. A comparative Langmuir– Blodgett study of crude oils from North Sea, European continent and Venezuela. Colloid & Polymer Science. 1998;276(9):800.
55. Freer EM, Radke CJ. Relaxation of asphaltenes at the toluene / water interface: diffusion exchange and surface rearrangement The Journal of Adhesion. 2004;80(6):481-96.
56. Ortiz DP, Baydak EN, Yarranton HW. Effect of surfactants on interfacial films and stability of water-in-oil emulsions stabilized by asphaltenes. Journal of Colloid and Interface Science. 2010;351(2):542-55.
57. Spiecker PM, Kilpatrick PK. Interfacial rheology of petroleum asphaltenes at the oil-water interface. Langmuir: The ACS Journal Of Surfaces And Colloids. 2004;20(10):4022-32.
58. Spiecker PM, Gawrys KL, Kilpatrick PK. Aggregation and solubility behavior of asphaltenes and their subfractions. Journal of Colloid And Interface Science. 2003;267:178-93.
59. Czarnecki J, Moran K. On the stabilization mechanism of water-in-oil emulsions in petroleum systems. Energy and Fuels. 2005;19(5):2074-9.
60. Czarnecki J. Stabilization of water in crude oil emulsions. Part 2. Energy and Fuels 2009;23(2):1253-7.
61. Xu Y, Dabros T, Hamza H, Shefantook W. Destabilization of water in bitumen emulsion by washing with water. Petroleum Science and Technology. 1999;17:1051.

62. Wu X. Investigating the stability mechanism of water-in-diluted bitumen emulsions through isolation and characterization of the stabilizing materials at the interface. *Energy and Fuels*. 2003;17:179-90.
63. Fan Y, Tchoukov P, Pensini E, Dabros T, Czarnecki J, Masliyah J, et al. Asphaltene subfractions responsible for stabilizing water-in-crude oil emulsions. Part 1: interfacial behaviors. *Energy & Fuels*. 2014;28(6):6897.
64. Kokal S, Tang T, Schramm L, Sayegh S. Electrokinetic and adsorption properties of asphaltenes. 1995;94:253-65.
65. Acevedo S, Ranaudo MA, Garcia C, Castillo J, Fernandez A. Adsorption of asphaltenes at the toluene-silica interface: a kinetic study. *Energy and Fuels*. 2003;17:257-61.
66. Zahabi A, Gray MR, Dabros T. Kinetics and properties of asphaltene adsorption on surfaces. *Energy & Fuels*. 2012;26(1):1009.
67. Turgman-Cohen S, Fischer D, Kilpatrick P, Genzer J. Asphaltene adsorption onto self-assembled monolayers of alkyltrichlorosilanes of varying chain length. *ACS Applied Materials & Interfaces*. 2009(6):1347-57.
68. Saint-Just J. Catalyst characterization by adsorption of petroleum asphaltenes in solution. *Industrial & Engineering Chemistry Product Research and Development*. 1980;19(1):71-5.
69. Dudasova D, Silset A, Sjoblom J, Norwegian Univ Sci T. Quartz crystal microbalance monitoring of asphaltene adsorption/deposition *Journal of Dispersion Science and Technology* 2008;29(1):139-46.
70. Collins SH, Melrose JC. Adsorption of asphaltenes and water on reservoir rock minerals. SPE: Society of Petroleum Engineers; 1983. p. 249- 54.
71. Jada A, Debih H. Hydrophobation of clay particles by asphaltenes adsorption. *Composite Interfaces*. 2009;16(2/3):219-35.
72. Franco C, Patiño E, Benjumea P, Ruiz MA, Cortés FB. Kinetic and thermodynamic equilibrium of asphaltenes sorption onto nanoparticles of nickel oxide supported on nanoparticulated alumina. *Fuel*. 2013;105:408-14.
73. Balabin RM, Syunyaev RZ, Schmid T, Stadler J, Lomakina EI, Zenobi R. Asphaltene adsorption onto an iron surface: combined Near-Infrared (NIR), Raman, and AFM study of the kinetics, thermodynamics, and layer structure. *Energy & Fuels*. 2011;25(1):189.

74. McLean JD, Kilpatrick PK. Effects of asphaltene solvency on stability of water-in-crude-oil emulsions. *Journal of Colloid and Interface Science*. 1997;189(2):242.
75. Sanders RS, Chow RS, Masliyah JH. Deposition of bitumen and asphaltene-stabilized emulsions in an impinging jet cell. *Journal of Colloid and Interface Science*. 1995;174(1):230.
76. Fang H, Zhang L, Luo L, Zhao S, An J, Xu Z, et al. A study of thin liquid films as related to the stability of crude oil emulsions. *Journal Of Colloid And Interface Science*. 2001;238(1):177-82.
77. Nassar NN, Hassan A, Pereira-Almao P. Effect of the particle size on asphaltene adsorption and catalytic oxidation onto alumina particles. *Energy & Fuels*. 2011;25(5):3961.
78. Ansari N. Thermogravimetric Analysis of Solvent Interaction with Model TSRU Tailings Components. Canada: University of Alberta (Canada); 2013.
79. Foo KY, Hameed BH. Insights into the modeling of adsorption isotherm systems. *Chemical Engineering Journal*. 2010;156(1):2-10.
80. Langmuir I. The constitution and fundamental properties of solids and liquids. Part I. Solids. *Journal of the American Chemical Society*. 1916;38(11):2221-95.
81. Freundlich HMF. Uber die adsorption in losungen. *Journal of Physical Chemistry*. 1906;57(A):385-470.
82. Mohammadi M, Khamehchi E, Sedighi M. The prediction of asphaltene adsorption isotherm constants on mineral surfaces. *Petroleum Science & Technology*. 2014;32(7):870-7.
83. Nassar NN, Hassan A, Pereira-Almao P. Metal oxide nanoparticles for asphaltene adsorption and oxidation. *Energy & Fuels*. 2011;25(3):1017-23.
84. Tombacz E, Szekeres M. Surface charge heterogeneity of kaolinite in aqueous suspension in comparison with montmorillonite. *Applied Clay Science*. 2006(1-4):105.
85. Fritschy G, Papirer E. Interactions between a bitumen, its components and model fillers. *Fuel*. 1978;57:701-4.
86. Saravanan L, Subramanian S. Surface chemical studies on the competitive adsorption of poly(ethylene glycol) and ammonium poly(methacrylate) onto alumina. *Journal of Colloid And Interface Science*. 2005;284:363-77.
87. Nassar NN, Hassan A, Pereira-Almao P. Effect of surface acidity and basicity of aluminas on asphaltene adsorption and oxidation. *Journal of Colloid And Interface Science*. 2011;360:233-8.

88. Zheivot VI, Parkhomchuk EV, Sashkina KA, Melgunova EA, Zaikovskii VI, Moroz EM. Silica and alumina based functional materials: substructures, adsorption and gas chromatographic properties. *Microporous and Mesoporous Materials*. 2015;202:57-67.
89. Morrow BA, McFarlan AJ. Infrared and gravimetric study of an aerosil and a precipitated silica using chemical and hydrogen/deuterium exchange probes. *Langmuir*. 1991;7(8):1695-701.
90. Bermudez A, Salazar R. Synthesis and characterization of the polystyrene- asphaltene graft copolymer by FT-IR spectroscopy. *CT&F - Ciencia, Tecnologia y Futuro*. 2008.
91. Della Volpe C, Dirè S, Pagani E. A comparative analysis of surface structure and surface tension of hybrid silica films. *Journal of Non-Crystalline Solids*. 1997;209:51-60.
92. Guo X, Liu X, Xu B, Dou T. Synthesis and characterization of carbon sphere-silica core-shell structure and hollow silica spheres. *Colloids and Surfaces A: Physicochemical and Engineering Aspects*. 2009;345:141-6.
93. Pasquarello A, Car R. Dynamical charge tensors and infrared spectrum of amorphous SiO<sub>2</sub>. *Physical Review Letters*. 1997;79(9):1766-9.
94. El-Naggar AY. Characterization of modified and polymer coated alumina surfaces by infrared spectroscopy. *Journal of Spectroscopy - Hindawi Publishing Corporation* 2013;2013:706960.
95. Ledoux RL, White JL. Infrared study of the OH groups in expanded kaolinite. 1964:244.
96. Frost RL, Kristóf J, Makó É, Horváth E. A DRIFT spectroscopic study of potassium acetate intercalated mechanochemically activated kaolinite. *Spectrochimica Acta Part A: Molecular and Biomolecular Spectroscopy*. 2003;59:1183-94.
97. Frost RL, Makó É, Kristóf J, Klopogge JT. Modification of kaolinite surfaces through mechanochemical treatment—a mid-IR and near-IR spectroscopic study. *Spectrochimica Acta Part A: Molecular and Biomolecular Spectroscopy*. 2002;58(13):2849-59.
98. Adamson AW, Gast AP. *Physical Chemistry of Surfaces*: Wiley, c1997. 6th ed., New York; 1997.
99. Rouquerol F, Rouquerol J, Sing KSW. *Adsorption by Powders and Porous Solids : Principles, Methodology, and Applications*: Academic Press, San Diego; 1999.
100. Kasprzyk-Hordern B. Chemistry of alumina, reactions in aqueous solution and its application in water treatment. *Advances in Colloid and Interface Science*. 2004;110(1–2):19-48.

101. Kurhinen M, Pakkanen TA. Diffuse reflectance infrared spectroscopy study of Co-2(CO)(8) supported on alumina:
102. Goncalves MLA, Teixeira MAG, Pereira RCL, Mercury RLP, Matos JR. Contribution of thermal analysis for characterization of asphaltenes from Brazilian crude oil. *Journal of Thermal Analysis and Calorimetry*. 2001;64(Generic):697-706.
103. Schucker RC. Thermogravimetric determination of the coking kinetics of Arab heavy vacuum residuum. *Ind Eng Chem Process Des Dev*; (United States). 1983:615.
104. Trejo F, Rana MS, Ancheyta J. Thermogravimetric determination of coke from asphaltenes, resins and sediments and coking kinetics of heavy crude asphaltenes. *Catalysis Today*. 2010;150(3-4):272-8.
105. Friedman HL. Kinetics of thermal degradation of char-forming plastics from thermogravimetry. Application to a phenolic plastic. *Journal of Polymer Science Part C: Polymer Symposia*. 1964;6(1):183-95.
106. Flynn JH, Wall LA. A quick, direct method for the determination of activation energy from thermogravimetric data. *Journal of Polymer Science Part B: Polymer Letters*. 1966;4(5):323-8.
107. Collett GW, Rand B. Thermogravimetric investigation of the pyrolysis of pitch materials. A compensation effect and variation in kinetic parameters with heating rate. *Thermochimica Acta*. 1980;41(2):153-65.
108. Slade PE, Jenkins LT. *Techniques and Methods of Polymer Evaluation*: M. Dekker, New York; 1966.
109. Toop DJ. Theory of life testing and use of thermogravimetric analysis to predict the thermal life of wire enamels. *Electrical Insulation, IEEE Transactions on*. 1971;EI-6(1):2-14.
110. Qu X, Alvarez PJJ, Li Q. Impact of sunlight and humic acid on the deposition kinetics of aqueous fullerene nanoparticles (nC60). *Environmental Science and Technology -Washington DC-*. 2012;46(24):13455-62.
111. Baradel N, Fort S, Halila S, Badi N. Synthesis of single-chain sugar arrays. *Angewandte Chemie International Edition*. 2013(8):2335.
112. Moya SE, Irigoyen J. Recent advances in the use of the quartz crystal microbalance with dissipation for the study of the collapse of polyelectrolyte brushes. *Journal of Polymer Science Part B: Polymer Physics*. 2013(14):1068.

113. Frost R, Svedhem S. Characterization of nanoparticle-lipid membrane interactions using QCM-D. *Methods In Molecular Biology* (Clifton, NJ). 2013;991:127-37.
114. Nam DH, Lee J-O, Sang B-I, Won K, Kim YH. Silaffin peptides as a novel signal enhancer for gravimetric biosensors. *Applied Biochemistry and Biotechnology*. 2013(1):25.
115. Ozdemir MS, Marczak M, Bohets H, Bonroy K, Roymans D, Stuyver L, et al. A label-free potentiometric sensor principle for the detection of antibody-antigen interactions. *Analytical Chemistry*. 2013(9):4770.
116. Lin S, Wiesner MR. Deposition of aggregated nanoparticles - a theoretical and experimental study on the effect of aggregation state on the affinity between nanoparticles and a collector surface. *Environmental Science and Technology -Washington DC-*. 2012;46(24):13270-7.
117. Gall I, Herzberg M, Oren Y. The effect of electric fields on bacterial attachment to conductive surfaces. *Soft Matter*. 2013;9(8):2443.
118. Salas C, Rojas OJ, Lucia LA, Hubbe MA, Genzer J. On the surface interactions of proteins with lignin. *ACS Applied Materials & Interfaces*. 2013;5(1):199-206.
119. Farooq U, Sjöblom J, Øye G. Desorption of asphaltenes from silica-coated quartz crystal surfaces in low saline aqueous solutions. *Journal of Dispersion Science & Technology*. 2011;32(10):1388-95.
120. Hannisdal A, Ese M-H, Hemmingsen PV, Sjöblom J. Particle-stabilized emulsions: effect of heavy crude oil components pre-adsorbed onto stabilizing solids. *Colloids and Surfaces A: Physicochemical and Engineering Aspects*. 2006;276(1-3):45-58.
121. Rodahl M, Hook F, Krozer A, Brzezinski P, Kasemo B. Quartz crystal microbalance setup for frequency and q-factor measurements in gaseous and liquid. *Review of Scientific Instruments*. 1995;66(7):3924.
122. Keiji Kanazawa K, Gordon JG. The oscillation frequency of a quartz resonator in contact with liquid. *Analytica Chimica Acta*. 1985;175:99-105.
123. Sauerbrey G. Verwendung von schwingquarzen zur wägung dünner schichten und zur mikrowägung. *Zeitschrift für Physik*. 155(2):206-22.
124. Cho N-J, Kanazawa KK, Glenn JS, Frank CW. Employing two different quartz crystal microbalance models to study changes in viscoelastic behavior upon transformation of lipid vesicles to a bilayer on a gold surface. *Analytical Chemistry*. 2007(18):7027.

125. Voinova MV, Rodahl M, Jonson M, Kasemo B. Viscoelastic acoustic response of layered polymer films at fluid-solid interfaces: continuum mechanics approach. 1998.
126. Ruso JM, Piñeiro Á. Proteins in Solution and at Interfaces : Methods and Applications in Biotechnology and Materials Science: John Wiley & Sons Inc., [2013], Hoboken, New Jersey; 2013.
127. Jouault N, Corvis Y, Cousin F, Jestin J, Barré L. Asphaltene adsorption mechanisms on the local scale probed by neutron reflectivity: transition from monolayer to multilayer growth above the flocculation threshold. *Langmuir: The ACS Journal Of Surfaces And Colloids*. 2009;25(7):3991-8.
128. Castillo J, Fernández A, Ranaudo M, Acevedo S. New techniques and methods for the study of aggregation, adsorption, and solubility of asphaltenes. Impact of these properties on colloidal structure and flocculation *Petroleum Science & Technology*. 2001;19(1/2):75.
129. Moschopedis SE, Fryer JF, Speight JG. Investigation of asphaltene molecular weights. *Fuel*. 1976;55:227-32.
130. Goual L, Horváth-Szabó G, Masliyah JH, Xu Z. Adsorption of bituminous components at oil/water interfaces investigated by quartz crystal microbalance: implications to the stability of water-in-oil emulsions. *Langmuir: The ACS Journal Of Surfaces And Colloids*. 2005;21(18):8278-89.
131. Moulder JF. *Handbook of X-ray Photoelectron Spectroscopy : A Reference Book of Standard Spectra for Identification and Interpretation of XPS Data*: Physical Electronics, Eden Prairie, Minn. ; 1995.
132. Östlund J-A, Nydén M, Scott Fogler H, Holmberg K. Functional groups in fractionated asphaltenes and the adsorption of amphiphilic molecules. *Colloids and Surfaces A: Physicochemical and Engineering Aspects*. 2004;234:95-102.
133. Niemantsverdriet JW. *Spectroscopy in Catalysis : An Introduction*: VCH Verlagsgesellschaft Weinheim, Germany 1995.
134. Siskin M, Kelemen SR, Eppig CP, Brown LD, Afeworki M. Asphaltene molecular structure and chemical influences on the morphology of coke produced in delayed coking. *Energy and Fuels*. 2006;20(3):1227-34.
135. Araújo RS, Azevedo DCS, Cavalcante Jr CL, Jiménez-López A, Rodríguez-Castellón E. Adsorption of polycyclic aromatic hydrocarbons (PAHs) from isooctane solutions by mesoporous

molecular sieves: influence of the surface acidity. *Microporous and Mesoporous Materials*. 2008;108(1–3):213-22.

136. Gonzalez MF, Stull CS, Lopez-Linares F, Pereira-Almao P. Comparing asphaltene adsorption with model heavy molecules over macroporous solid surfaces. *Energy & Fuels*. 2007;21(1):234-41, JAN.

137. López-Linares F, Carbognani L, González MF, Sosa-Stull C, Figueras M, Pereira-Almao P. Quinolin-65 and violanthrone-79 as model molecules for the kinetics of the adsorption of C7 Athabasca asphaltene on macroporous solid surfaces. *Energy & Fuels*. 2006;20(6):2748-50.

138. Dubey ST, Waxman MH. Asphaltene adsorption and desorption from mineral surfaces. *SPE (Society Of Petroleum Engineers)* 1991:389.

139. da Costa LM, Stoyanov SR, Gusarov S, Tan X, Gray MR, Stryker JM, et al. Density functional theory investigation of the contributions of  $\pi$ - $\pi$  stacking and hydrogen-bonding interactions to the aggregation of model asphaltene compounds. *Energy & Fuels*. 2012;26(5):2727-35.

140. Simon Ivar A. Association of Petroleum Asphaltenes and the Effect on Solution Properties. *Handbook of Surface and Colloid Chemistry*. Third Edition ed. Boca Raton, Florida: CRC Press; 2008. p. 703-18.

141. Sedghi M, Goual L, Welch W, Kubelka J. Effect of asphaltene structure on association and aggregation using molecular dynamics. *The Journal of Physical Chemistry B*. 2013;117(18):5765-76.

142. Murgich J. Intermolecular forces in aggregates of asphaltenes and resins *Petroleum Science and Technology*. 2002;20(9-10):983-97.

143. Porte G, Zhou H, Lazzeri V. Reversible description of asphaltene colloidal association and precipitation. *Langmuir*. 2003;19(1):40-7.

144. Gray MR, Tykwinski RR, Stryker JM, Tan X. Supramolecular assembly model for aggregation of petroleum asphaltenes. *Energy & Fuels*. 2011;25(7):3125-34.